1-1-2002

New developments using carbon dioxide as a solvent : monolayers and nanocomposites.

Chuntao, Cao
University of Massachusetts Amherst

NEW DEVELOPMENTS USING CARBON DIOXIDE AS A SOLVENT: MONOLAYERS AND NANOCOMPOSITES
1. REACTIONS OF ORGANOSILANES WITH OXIDIZED SILICON SURFACES IN CARBON DIOXIDE
2. POLYMER/POLYMER NANOCOMPOSITES SYNTHESIZED IN CARBON DIOXIDE

A Dissertation Presented

by

CHUNTAO CAO

Submitted to the Graduate School of the
University of Massachusetts Amherst in partial fulfillment
of the requirements for the degree of

DOCTOR OF PHILOSOPHY

February 2002

Polymer Science and Engineering

NEW DEVELOPMENTS USING CARBON DIOXIDE AS A SOLVENT: MONOLAYERS AND NANOCOMPOSITES
1. REACTIONS OF ORGANOSILANES WITH OXIDIZED SILICON SURFACES IN CARBON DIOXIDE
2. POLYMER/POLYMER NANOCOMPOSITES SYNTHESIZED IN CARBON DIOXIDE

A Dissertation Presented

by

CHUNTAO CAO

Approved as to style and content by:

Thomas J. McCarthy, Chair

Alan J. Lesser, Member

Paul M. Lahti, Member

Thomas J. McCarthy, Department Head
Polymer Science and Engineering

To Yujing

ACKNOWLEDGMENTS

First of all, I would like to thank Dr McCarthy and Dr. Hsu. The trust they gave me is the most precious thing I have ever had.

Dr. McCarthy, my advisor, is really a great person. He helped me on almost everything. I am lucky to be able to work for him. I would also like to thank Dr. Lesser and Dr. Lahti for sitting in my committee. They gave me many suggestions. Dr. Lesser also helped me a lot on my composites project, especially the mechanical part.

I want to thank PSE staff. They keep the department running, and make everyone's life easy. Most of them helped me directly, and I made a lot of friends.

The McCarthy group is like a family. Members help each other. I had great discussion with almost everyone. And I really enjoy it. I will miss these names: Wei, Ed, Kelyn, Meng, Gene, Rick, Heather, Alex, Chris, Jeff, Didem, Terry, Xinqiao, Kate, Misha, Margarita, Kevin, Ebru, Ilke, Ricardo, and Jack!

It is impossible to list the names of all my friends. However, the help is always priceless. Here I only mention a couple of them who are not in Amherst any more: Heather Hayes and Yoko Aoyama. They both support me a lot. Hui Li is my friend in UChicago. He helped me to settle down in America, and he is a true friend.

Finally, I would like to thank both my parents and parents-in-law for their trust and understanding. I also want to thank my sister, Liqing, and my brother-in-law for supporting the whole family while I am away in another country. My wife, Yujing, is the biggest support for me in these four years. We suffer together and enjoy together. Thank her for sharing the life with me.

ABSTRACT

NEW DEVELOPMENTS USING CARBON DIOXIDE AS A SOLVENT: MONOLAYERS AND NANOCOMPOSITES
1. REACTIONS OF ORGANOSILANES WITH OXIDIZED SILICON SURFACES IN CARBON DIOXIDE
2. POLYMER/POLYMER NANOCOMPOSITES SYNTHESIZED IN CARBON DIOXIDE

FEBRUARY 2002

CHUNTAO CAO, B.S., UNIVERSITY OF SCIENCE AND TECHNOLOGY OF CHINA

M.S., UNIVERSITY OF CHICAGO

M.S., UNIVERSITY OF MASSACHUSETTS AMHERST

PH.D., UNIVERSITY OF MASSACHUSETTS AMHERST

Directed by: Professor Thomas J. McCarthy

The aim of this research was to explore new directions for carbon dioxide. The first project emphasized silyl monolayer synthesis. Silylation reactions were performed in both liquid and supercritical carbon dioxide. Different monofunctional organosilanes reacted with silica surfaces, forming covalently attached monolayers. These monolayers were characterized using contact angle measurements, X-ray photoelectron spectroscopy, and ellipsometry. Reaction kinetics were established, and compared with silylations in organic solvents. The reaction rate in CO_2 is higher than that in conventional solvents while the final coverage is slightly lower than the optimized conditions for conventional solvents. Other multi—functional silanes were also studied. The silylation of nanoporous silica surfaces showed bonding densities almost as high as the maximum

value reported in literature for small-pore substrates. Overall, CO_2 is a good solvent for silylations on silica surfaces.

The second project was to synthesize polymer/polymer nanocomposites using a CO_2-assisted templating method. Semicrystalline polymers are composed of tens-of-nanometer thick crystalline lamellae and an amorphous matrix. CO_2 normally swells only the amorphous and interlamellar regions. The goal of this research was to selectively bring monomers to the amorphous and interlamellar regions with the help of CO_2. In situ polymerization and precipitation fixes the structure, replicating the nano-structure of the semicrystalline polymer substrate. Ring-opening metathesis polymerization was performed inside of CO_2-swollen poly(4-methyl-1-pentene) (PMP) of high crystallinity. Several polymer/polymer nanocomposites were successfully produced using this method. They were characterized by a variety of techniques, such as transmission electron microscopy (TEM), differential scanning calorimetry (DSC), thermal gravimetric analysis (TGA) and wide angle X-ray diffraction (WAXD). Infrared studies and TEM indicated that one type of composite, polynorbornene/PMP, had a gradient distribution of polynorbornene inside of the PMP matrix. Another composite, polyoctenamer/PMP prepared by cis-cyclooctene polymerization, exhibited very interesting mechanical properties. The poly(dicyclopentadiene)/PMP composites are unique nanometer-scale blends of a highly crosslinked thermoset with a thermoplastic polymer.

TABLE OF CONTENTS

LIST OF TABLES

Table Page

LIST OF FIGURES

Figure Page

CHAPTER 1

OVERVIEW

Carbon dioxide, in both subcritical (liquid) and supercritical states, has attracted much interest, mainly because it is nontoxic, nonflammable, inexpensive, and recyclable, while at the same time, because of its low critical point (T_c = 31.1 °C, P_c = 72.8 atm (1070 psi)), using it is fairly manageable. All CO_2 related research can be marked as "green" due to the obvious environmental consideration. Five to ten years ago, "to be environment-friendly" was the focus of CO_2 research. To reduce the usage of toxic materials and eliminate the waste handling process, people tried all means to replace organic or aqueous solvents with CO_2 for many traditional processes, such as extractions, homogeneous organic reactions, polymerizations, etc. It proved a big success in academia. On the other hand, the high cost of handling high-pressure CO_2 hinders major industrial applications. Recently, more and more CO_2 papers have appeared in "hot" areas, such as surface and interface modifications, drug delivery, bioactive materials, photolithography, and nanocrystal growth. With "green" still in consideration, many researchers are also taking advantage of CO_2's other properties, for example, tunable solubility, high diffusivity, low surface tension, no costly solvent removal step. Besides the scientific curiosity, one important reason is that, by producing high value-added products, the high cost of using CO_2 may be offset. The work presented in this thesis follows the trend. One section deals with monolayers, and the other focuses on nanocomposites.

A monolayer, by name, means a single molecular layer at a surface or interface. The importance of monolayers can never be over-estimated because it provides a highly controlled organic surface, which sets the foundation for studies of wettability, adhesion, adsorption, surface reactions, surface patterning, biocompatibility, etc. Monolayers can be either covalently attached, like polymer "brushes" and alkyl chains attached onto hydrogen-terminated silicon by radical reactions, or self-assembled through non-covalent interactions, for example, alkylthiolates on gold surface and trichlorosilanes absorbed onto silica. In work described in Chapter 2, the industrially important reaction, silylation, was performed in both liquid and supercritical CO_2. Different mono-functional organosilanes reacted with silica surfaces, forming covalently attached monolayers. These monolayers were well characterized using contact angle measurements, X-ray photoelectron spectroscopy, and ellipsometry. Reaction kinetics was established, and the comparison with reactions in conventional solvents (like toluene) was made. The reaction rate in CO_2 is higher than that in conventional solvents while the final coverage is slightly lower than the optimized conditions for conventional solvents. The study was also extended to multi-functional silanes, looking into the formation of self-assembled monolayers (SAMs) in CO_2. Both single surfaces (silicon wafers) and nanoporous silica gel surfaces were evaluated. Because of CO_2's low surface tension and high diffusivity, the surface silylation of nanoporous silica gel in CO_2 showed a bonding density almost as high as the maximum value reported in the literature for small-pore substrates. Portions of the work described in this chapter were presented at the 1999 New Orleans ACS meeting,[1] and later published in *Langmuir*.[2]

The second project concerns nanocomposites. This project appears like an extension of the previous research done by Watkins and Kung in the McCarthy group. However, new concepts were incorporated and new methods were used.

There are numerous ways to synthesize nanometer-scale materials. One general method is templating, taking available nano-materials as templates to make new nanostrucures. Single-phase nano-objects, like nanotubes or gold colloids, are perfect nanotemplates by themselves. For multi-phase substrates, two criteria are needed to qualify as nanotemplates. First, at lease one phase should have one or more dimensions in the range of 1 nanometer to 100 nanometer. Second, material should be able to enter different phases selectively. Semicrystalline polymers are composed of tens of nanometer thick crystalline lamellae and an amorphous matrix, which fulfills the first requirement. At the same time, CO_2 can selectively bring small molecules into the amorphous phase rather than crystalline phase. It is quite obvious that the combination of semi-crystalline polymers and CO_2 may prove to be a new way to produce nanocomposites. The possibility and feasibility of synthesizing polymer/polymer nanocomposites using CO_2 was explored in this thesis by in situ polymerization of a second monomer inside of CO_2 swollen semi-crystalline polymers.

The first example is discussed in Chapter 3. A ring-opening metathesis polymerization (ROMP) catalyst, Grubbs' catalyst was first incorporated into poly(4-methyl-1-pentene) (PMP). Norbornene was then diffused into this catalyst-embedded substrate with the help of CO_2. Upon contact with the catalyst, norbornene polymerized and precipitated out inside of PMP substrate. The newly formed polynorbornene was only found in the amorphous and interlamellar regions of PMP, producing a novel

polynorbornene/PMP nanocomposites. The resulting composites were characterized by a variety of techniques. The nano-scale distribution of polynorbornene was easily detected by transmission electron microscopy (TEM). Differential scanning calorimetry (DSC) and thermal gravimetric analysis (TGA) were used to look at the thermal behaviors. Wide angle X-ray diffraction (WAXD) monitored the changes in crystallinity. It is possible that these composites have gradient structure due to the monomer diffusion gradient. TEM, scanning electron microscopy (SEM) and Infrared-microscopy proved that it indeed is the case. A hypothesis on the origin of this gradient structure was finalized in Chapter 4 with the work of using other monomers. The effect of various reaction conditions on the final composition and structure was studied systematically. This work was presented in 2000 San Francisco ACS meeting,[3] and will be published soon.

The second example (Chapter 4) is related to the first one, with an emphasis on the relationship between structure and mechanical properties. While the Grubbs' catalyst was still the catalyst of choice, monomers used for this work were cyclooctene and dicyclopentadiene. ROMP of cyclooctene gives polyoctenamer, a diene elastomer with a Tg of about -100 °C, while poly(dicyclopentadiene) is a highly-crosslinked thermoset. Thus, rubber/PMP and thermoset/PMP composites were obtained, respectively. These non-classical polymer blends showed phase separation on the order of tens of nanometer because both polyoctenamer and poly(dicyclopentadiene) only exist in the amorphous and interlamellar regions of PMP. As it was relatively difficult to control the concentration of poly(dicyclopentadiene), most of the studies were on polyoctenamer/PMP nanocomposites. By varying the composition using experimental

parameter control, a series of composites with different polyoctenamer concentrations and different structures were formed, and these composites showed different mechanical properties. TEM, SEM and WAXD were again used together with the mechanical measurements to reveal the fracture mechanics. Structure and property relationship in the nanometer range was established. Upon success in making these nanocomposites, further structure manipulations, like annealing, foaming, swelling, and extraction, were performed. Part of this work was presented in 2001 San Diego ACS meeting.[4] A formal paper is in preparation.

CHAPTER 2

REACTIONS OF ORGANOSILANES WITH OXIDIZED SILICON SURFACES IN CARBON DIOXIDE

2.1 Background

2.1.1 Silylations

Chemical modification of silica surfaces using silane agents has a wide range of applications. It is well known that, for glass fiber-reinforced polymer composites, the fiber surface has to be treated with silanes to improve interfacial adhesion.[5] Silanes with alkyl or fluoroalkyl side chains can help to construct low-energy hydrophobic surfaces.[6-12] The silica stationary phase in normal chromatography is hydrophilic due to the large amount of silanols on the surface. Polar molecules and polar groups on biomolecules interact strongly with the surface of silica gel. Hydrophobizing the stationary phase with silanes is the essential step towards reversed-phase chromatography for separation of biomolecules.[13-16] Surface silylations also find applications in many research frontiers, like making biocompatible surfaces,[17-20] and forming monolayers for lithography, micropatterning, and sensors.[21-25] This chemistry is also the basis for much fundamental research on controlled surfaces.[26-31] The general silylation on silica surfaces is illustrated below.

Equation 2.1:

$$Si_{solid} - OH + R(Me)_{3-n} SiX_n = Si_{solid} - O - SiR(Me)_{3-n} X_{n-1} + HX$$

Here, R can be methyl groups, long alkyl chains, perfluoroalkyl chains, and other end-functionalized long chains. X designates the leaving functional groups, such as -Cl, $-N(Me)_2$, -OR, and -OH. Monofunctional silanes (n=1) give covalently-attached monolayers on the surface, while trifunctional silanes (n=3) can form both self-assembled monolayers (SAMs) and multilayers, depending on conditions.[32,33] Chlorosilanes are the most important, and have been studied thoroughly. For chlorosilanes, the reaction shown above normally will not happen directly without water or catalysts at low temperature. Direct reactions occur only in gas phase (>300 °C).[34] At ambient temperature, water is usually required to first hydrolyze the chlorosilanes to silanols before the condensation onto surfaces can proceed.[24,35]

There are two major methods to carry out these modifications: vapor-phase reaction and reaction in solution (water or organic solvents). The latter is of more importance and must be used for silanes having low vapor pressures. As society raises concerns about environmental problems, research on reducing the use of volatile organic compounds and reducing the generation of aqueous waste has become increasingly important. Given the huge number of silane applications in industry and the huge amount of organic and aqueous waste generated, the effect of finding an alternative solvent or processing should not be underestimated.

2.1.2 Supercritical CO_2

Figure 2.1 is the phase diagram of a pure matter. Above certain temperature and pressure (defined as critical point), it reaches supercritical state. In this supercritical region, the boundary of liquid and gas disappears. Supercritical fluids (SCFs), the

matter in the supercritical state, generally have gas-like diffusivity and can have liquid-like density. They have no surface tension and very low viscosity. The solvent strength of supercritical fluids is tunable because the density of SCFs can change dramatically by temperature and pressure adjustment. Some books and review articles are available for the general behavior and specific applications of supercritical fluids.[36-38]

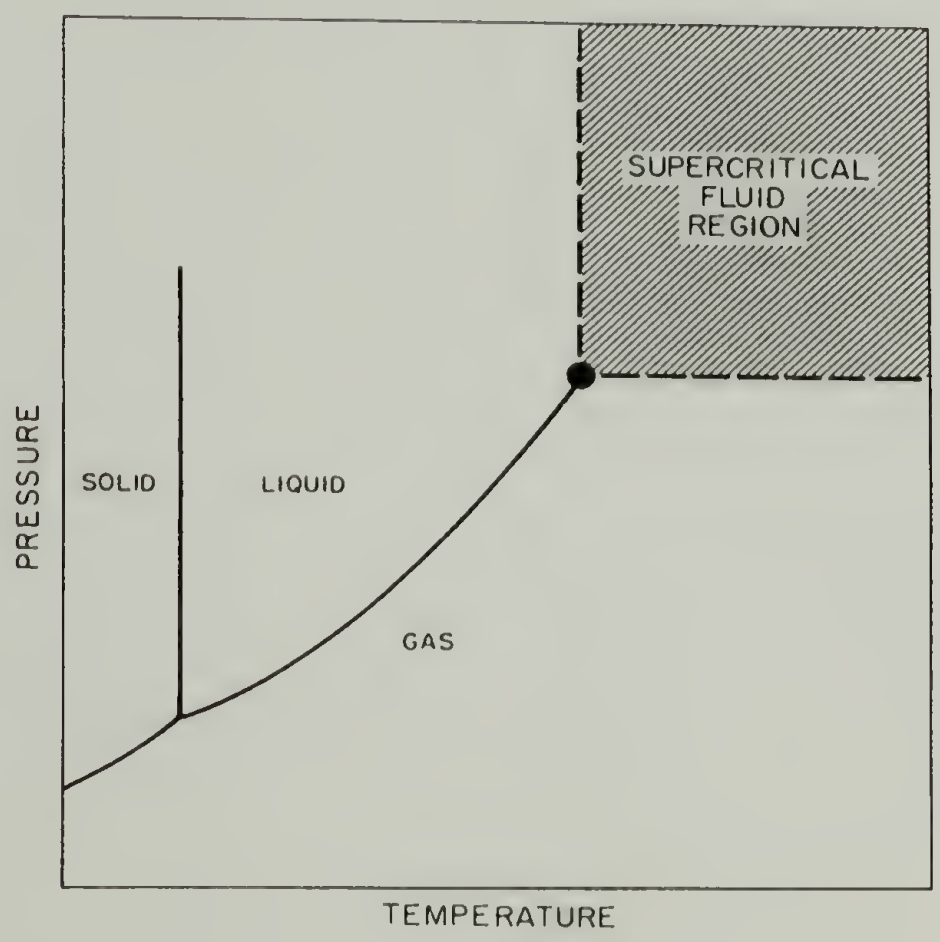

Figure 2.1: Phase diagram of a pure matter.[32]

Carbon dioxide has a fairly low critical point of 31.1 °C and 72.8 atm (1070 psi). The supercritical state is easily achievable under relatively mild conditions, making CO_2 an attractive candidate for both fundamental studies and industrial applications of supercritical fluids. Plus, CO_2 is both nontoxic and nonflammable. It is abundant and inexpensive. Though it is a major target of greenhouse gases to blame for the global

warming, CO_2 can be easily recycled because it is in the gas phase at ambient conditions. No solvent residue is left behind after releasing CO_2 as a gas, which efficiently reduces the time and cost of solvent separation and drying. Just like most supercritical fluids, supercritical CO_2 has very high self-diffusivity, relatively low viscosity, and zero surface tension. A comparison of some physical properties among liquids, gases and supercritical fluids is listed in Table 2.1.[39] Even for liquid CO_2 at room temperature, the self-diffusivity is $10^{-3} - 10^{-4}$ cm^2/sec, an order of magnitude higher than the diffusivity of solutes in normal liquids.[36]

Table 2.1: Physical property comparison for liquids, gases, and supercritical fluids.[34]

	diffusivity (cm^2/sec)	viscosity (cps)	density (g/ml)	surface tension (dyn/cm)
Liquid	10^{-5}	1	1.0	20-50
Supercritical Fluid	10^{-3}	0.03	0.2-1.0	0
Gas	10^{-1}	10^{-5}	10^{-3}	-

The solvent strength of CO_2 is similar to typical non-polar solvents. It can dissolve many small organic molecules to a certain extent. At the same time, most strongly polar molecules and high molecular weight molecules are not soluble in CO_2. However, by adding co-solvents or surfactants, the solubility of other molecules in CO_2 can be greatly enhanced. Another unique way of manipulating solvent properties of supercritical CO_2 takes advantage of the tunable solvent strength of supercritical fluids. Figure 2.2 shows the dependence of CO_2 density on pressure and temperature.[40,41] Just by external control of temperature and pressure, the CO_2 density can have dramatic changes, making it possible to selectively dissolve or precipitate certain types of molecules or fractions during various processing periods.

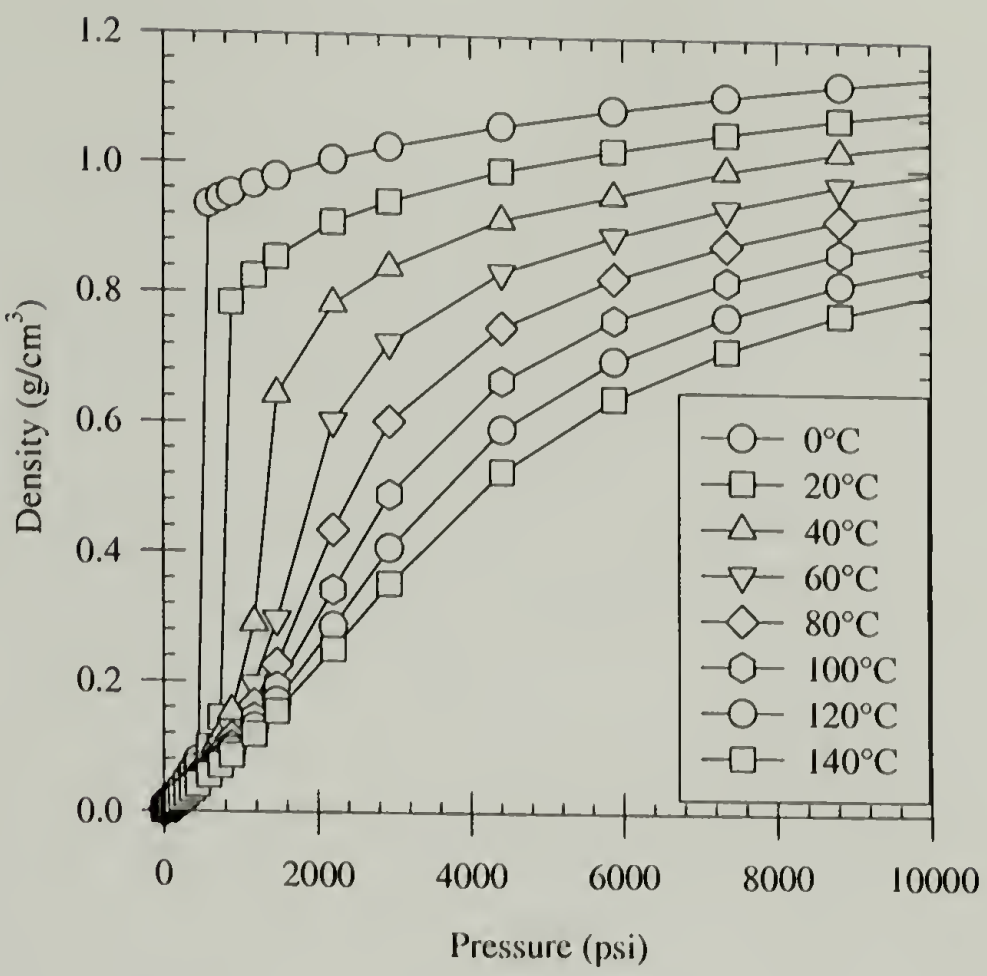

Figure 2.2: Density of CO_2 as a function of pressure at different temperature.[36]

2.1.3 Silica and supercritical CO_2

The combination of silica and supercritical fluids is not a new concept. Supercritical drying plays an important role in aerogel synthesis.[42] During the sol-gel process, the very fine open structure of the wet gel will collapse upon drying due to the powerful capillary force on the cell walls by solvent evaporation and shrinking. To make the extremely light aerogels, the drying process is carried out in the supercritical region of the solvents, normally alcohols.[43,44] As the critical points of alcohols are usually very high, exchanging the original solvent with supercritical CO_2 after the sol-gel step lowers the processing temperature and pressure, but with extra steps. It has also been shown in the literature[45] that aerogels can be formed directly in supercritical CO_2

by a modified sol-gel procedure to avoid water. Drying using supercritical CO_2 gives hydrophilic surfaces while supercritical methanol makes the surface hydrophobic.

Silylation of silica surfaces in supercritical CO_2 was pioneered by researchers at Xerox.[46] The main task there was to find a new solvent-based procedure to modify the surface of toner additives, such as fumed silica, metal, and metal oxide, all within a 5 to 500 nm particle size range. Gas phase treatment with volatile organosilanes usually does a good job. However, when the chosen organosilanes have low vapor pressures, and gas phase reactions are not possible, silylation in conventional solvents has a series of problems. Using supercritical CO_2, instead, eliminates the use of toxic and/or flammable solvents, removes the solvent separation step, reduces the reaction time, and avoids the serious "caking" problem — agglomerations of oxide powders due to traditional solvent process.

Besides inventing a novel industrial procedure, Tripp and co-workers[47,48] continued research on the interaction of supercritical CO_2 with fumed silica using infrared spectroscopy and also demonstrated that hexamethyldisilazane reacts with and n-octadecyltrichlorosilane physisorbs to surfaces that had been extracted (dried) with CO_2. These researchers point out several issues concerning the silica-CO_2 system that need to be considered in silylation chemistry. CO_2 weakly physisorbs to silica with an interaction strength similar to that of carbon tetrachloride. Carbon dioxide extracts the adsorbed water from the silica surface, which sets it apart from conventional solvents. Generally, water adsorbs to silica from organic solvents. Water is required to convert chlorosilanes to silanols, which in turn condense with surface silanols. Aminosilanes do not require water to react but have the disadvantages that they are not as available as the

chlorosilanes and that the amine product can react with CO_2 to form carbamates that can compete for adsorption sites.

2.2 Research introduction

The ultimate goal of this work is to investigate silylations on silica surfaces using organosilanes in carbon dioxide. Dr. Fadeev (previously in our group) has prepared a large number of covalently attached monolayers on single surfaces (polished silicon wafers) using monofunctional silanes ($ClSiR_3$)[8] and compared these monolayers with those prepared from di- and trifunctional silanes (Cl_2SiR_2, Cl_3SiR).[33] Conditions were optimized for both solution and vapor reactions. In the work reported here, monolayers prepared using CO_2 as a solvent were compared with those prepared in organic solvents and in vapor phase under optimized conditions. Unlike the anhydrous conditions used by Tripp et al.,[48] hydrated (undried) silica surfaces were used and no pre-extraction of the adsorbed water layer by CO_2 was performed before silylation (the water may dissolve during reaction but remains in the reaction vessel). Monofunctional silanes were the main silylation agents because of the simple reaction mechanism while di- and tri functional silanes were also tested later to extend the research scope, and to have a look at the self-assembly of tricholorosilanes. There were in total two monofunctional dimethylaminosilanes, six monofunctional chlorosilanes, two dichlorosilanes, and three trichlorosilanes used. Surface modification of nanoporous silica gel in CO_2 is of significant interest and was studied to a certain depth, while

silicon wafer single surfaces were the substrates used in most studies because of the abundant characterization tools for monolayers on flat surfaces.

2.3 Experimental section

2.3.1 Materials

Polished silicon wafers with a native oxide layer were obtained from International Wafer Service (<100> orientation, P/B doped, resistivity from 20.0 to 40.0 Ωcm). Two nanoporous silica gels, SG-300 with 300 Å pore size and ~160 m^2/g specific surface area and SG-60 with 60 Å pore size and ~500 m^2/g specific surface area, were obtained from Supelco, Inc. These silica surfaces all contain about 4.5 to 5 silanols per square nm.[49] All amino, and chlorosilanes (see Table 2.2) were obtained from Gelest and used as received. Ethanol, methanol, 2-propanol, dichloromethane (HPLC grade), sulfuric acid, and hydrogen peroxide were obtained from Fisher and used as received. Ethyldiisopropylamine (EDIPA) and anhydrous toluene were obtained from Aldrich and used as received. Hexadecane was obtained from Aldrich and vacuum-distilled prior to use. Carbon dioxide (Coleman grade 99.99%, Merriam Graves) was passed through activated alumina and Q-5 catalyst (Englehard Industries) to remove water and oxygen, respectively. An Isco 100DM high-pressure syringe pump fitted with a heating/cooling jacket was used to deliver CO_2 at the required pressure and

Table 2.2: Silanes used in the research.

Aminosilanes:

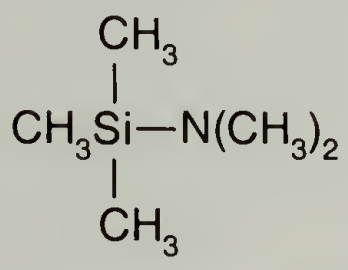

(dimethylamino)tri-methylsilane (DTMS)

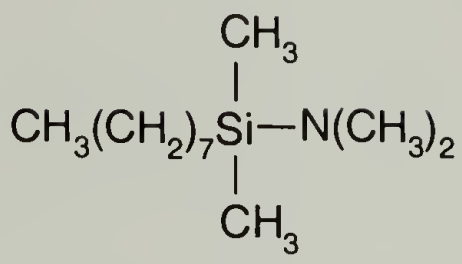

(dimethylamino)-n-octyl-dimethylsilane (DODS)

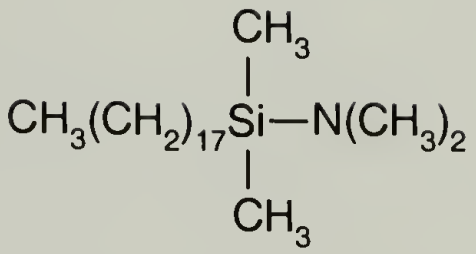

(dimethylamino)-n-octadecyl-dimethylsilane (DODDS)

Monochlorosilanes:

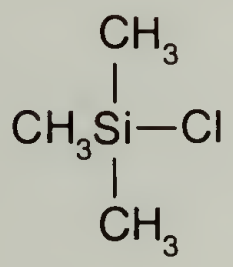

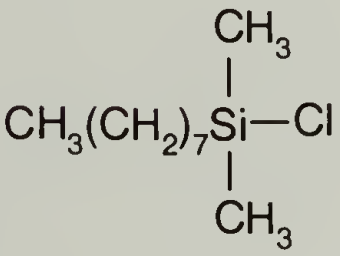

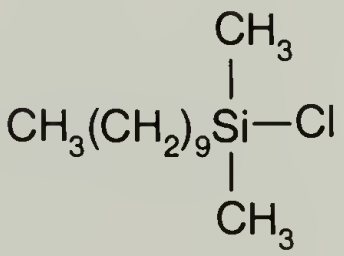

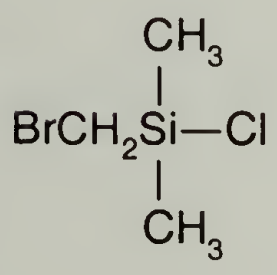

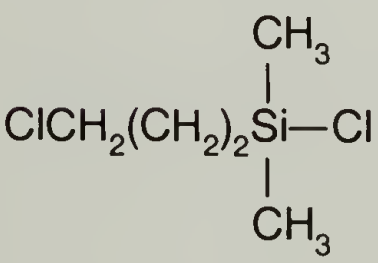

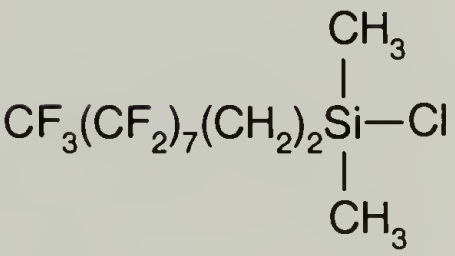

Dichlorosilanes:

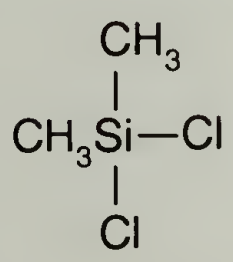

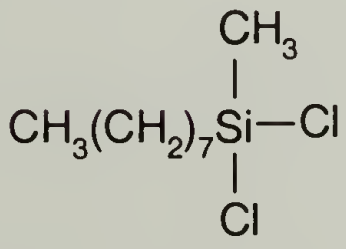

Trichlorosilanes:

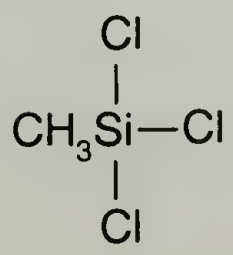

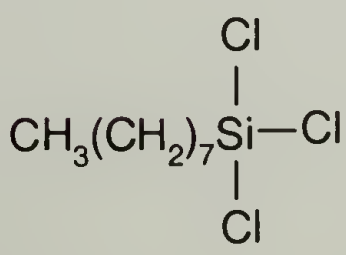

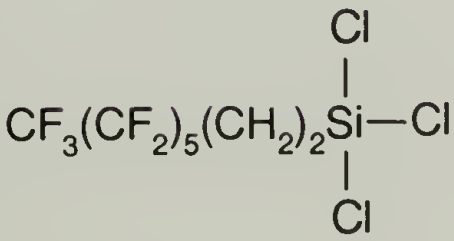

temperature. Water with resistivity of 18.2 MΩcm was obtained by further purifying the house RO water using a Millipore Milli-Q water system including reverse osmosis, ion-exchange and filtration steps.

2.3.2 High-pressure reaction setup

By submerging clean wafers into pre-prepared silane solutions, silylation in conventional solvents is simple and straightforward. However, performing the same

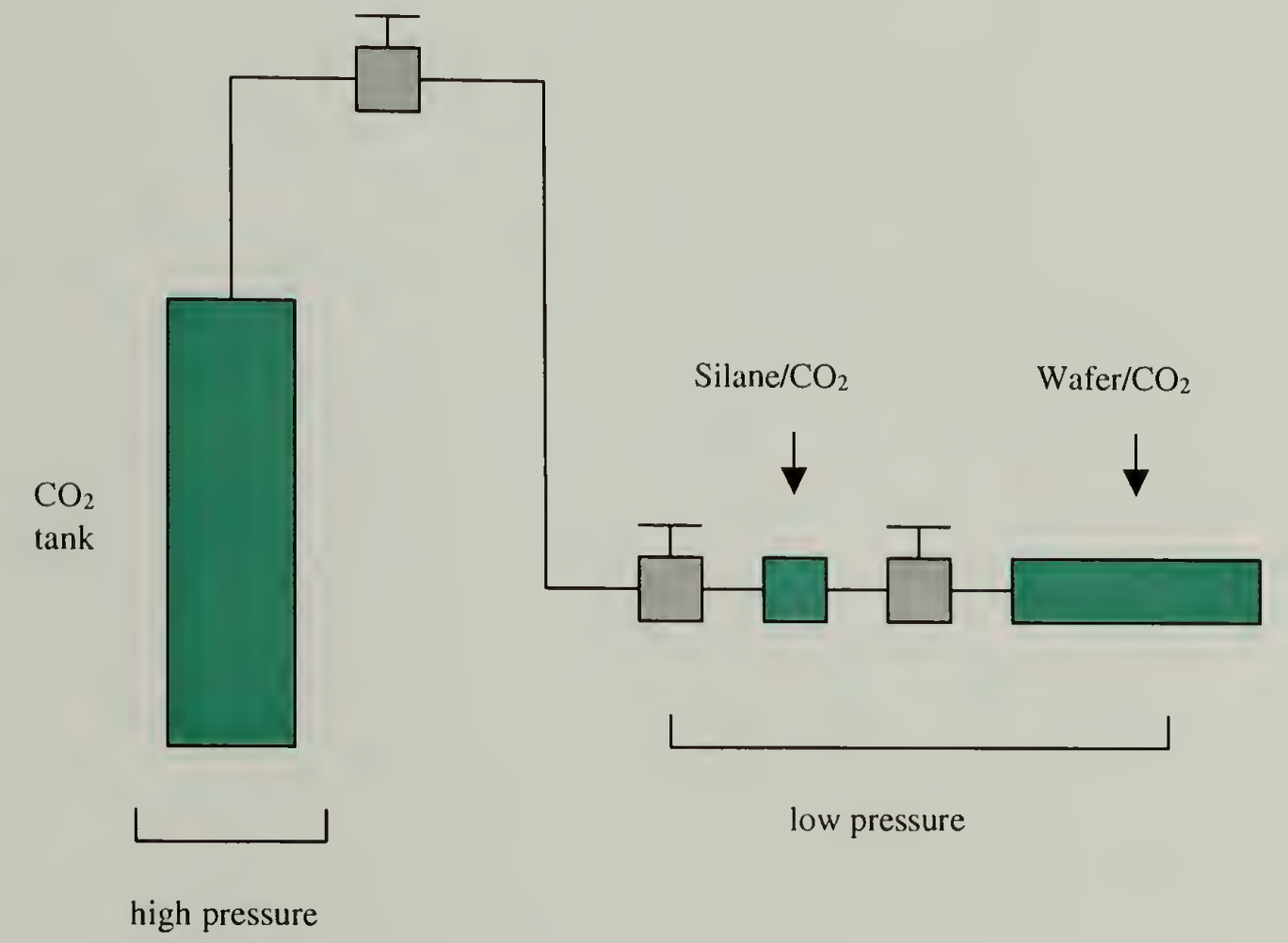

Figure 2.3: Schematic high-pressure silylation setup.

reaction in stainless steel vessels sealed for holding pressure is non-trivial. It is difficult to transfer wafers into the sealed vessel. If the silane and wafers are put together in the vessel prior to CO_2 filling, the data will be misleading due to quick vapor phase

reactions occurring before infusion of CO_2. To solve the problem, an extra small high-pressure vessel was used, and a pressure gradient transferred the silane/CO_2 solution into the wafer/CO_2 vessel, as illustrated in Figure 2.3.

2.3.3 Experimental procedures

2.3.3.1 Preparation of silica substrates

Silicon wafers (100 mm diameter) were cut into 1.5 cm x 1.5 cm samples. Each sample was placed in a 20 mL scintillation vial and covered with a freshly prepared solution of sulfuric acid and 30% aqueous hydrogen peroxide (v/v = 70/30). After ten hours, the acidic solution was decanted, and the wafers were immediately covered with Milli-Q water. The water was decanted after 30 seconds. This washing process was repeated seven times. The wafers were stored under Milli-Q water in the same vial and used within 2-3 days. Beyond this time, they were recleaned to avoid contamination buildup. Wafers cleaned using this procedure exhibited advancing contact angles lower than 10° and 0° receding contact angles. Porous silica gels were heated at 120 °C in a clean oven for 24 hours prior to modification.

2.3.3.2 Silylation of single surfaces in CO_2

The cleaned silicon wafers were removed from Milli-Q water, dried with a stream of nitrogen for 20 seconds, and placed in a nitrogen-purged 8.5 mL stainless steel high-pressure vessel. This drying procedure leaves a thin layer of water adsorbed on the silicon wafer surface. The vessel was then filled through a needle valve with ~5.0 g of CO_2 at room temperature (23 °C, 950 psi, ρ~0.6 g/cm^3). A second stainless steel vessel (0.35 mL) containing ~1 mmol silane was connected to the reaction vessel through a

valve. This vessel was filled with CO_2 (23 °C, 950 psi) and was connected by another needle valve to a syringe pump set at 1200 psi CO_2 at 23 °C. By opening both valves at the same time, the CO_2 pressure gradient pushed the silane from the smaller vessel into the reaction vessel. The valve to the syringe pump was closed leaving a solution of ~1 mmol silanes and 6.5-6.9 g CO_2 in an ~8.9 mL reactor. After the desired reaction time, the silane/CO_2 solution was vented into ethanol. The wafers were removed, and rinsed with methylene chloride, acetone, and methanol sequentially. The wafers were then submerged in a methanol solution for two hours. Finally, the silicon wafers were dried under a stream of nitrogen for 30 seconds. Contact angle measurements were taken immediately.

2.3.3.3 Silylation of nanoporous silica in CO_2

Silica gel (~0.5 g) and a 3-5 times molar excess (based on surface silanols) of (dimethylamino)octadecyldimethylsilane (DODDS) were introduced into a 8.5 mL stainless steel high-pressure vessel. CO_2 was introduced at room temperature (23 °C, 3000 psi, $\rho \approx 0.75$ g/cm^3). The vessel was then heated to the desired temperature and kept for the desired period of time. The vessel was allowed to cool and the CO_2 was vented. The modified silica was washed on a porous glass filter sequentially with toluene (20ml × 2), isopropanol (20ml × 2), ethanol (20ml × 2), ethanol/water (20ml × 2), and ethanol (20ml × 2), and was dried in an oven at 100 °C for 10 hours.

2.3.3.4 Silylation of porous silica in toluene

Silica gel was added to toluene followed by a 3-5 times molar excess (based on surface silanols) of DODDS. The silane concentration in toluene was the same as that in CO_2. The mixture was stirred and heated at the desired temperature for the desired

period of time. The toluene solution was decanted and the modified silica samples were washed as described above.

2.3.4 Characterization techniques

The monolayers formed on silicon wafers can be analyzed using classical surface techniques, such as wettability, ellipsometry and X-ray photoelectron spectroscopy. The monolayers formed on the surface of nanoporous silica gel can be characterized by IR and carbon elemental analysis.

2.3.4.1 Wettability

Contact angle measurement is the simplest, and still powerful, surface characterization tool. It is governed by the following Young's equation:

Equation 2.2:

$$\gamma_{lv}\cos\theta = \gamma_{sv} - \gamma_{sl}$$

γ_{lv}, γ_{sv} and γ_{sl} are the interfacial tensions for the liquid/vapor, solid/vapor, and solid/liquid interfaces, respectively. Contact angle is in close connection with surface tension, and very sensitive to chemical and topolographical changes in the film's top skin layer of a few angstroms thick. For mixed or incomplete monolayers, the Israelachvili-Gee equation[50] proves to be fairly accurate. f_1 and θ_1 are the surface

Equation 2.3:

$$(1+\cos\theta)^2 = f_1(1+\cos\theta_1)^2 + f_2(1+\cos\theta_2)^2$$
$$f_1 + f_2 = 1$$

coverage and contact angle, respectively, for the first component, and f_2 and θ_2 are for the second component.

In this study, contact angle measurements were made with a Ramé-Hart telescopic goniometer and a Gilmont syringe with a 24-gauge flat-tipped needle. The probe fluid used was water, purified as described above. Dynamic advancing (θ_A) and receding (θ_R) angles were recorded while the probe fluid was added to and withdrawn from the drop, respectively. The values reported are averages of 5-10 measurements made on different areas of the sample surface. The modified surfaces exhibited very homogeneous surfaces as evidenced by contact angle and all measurements for all surfaces were within ± 2° of the averages.

2.3.4.2 Ellipsometry

Ellipsometry is a simple technique for measurement of thin film thickness and refractive index. The sample thickness can be measured from a few angstroms to microns. Understanding detailed theory involves some physics and geometry, which is beyond the coverage of this research. Interested readers are referred to some nicely written books.[51] Only general concept will be mentioned here. When an incident light strikes an interface, some of the light will be reflected while some other will be refracted. If the incident light is linearly-polarized, the outcoming reflected light will be elliptically-polarized due to the refractive indices of substrates and the thickness of the film. So the elliptically-polarized light coming from the interface contains information on thickness and refractive index. In practice, a NULL type ellipsometer has the following component setup. A monochromatic (632.8 nm) linearly-polarized collimated laser is the beam source. The incident angle is chosen (normally 75 °). The laser passes

a depolarizer first, becoming circularly-polarized. Then an adjustable polarizer makes it linearly-polarized again. A quarter-wave compensator changes it to an elliptically-polarized state before it strikes the interface. After striking the interface, the laser can be either linearly-polarized or elliptically-polarized, depending upon film properties like refractive index and thickness. For each sample, it is possible to get a linearly-polarized light by adjusting the position of the polarizer. Then a NULL condition (maximum extinction) is easily achieved by rotating the analyzer and detected by a photomultiplier. To get good measurements, there are some requirements: 1) sharp interface; 2) small roughness; 3) transparent film; 4) relatively large surface cross-section (millimeter size).

A Rudolph Research AutoEL-II automatic ellipsometer was used in this research. The light source was a He-Ne laser (λ = 632.8 nm), the incident angle was 70.0° (from the normal), and the compensator was set at -45°. By assuming a two-layer model (monolayer/silicon oxide on the silicon substrate), the thickness was calculated using "dafIBM" software. For extremely thin films (less than 50 Å thick), the refractive index of monolayers has to be known in order to calculate the thickness.[51,52] According to a literature report,[53] the value of 1.45 was estimated for the refractive index for hydrocarbon monolayers, and a value of 1.35 was used for the refractive index of perfluorohydrocarbons.[54] The thickness of the silicon oxide layer (~22 Å) on top of silicon wafers was measured for each sample prior to modification. At least five measurements were made, and average results are reported.

2.3.4.3 X-ray photoelectron spectroscopy

The working theory of XPS is relatively simple. When X-ray radiation strikes the surface, the inner-shell electrons of atoms on the surface will absorb the photon's

energy following quantum rules. If they have enough energy to overcome the binding energy, they escape from the surface. These electrons are called photoelectrons. The kinetic energy of a photoelectron equals the difference between the photon energy absorbed by the electron and the binding of that electron, as shown in the following equation:

Equation 2.4:

$$E_k = h\gamma - E_b$$

Each inner-shell electron has its own characteristic binding energy. Knowing binding energy allows identification of the element. That is why XPS is also known as electron spectroscopy for chemical analysis (ESCA). The binding energy of inner-shell electrons is also sensitive to the electronic environment of the atom. The small "chemical shift" of the binding energy gives information about chemical structures. After the ejection of a photoelectron, the excited atom can relax by one of two mechanisms. To fill the hole created by the photoelectron, an electron from an outer shell can come down, and release certain amount of energy equal to the energy difference of the two orbitals. This energy can be emitted as X-ray radiation, or it can be given to another electron in an outer shell and let it escape from surface. Such a electron is called an Auger electron. The kinetic energy of Auger electrons is also characteristic of the elemental composition.

The sampling depth of XPS can be better understood by a little detailed discussion.[55] Except for those photoelectrons right on the surface, most of the photoelectrons emitted from atoms have to travel a certain distance before escaping

from the surface. During the travel, they can experience elastic and inelastic interactions. Inelastic scattering will decrease the kinetic energy of photoelectrons, and hence reduce their chances of escaping from surface. No-loss emission is limited to only a few atomic layers below the surface, which makes the XPS technique surface sensitive. The intensity of the photoelectrons that suffer no loss in kinetic energy after traveling a distance z is assumed to follow an exponential decay law:

Equation 2.5:

$$I(z) = I^{i} \exp\left(\frac{-z}{\lambda_a(E_k)\sin\theta} \right)$$

I^i is the initial photoelectron intensity generated at a given point in the sample. θ is the takeoff angle measured between the surface and the direction of emitted photoelectrons to the analyzer. z is the normal distance from the given point to surface. $\lambda_a(E_k)$ is the attenuation length of the photoelectron with kinetic energy E_k. There are four distances to be defined. The inelastic mean free path is defined to be the average distance (in nanometers) that an electron having a given energy travels between successive inelastic collisions. The attenuation length is the average distance (in nm) that an electron having a given energy travels between successive inelastic collisions as derived from a particular model in which elastic electron scattering is assumed to be insignificant. The measured attenuation length is shorter than the inelastic mean free path because of the neglect of elastic scattering. The escape depth is the distance (in nm) normal to the surface at which the probability of an electron escaping without significant energy loss due to inelastic scattering process drops to 1/e (36.8%) of its original value. It is equal

to $\lambda_a \sin\theta$. Thus, small takeoff angles give more surface sensitive results. Depth profiling can be obtained by gradually changing θ in an experiment. Finally, the sampling depth is the distance (in nm) normal to the surface from which a specific percentage of the detected electrons originate. Usually this specific percentage is 95% of the observed signal, which sets the sampling depth equal to three times the escape depth ($3\lambda_a \sin\theta$).

In this study, X-ray photoelectron spectra (XPS) were obtained using a Physical Electronics 5100 spectrometer with a Mg K_α X-ray source (15 kV, 400 W) at pressures less than 10^{-8} Torr. Spectra were acquired at both 15° and 75° takeoff angles (between the wafer surface and the entrance lens of the detector optics). Samples were rinsed with ethanol and vacuum-dried for at least 4 hours at 10 mTorr before being introduced to the XPS spectrometer. Given a calculated attenuation length for C_{1s} electrons of 2.6 nm with a M_g K_α source,[55] the typical sampling depths for 15° and 75° takeoff angles are 2.0 nm and 7.5 nm, respectively.

2.3.4.4 Elemental analysis

All the surface characterization techniques mentioned above require flat surfaces. For small particles and porous materials, Infrared and elemental analysis are two typical techniques used in the literature. The IR technique takes experience and we will skip that because elemental analysis itself provides enough information.

The amount of monolayers on flat silicon wafers is too small to be detected. However, when the specific surface area is on the order of hundreds of square meters per gram, like the porous silica gels we used, it becomes significant, and can be easily detected by classic elemental analysis. Different elements have different detection

methods. In this case, carbon analysis was performed with a 240XA Elemental Analyzer made by Exeter Analytical of North Chelmsford, MA, using the classical modified Pregl technique. A 3-5 mg sample was weighted to the nearest μg and combusted in an oxygen atmosphere at 1000 °C. The resulting CO_2 was detected and quantified after the instrument was standardized with NIST micro-analytical grade acetanilide. Carbon appears only in the monolayers, not in the silica gel. A complete burning process transforms all carbon atoms in the monolayer to carbon dioxide gas molecules, the amount of which can be quantitatively measured. Thus, the weight percentage in the sample can be calculated. The relationship between carbon content and silane bonding density is shown in the following equation:

Equation 2.6:

$$\rho(group/nm^2) = \frac{N_A \times 10^{-18} \times \%C}{1200 \times n_c - \%C \times F_w} \times \frac{1}{S}$$

ρ: bonding density;
%C: carbon percentage from chemical analysis;
N_A: Avogadro constant;
n_c: number of carbons in the silane molecule;
F_w: corrected formula weight of silanes;
S: specific surface area of porous silica.

2.4 Results and discussions

2.4.1 Solvent state

Carbon dioxide has a critical point of 31.1 °C and 1070 psi (73.8 bar). To determine whether the state of CO_2 (liquid or supercritical) has an effect on the reaction, a first series of reactions both in the supercritical state (above 31.1 °C and 1070 psi) and

subcritical state (liquid CO_2 at room temperature) were conducted. Water contact angle data for silicon samples reacted with (dimethylamino)trimethylsilane (DTMS) and (dimethylamino)*n*-octyldimethylsilane (DODS) for 24 hours are shown in Table 2.3.

Table 2.3: Water contact angles of trialkylsilane monolayers prepared in liquid and supercritical carbon dioxide.[a]

silane	Reaction temperature(°C)	Reaction pressure(psi)	Contact angles θ_A(°)	θ_R(°)
DTMS[b]	23	1200	91	81
DTMS	40	2200	96	84
DTMS	78	4400	96	85
DTMS	100	6000	94	84
DODS[c]	23	1200	103	90
DODS	40	2200	103	90

[a]Reactions were carried out for 24 hours; CO_2 density ~0.77 g/mL.

[b](dimethylamino)trimethylsilane. [c](dimethylamino)*n*-octyldimethylsilane.

The data indicate that, for surfaces prepared with DTMS, contact angles (and bonding density) increase when the temperature is raised from 23 to 40 °C, but that there is no further increase at higher temperatures. DODS-derived surfaces showed no difference between liquid and supercritical CO_2. The contact angles of the DODS-derived monolayers are rather insensitive to bonding density differences at high coverage because the *n*-octyl groups shield surface silanols from the probe fluid. The differences in yield (bonding density) between reactions of DTMS above and below the critical temperature was reproducible and could be attributed to several causes including reaction rate, diffusivity and structure of the monolayer as a function of temperature, but there is no intention to speculate regarding this. A general comment will be made

concerning the complexity of this reaction in the next paragraph. Using the Israelachvili-Gee equation[50] (Equation 2.3) and the values of 108° for trimethylsilyl[8] and 0° for silanol, it is calculated (using advancing contact angle values) that the surface prepared at 23 °C contains 86% trimethylsilyl and 14% silanol groups and the surface prepared at 40 °C contains 90% trimethylsilyl and 10% silanol groups. They are thus not very different.

A comment is made here regarding "complete" trialkylsilyl monolayers. The McCarthy group has reported[8,56] detailed studies of trialkylsilyl monolayers that indicate that "complete" monolayers (of the same silane) can differ in bonding density and that this depends on the reaction conditions. The silanes react with the surface by random covalent reaction with silanols. Silica contains[49] 4.5-5 silanols per nm^2 and the maximum bonding density of trialkylsilyl groups[57-60] is 2.6-2.8 groups/nm^2, thus there are residual silanols present on all modified surfaces. This differs significantly from close-packed self-assembled monolayers that contain about 4.5-5 groups/nm^2.[11,61-63] As the random covalent attachment reaction occurs, "sub-nanopores"[56] between groups are formed and the reaction is complete when the sub-nanopores are all smaller than the cross section of the silane reagent. It has been shown[56] that binary mixed monolayers can be prepared by subsequent reaction with smaller silane reagents. The size of the sub-nanopores and thus the distance between groups (and bonding density) depends on reaction conditions. There are surface silanols in these sub-nanopores and whether or not water as a probe fluid can interact with the silanols depends on the nanopore size. Complete monolayers prepared in toluene at 60-70 °C, in toluene at room temperature, and in the vapor phase at 60-70 °C exhibit water contact angles of θ_A/θ_R = 105°/91°,

105°/96° and 108°/96°, respectively[8]. Apparently, the sub-nanopores in the monolayer prepared in the vapor phase are smaller than those in the monolayer prepared at room temperature, which are smaller than those in the monolayer prepared in solution at elevated temperature.

2.4.2 Reaction kinetics

Standard reaction conditions of 23 °C and 1200 psi (liquid CO_2 with a density of ~0.77 g/mL) were chosen for subsequent experiments on single surface silicon samples. The data in Table 2.3 indicate that it is likely that denser silane monolayers can be formed in supercritical carbon dioxide. The data for the DODS-derived monolayers indicate that surfaces of identical wettability are formed in liquid and supercritical CO_2. XPS atomic concentration data of the trimethylsilyl and *n*-octyldimethylsilyl monolayers prepared at 23 °C and 1200 psi (24-hour reaction) are shown in Table 2.4.

Table 2.4: XPS atomic concentrations for trialkylsilyl monolayers prepared in liquid carbon dioxide.[a]

Silanes	Si		O		C	
	15°	75°	15°	75°	15°	75°
DTMS[b]	32.2	51.1	39.9	37.7	27.9	11.1
DODS[c]	22.8	50.0	19.4	27.0	57.8	23.0

[a]Reactions were carried out at 23 °C and 1200 psi for 24 hours.

[b](dimethylamino)trimethylsilane. [c](dimethylamino)*n*-octyldimethylsilane.

Nitrogen was not detected in the XPS spectrum indicating that dimethylamine-derived products did not adsorb or were completely removed in the post-reaction rinsing procedure. The severe take-off angle dependence of the carbon and silicon concentrations indicates that the monolayers, as expected, are very thin.

The kinetics of the reactions of DTMS and DODS with silicon wafers in liquid CO_2 was followed by water contact angle measurement; the data are plotted in Figure 2.4 and Figure 2.5. The data points for different reaction periods come from

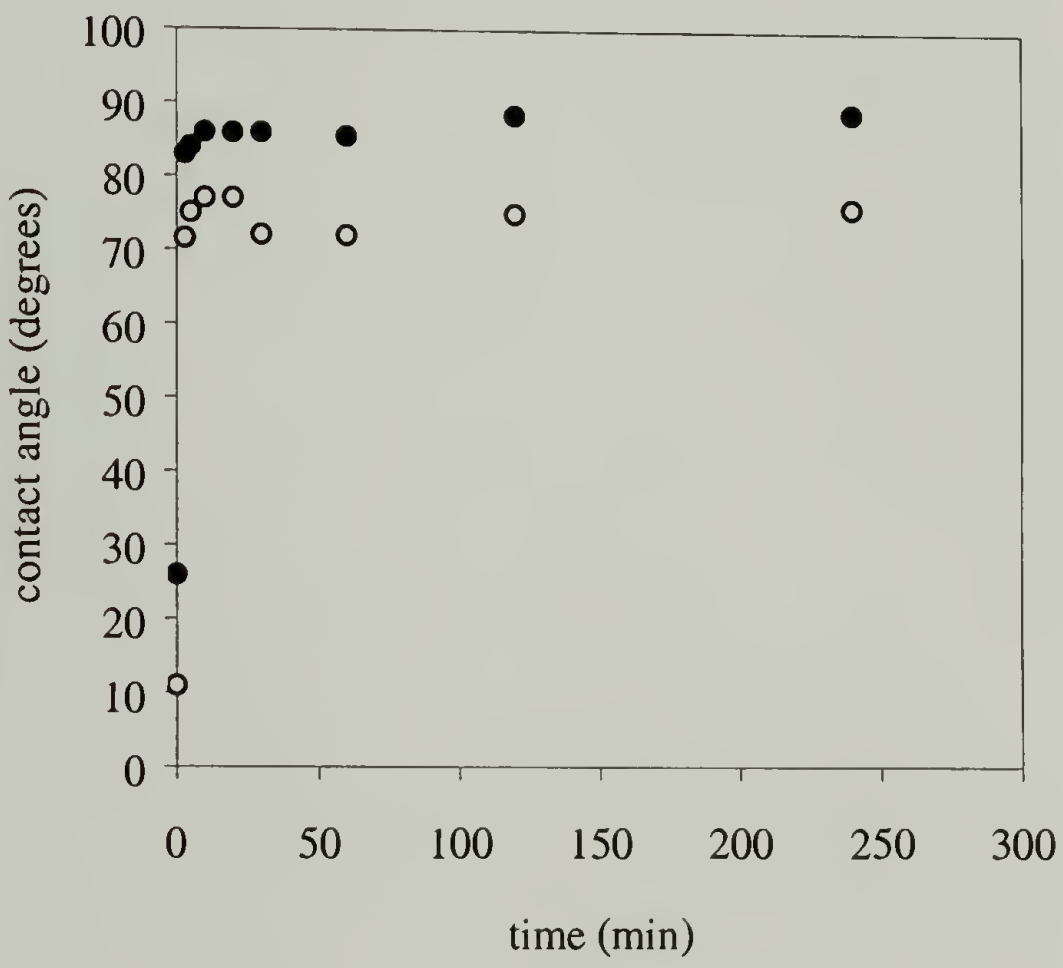

Figure 2.4: Rate of formation of trimethylsilyl monolayer prepared from DTMS in liquid CO_2. (23 °C, 1200 psi); θ_A - ●, θ_R - ○.

measurements on different samples. The initial stages of the reactions are extremely fast. Significant hydrophobization occurs rapidly, with θ_A/θ_R changing from 7°/0°

(initial silica surface) to 83°/72° for the DTMS-derived surface and to 92°/78° for the DODS-derived surface in three minutes of reaction. The reaction of DTMS in CO_2 is

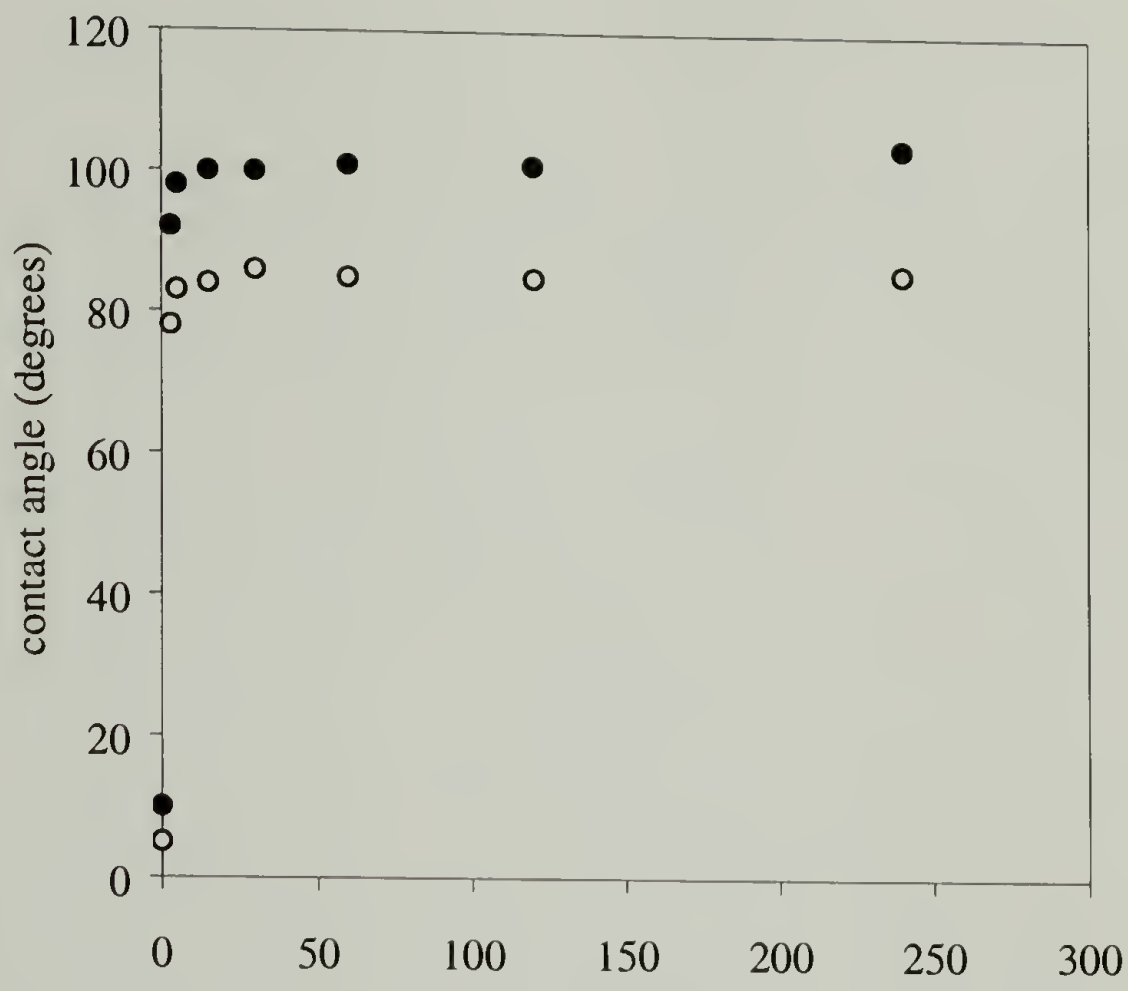

Figure 2.5: Rate of formation of n-octyldimethylsilyl monolayer prepared from DODS in liquid CO_2. (23 °C, 1200 psi); θ_A - ●, θ_R - ○.

faster than the corresponding reaction in toluene.[8] (In toluene, water contact angles are 80°/35° after 6 minutes of reaction at room temperature.) After the initial stage, the reactions slow considerably and contact angles increase very slowly over days. This sluggish late stage of reaction is not peculiar to carbon dioxide and is observed with toluene as the solvent as well. The low rate is due not only to the low concentration of accessible silanols, but also to the fact that the attached groups have to adopt conformations that expose unreacted surface silanols. For the reaction with DTMS, the contact angles are 89°/76° after 4 hours, 91°/81° after 1 day and 96°/85° after 5 days.

Using the Israelachvili-Gee equation [50](Equation 2.3), we calculate that water as a probe fluid senses trimethylsilyl and silanol groups in ratios of 78:22, 84:16, 86:14 and 90:10 after 3 minutes, 4 hours, 1 day and 5 days, respectively. Data for DTMS-derived surfaces prepared in toluene and in the vapor phase were discussed previously in the "solvent state" section. For the reaction with DODS, the contact angles are 104°/86° after 4 hours, 103°/90° after 1 day and 106°/88° after 5 days. Contact angles for the DODS-derived surfaces prepared in liquid CO_2 are comparable to those prepared in toluene at 60-70 °C θ_A/θ_R = 103/91°) and in toluene at room temperature (θ_A/θ_R = 106°/93°).[8] Water as a probe fluid does not sense silanols on any of these DODS-derived surfaces. The ellipsometric thickness values for DTMS- and DODS-derived monolayers (24-hour reaction) are 2 ± 2 Å and 6 ± 2 Å, respectively. The DODS value is considerably lower than that of fully stretched *n*-octyl chains observed in self-assembled monolayers prepared from the trichlorosilane.[53] This is consistent with data reported[33,54] for monofunctional silanes. The monolayers are disordered or loosely packed due to the lower bonding density and absence of strong lateral interactions.

An interesting contact angle behavior is observed in the early stages of the DTMS reaction (Figure 2.4). The receding contact angle increases over the first 10 min of reaction, levels (θ_R = 77° after 10 and 20 min of reaction) and then decreases (θ_R = 72° after 30 min of reaction). The contact angle hysteresis (θ_A - θ_R) also reaches a minimum value at 10-20 minutes of reaction. This decrease in θ_R and increase in hysteresis is explained as follows: At the intermediate bonding density achieved after 10-20 minutes of reaction, the trimethylsilyl groups are free to rotate and project a smooth, liquid-like surface, giving rise to low hysteresis. As bonding density increases

further, the trimethylsilyl groups impinge upon one another, becoming more crowded and less free to rotate and they project a rigid and rough surface to the probe fluid, contributing to high hysteresis. This behavior was observed as well for trimethylsilyl surfaces prepared in toluene.[8] For DODS in Figure 2.5, there is no similar decrease of hysteresis in the early stage, due to the long, flexible n-octyl groups of DODS.

2.4.3 Other silanes

As discussed above, aminosilanes do not require water or a catalyst to react with silica surfaces and this was the reason we chose DTMS and DODS for our initial experiments. Chlorosilanes are more readily available, but require water or amine catalysis to react with silica at moderate temperatures. It is found, however, that silicon wafers, prepared as described in the Experimental Section, react readily with chlorosilanes in CO_2 without amine catalysis. In fact, monolayers prepared with ethyldiisopropylamine(EDIPA) present (in slight excess over the molar equivalents of Si-Cl bonds) were of poorer quality than those prepared with only the chlorosilanes. This may be due to interactions between the amine or the amine hydrochloride product and silica. A range of mono-, di- and trichlorosilanes was studied and the surface analysis results are summarized in Table 2.5. Each of the modified surfaces described was prepared by reaction for 24 hours at 23 °C and 1200 psi (CO_2 density ~0.77g/mL) with ~0.1 M silane.

The monolayers prepared are of good quality and exhibit contact angles that are similar to those of surfaces prepared in toluene under optimized conditions.[8] Apparently there is a sufficient amount of water adsorbed to the silicon wafer to

hydrolyze enough chlorosilanes to prepare complete monolayers (the CO_2 is rigorously dried). Tripp et. al.[47] has shown that CO_2 may dissolve water from the surface under these conditions (their work was at 50 °C). Whether the chlorosilanes hydrolyze at the surface or hydrolyze in solution prior to adsorption depends on the relative rates of adsorption and dissolution. These kinetics issues are not addressed as good monolayers form under these conditions in 24 hours. The Me_3SiCl-derived surface exhibits water

Table 2.5: Contact angle, ellipsometry, and XPS data for silicon-supported layers prepared from Chlorosilanes in liquid CO_2.[a]

	θ_A/θ_R	thickness	XPS atomic % (15°)			
silane	(degrees)	(Å)	Si	O	C	Other
Me_3SiCl	92/82	3	27.7	39.7	32.7	
$C_8H_{17}SiMe_2Cl$	96/86	7	22.3	29.5	48.2	
$C_{10}H_{21}SiMe_2Cl$	99/87	6	20.7	25.3	54.0	
Me_2SiCl_2	101/76	11	25.5	30.6	43.9	
$C_8H_{17}SiMeCl_2$	104/91	18	17.9	20.5	61.7	
$MeSiCl_3$	88/61	10	28.8	42.1	29.1	
$C_8H_{17}SiCl_3$	107/90	21	13.4	16.2	70.4	
$C_8F_{17}(CH_2)_2SiMe_2Cl$	105/91	5	17.3	18.7	32.1	32.0^F
$C_6F_{13}(CH_2)_2SiCl_3$	114/95	11	12.4	14.4	30.1	43.1^F
$BrCH_2SiMe_2Cl$	84/69	2	31.1	32.1	33.1	3.7^{Br}
$Cl(CH_2)_3SiMe_2Cl$	83/68	3	26.6	37.0	32.9	3.5^{Cl}

[a]Reactions were carried out at 23 °C and 1200 psi for 24 hours.

contact angles of $\theta_A/\theta_R = 92°/82°$ which are indistinguishable from those on surfaces prepared from DTMS under identical conditions ($\theta_A/\theta_R = 91°/81°$). The *n*-octyldimethylchlorosilane-derived surface exhibits contact angles of $\theta_A/\theta_R = 96°/86°$; these are lower than those observed on DODS-derived surfaces prepared under the same conditions (103°/90°). All of the monochlorosilane-derived monolayers exhibit contact angles that are slightly lower than those prepared in toluene.[8] The dialkyldichlorosilanes and alkyltrichlorosilanes, however, yield surfaces when reacted in CO_2 that exhibit similar or higher contact angles than those prepared in toluene with EDIPA catalysis at 70 °C. The surfaces prepared in CO_2 from $(CH_3)_2SiCl_2$, *n*-$C_8H_{17}(CH_3)SiCl_2$, CH_3SiCl_3 and *n*-$C_8H_{17}SiCl_3$ exhibit contact angles of θ_A/θ_R = 101°/76°, 104°/91°, 88°/61° and 107°/90°, respectively. Values for the surfaces prepared in toluene are 92°/85°, 103°/90°, 80°/66° and 103°/89°, respectively.[8] The ellipsometric thickness data for these surfaces (Table 2.5) indicate that they are not monolayers, but are oligomeric layers approximately three times as thick as monolayers prepared from the monochlorosilanes. This oligomerization indicates that more than sufficient water is present to form monolayers. We do not have data for surfaces prepared in toluene to compare with the halogen-containing layers (the last 4 entries in Table 2.5).

2.4.4 Reactions with nanoporous silica

Silylation reactions with porous silica are widely used to prepare stationary phases for column chromatography and reaction of aminosilanes in toluene at elevated temperatures is a standard method. We compared the bonding density of

(dimethylamino)*n*-octadecyldimethylsilane (DODDS) - modified silica samples that were prepared in toluene with samples that were prepared in CO_2 at 7200 psi. Both sets of reactions were carried out at 70 °C (supercritical CO_2) and the silane concentrations were the same. The silica, SG-60, contained 60Å diameter pores and a specific surface area of ~500 m^2/g. Figure 2.6 shows bonding density values that were determined from carbon content (microanalysis) as a function of reaction time. Indistinguishable differences in bonding densities were observed for samples prepared in CO_2 and toluene; it is clear that CO_2 is a viable reaction medium for this process. After 24 hours,

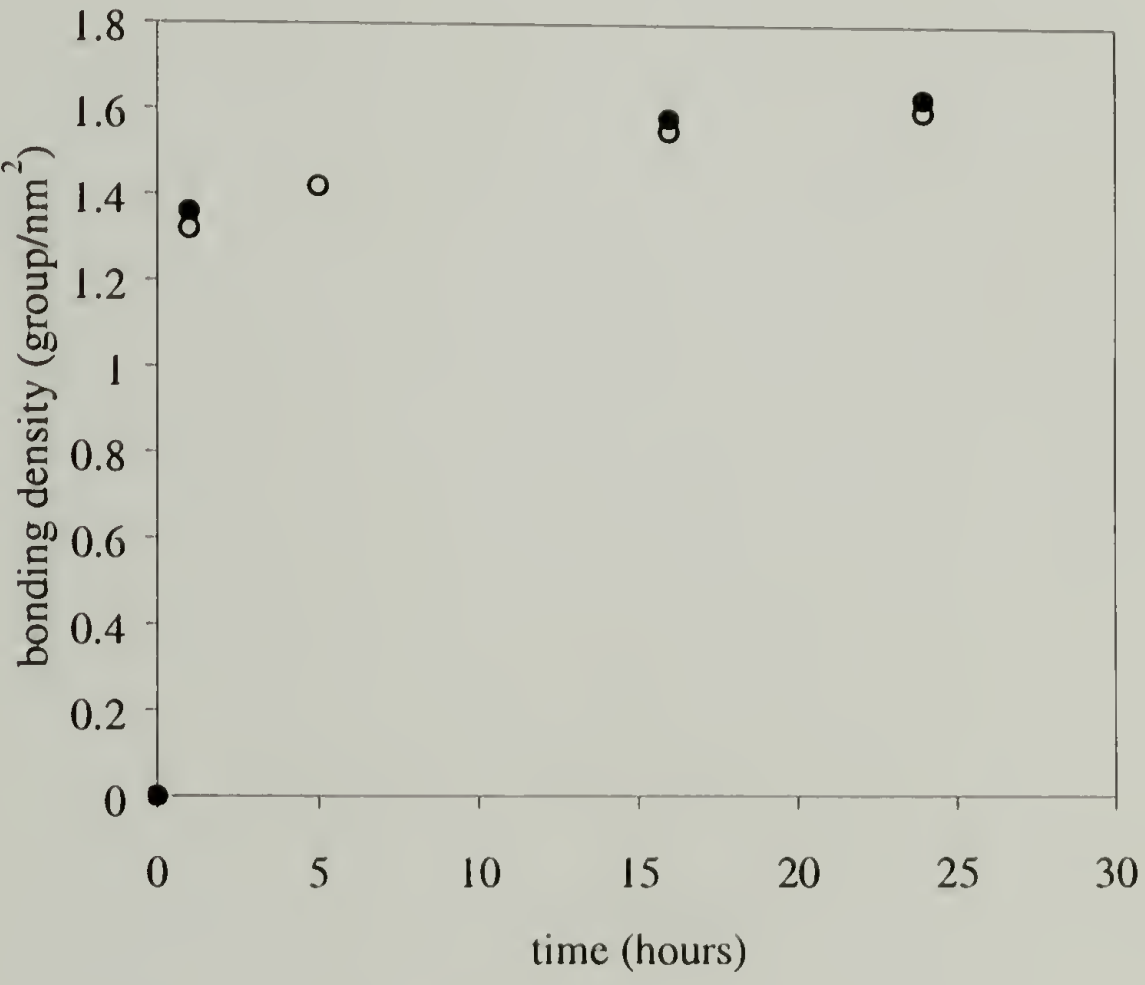

Figure 2.6 Comparison of bonding densities of n-octadecyldimethylsilyl groups as a function of reaction time. (Reactions of DODDS with SG-60 nanoporous silica were in toluene at 70 °C (●) and in CO_2 at 70 °C and 7200 psi.(○))

the bonding density reached as high as 1.6 silane groups/nm^2, which is typical of the maximum bonding density reported in the literature for small pore substrates.[57,59,60] The

reaction appears to be continuing after 24 h, so higher bonding densities can likely be achieved with longer reaction times, but the small pore diameter (which decreases even further upon reaction) makes it difficult for silane molecules to enter the pores, and the curvature of the surfaces of small pores results in a lower bonding density than the maximum value observed for the silica gel with larger pores. We also carried out silylations in CO_2 at 50 °C and 5400 psi using DODDS and two silica samples, SG-60 and SG-300 (that has 300 Å diameter pores).

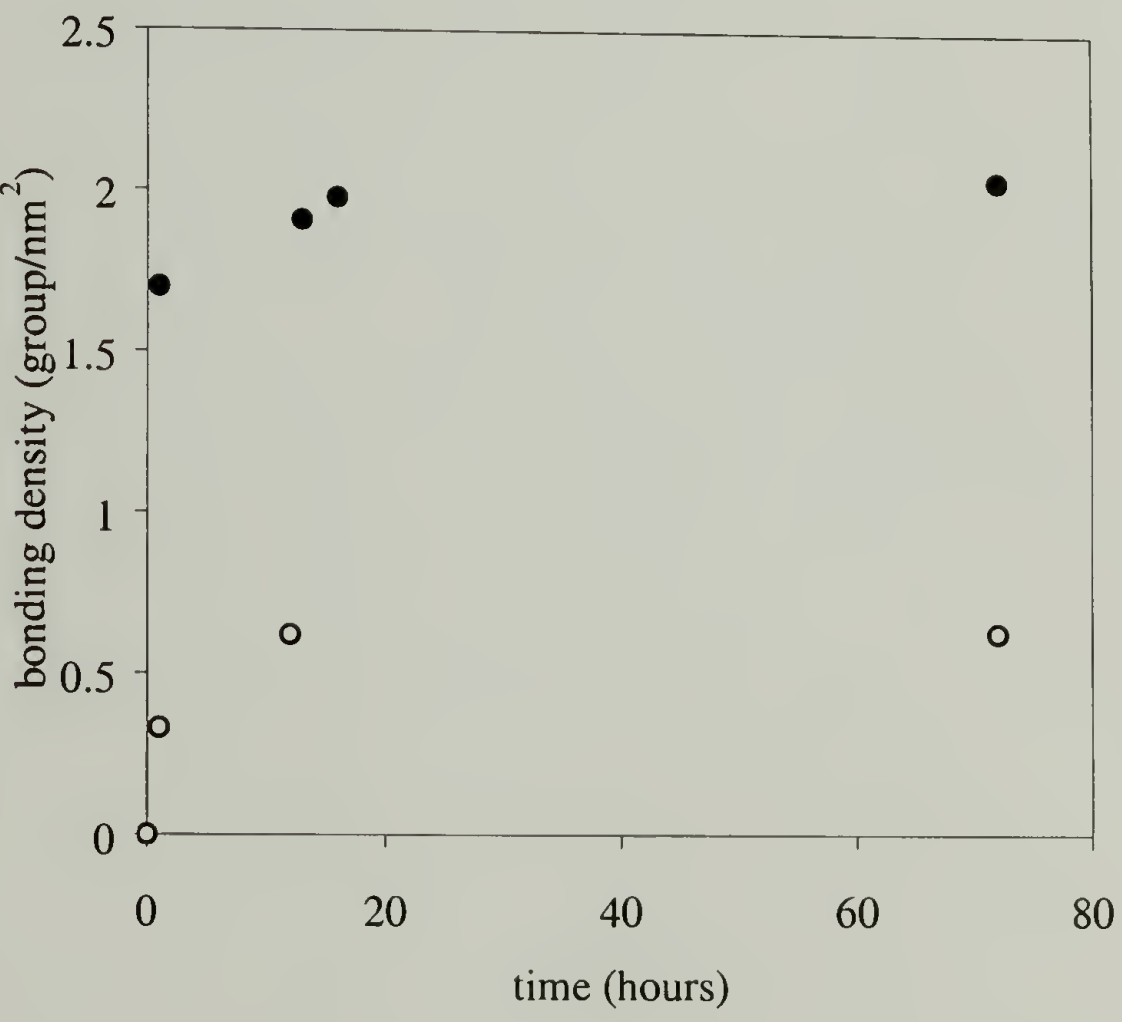

Figure 2.7: Comparison of bonding densities of n-octadecyldimethylsilyl groups as a function of reaction time for SG-60 (○) and SG-300 (●) nanoporous silica. (Reactions of DODDS were in CO_2 at 50 °C and 5400 psi.)

Figure 2.7 shows bonding density data for these modified silicas as a function of reaction time. Much lower bonding density was observed under these conditions than at

70° and 7200 psi for the SG-60 sample, but the bonding density in the silica with larger pores is significantly higher.

2.5 Conclusion

Liquid and supercritical carbon dioxide are viable reaction solvents for silylation reactions to form covalently attached monolayers to both single and porous silica surfaces. Reaction kinetics indicate that reactions with (dimethylamino)trialkylsilanes are rapid in the initial stages and very slow in the later stages. This is similar to what is observed in conventional solvents. Chlorosilanes also react readily with silicon wafers in the absense of amine catalysis and the reaction appears general. Monochlorosilanes yield monolayers; dichloro- and trichloro silanes yield oligomeric layers that are about three times as thick as the corresponding monolayers. By using silica surfaces that are not rigorously dried, a sufficient amount of water is introduced to the system to hydrolyze an excess number of chlorosilanes needed to form monolayers.

CHAPTER 3

SYNTHESIS AND CHARACTERIZATION OF POLYNORBORNENE/POLY(4-METHYL-1-PENTENE) NANOCOMPOSITES IN CARBON DIOXIDE

3.1 Background

3.1.1 Nanomaterials

The general definition of a nanomaterial is a material having at least one dimension in the nanometer range, usually 1 to 100 nm.[64] Materials with only one dimension in the nano range are nano-sheets. Nano-wires and nano-particles can be obtained when the number of dimensions in nanometer range increases. When a material is in the nanometer size range, phenomena associated with atomic and molecular interactions strongly influence its macroscopic properties. Most properties are unexpected, and often serve better for special interests than the traditional materials. As novel materials with special properties are becoming increasingly important to fulfill the society's need, "making things nano" has proved to be a great method to pursue. Another big driving force for nanotechnology is the information technology (IT) industry, where smaller patterning means the ability of constructing more transistors per unit area, which in turn gives faster information-transfer speed and higher information-storage capacity. Feynman, in his speech of "there is plenty of room at the bottom" during the American Physical Society annual meeting in 1959, first predicted the emergence of nanotechnology and its applications. The speech was published in 1960.[65] Forty years later, nanoscience and nanotechnology have become scientific fashions in almost all research areas. Some observers have begun to call nanotechnology the third

megatrend characterizing the US R&D enterprise in the past fifteen years, right after information technology and biotechnology, according to Mihail C. Roco, a senior advisor of the National Science Foundation.

Intuitively, there are two ways to make nano-objects: "cut" and "build", which are also referred to as "top-down" and "bottom-up", respectively. The "cut" approach means to reduce the dimensions of the material from macroscopic range to nanometer range, as in electron beam lithography,[66] and X-ray lithography.[67] The electronics industry largely relies on this approach (mainly photolithography) to make integrated circuits and micro-processing chips. It has been a great industrial success to make micrometer and sub-micrometer size features while getting down into the range of less than 100 nm is still a big hurdle along the road. On the other hand, there are many ways to "build", which is assembling atoms or small molecules with angstrom size into bigger structures. There are numerous methods in this approach. However, they are not industry-favored due to high cost or scale-up difficulties. Examples include dendrimer synthesis,[68] carbon nanotube synthesis,[69,70] and molecular self-assembling through secondary interactions.[71] Scanning Tunneling Microscope (STM) manipulation[72] and Atomic Force Microscope (AFM) tip modification[73,74] can belong to either one of the two categories, depending on the perspective.

3.1.2 Nanotemplating and semicrystalline polymers

Both "cut" and "build" approaches mentioned above are direct methods. However, not all nanomaterials can be synthesized directly. A common way to get around is taking an indirect route – "templating", using available nano-materials as

templates to synthesize new materials while preserving the original nano-structures during the process. The templates can be synthetically available materials, like di-block copolymers,[75,76] dendrimers,[77] and carbon nanotubes,[78] or natural materials, for example, clay,[79] colloidal silica,[80,81] and DNA.[82]

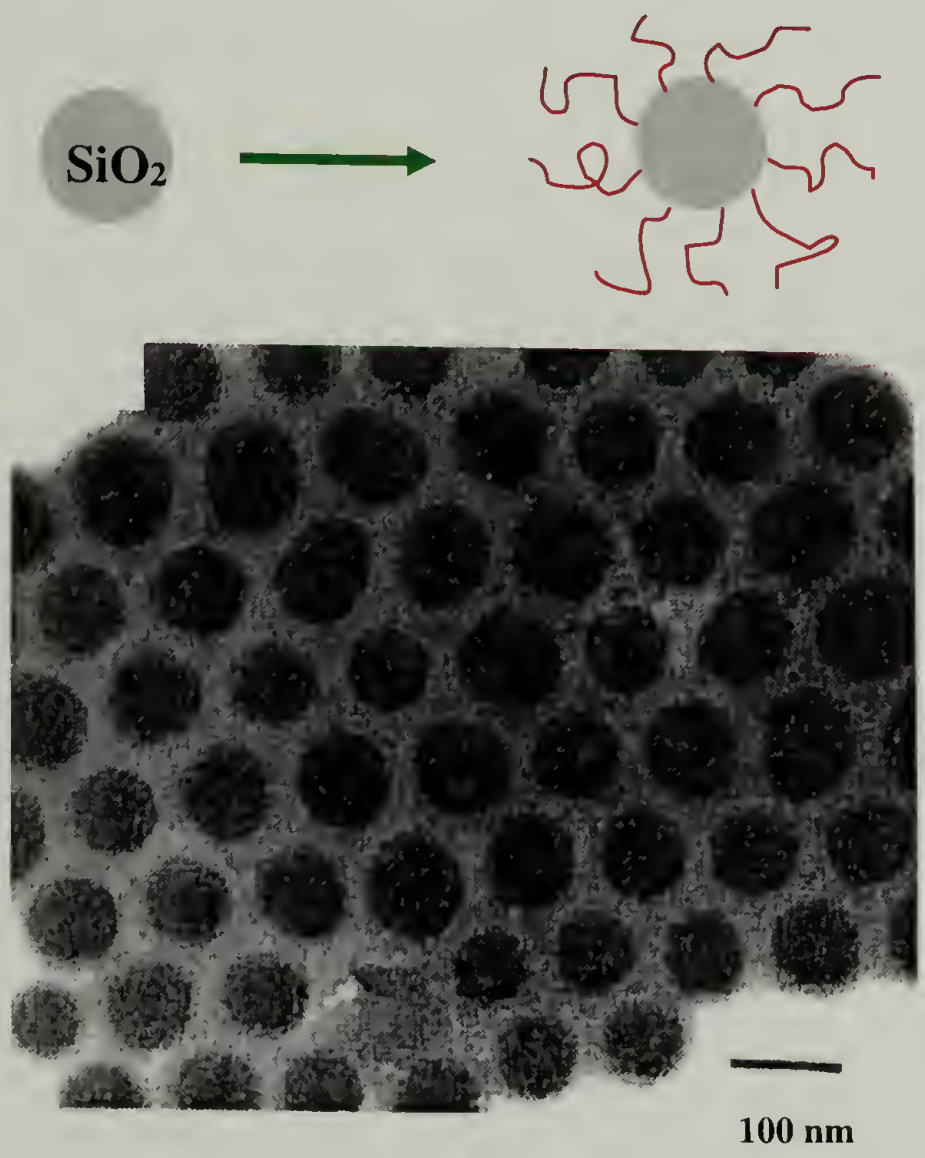

Figure 3.1: TEM micrograph of a hybrid of polystyrene/SiO_2 nanoparticles.[81]

Figure 3.1 is an example of using colloidal silica particles as a nanotemplate. The surface of silica particles is modified by silanes with a chloride end-functionality. Sequential Atom Transfer Radical Polymerization (ATRP) of styrene gives relatively uniform chain-length polystyrene growing from surface. After evaporating the solvent, a highly structure-ordered organic/inorganic hybrid is formed.

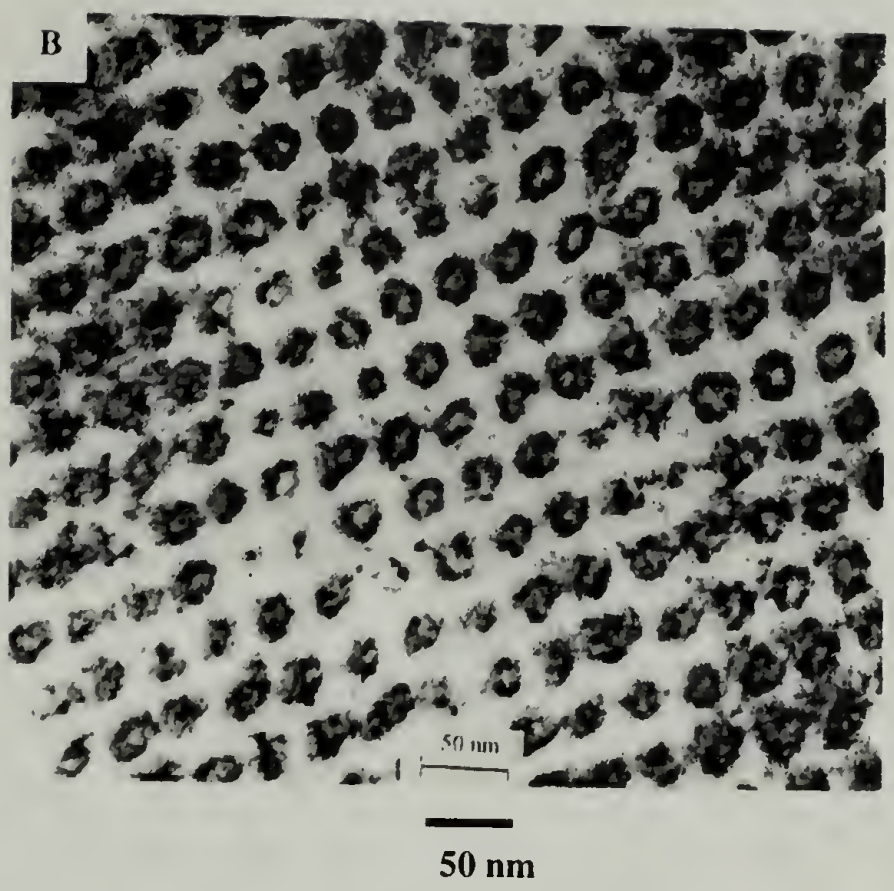

Figure 3.2: TEM micrograph of PAA nanochannels filled with CdS particles (end-on view)[83]

Fig 3.2 shows another example using diblock copolymers as a nanotemplate. Here poly(2-cinnamoylethyl methacrylate) (PCEMA) and poly(t-butyl acrylate) (PtBA) di-block copolymer is synthesized with PCEMA as a major phase. This diblock undergoes micro-phase separation to form PtBA cylinders inside of the PCEMA matrix. PtBA is hydrolyzed to poly(acrylic acid) (PAA), and CdS nanocrystals are synthesized inside of the PAA cylinders.

To get the new materials, the final step usually involves removal of the original template by dissolution or degradation. Nanocomposites are formed if the original templates are not removed after the templating process. Single-phase nano-objects, like carbon nanotubes or gold colloids, are perfect nanotemplates by themselves. For multi-phase substrates, two criteria are needed to qualify as nanotemplates. First, at lease one

phase should have one or more dimensions in the range of 1 nanometer to 100 nanometer. Second, material should be able to enter different phases selectively.

Because of the easy processibility, well-ordered nanostructures from micro-phase separation, and numerous synthetic methods, di-block copolymers have long been the favorite nanotemplates for many researchers. However, there is another family of nano-structured polymers almost forgotten by most people – semicrystalline polymers. Semicrystalline polymers contain both crystalline phase and amorphous phase. At low resolution of micrometer to millimeter scale, they show spherulitic structures; while in the tens of nanometer range, they are composed of layer-like crystallites (lamellae) separated by disordered regions.[84] In fact, Haward in 1970[85] already stated that polyolefins like polyethylene or polypropylene could be regarded as dispersions of crystals held together by rubber. Nowadays, using modern polymer physics language, It can be said that semicrystalline polymers are dispersions of tens-of-nanometer thick crystalline lamellae held together by amorphous phases. Although the thickness of crystalline lamellae is affected by process conditions, it is relatively uniform for the same sample. Thus, semicrystalline polymers can be a potentially cheap source for nano-templates, providing that molecules can be selectively deposited into one phase.

Figure 3.3: TEM micrograph of polycthylcne.[84]

3.1.3 Polymers and CO_2

The research on polymers using CO_2 has grown significantly in recent years. It has been moving from traditional areas like extraction[36] to polymer synthesis[86] and special processing, like foaming[87,88], Sol-Gel process[45] and particle formation.[89,90] Now it even covers frontier areas like photolithography,[91,92] bioactive polymers[93]and nanocomposites.[94] There are several excellent review articles and books available in this area.[36,38,95-98]

Several years ago, the McCarthy group developed a unique method to modify polymer substrates in the solid state.[94,99] It involves carrying out chemical reactions, including polymerizations, within CO_2-swollen polymer substrates. This method offers several advantages. (i) It is an environmentally safe procedure because carbon dioxide is nonflammable and nontoxic. (ii) Carbon dioxide, at both subcritical and supercritical states, has high diffusivity and low surface tension (supercritical CO_2 has zero surface

tension).[36] (iii) As CO_2 is a gas at ambient conditions, post-reaction procedure is simple and no costly solvent recovery is needed. (iv) Dense CO_2 can dissolve many small organic molecules[100] and swell most polymers,[101] making this approach a versatile tool to modify a wide range of polymers by a wide range of methods.

Beyond these obvious advantages, CO_2 has another unique property. For most semicrystalline polymer substrates, it only swells the amorphous phase, thus all reactions are confined to the amorphous region. This solves the problem of using semicrystalline polymers as nanotemplates. By selectively putting materials into the amorphous regions using CO_2, polymer-based nanocomposites should be easily synthesized using the templating method.

One major objective in the early research of making polymer/polymer composites in CO_2 is to reduce domain size of phase-separated polymer blends. To get enhanced properties, polymer composites can be prepared by blending different polymers together.[102] However, physical blending of immiscible polymers normally results in macro-phase separation, which dramatically impairs mechanical properties. A lot of research, including reactive blending[103,104] and addition of di-block copolymers,[105] has been done to reduce the domain size of separated phases. In our case, monomers are carried into polymer substrates by CO_2. As CO_2 normally swells only the amorphous region of semicrystalline polymers, subsequent polymerization occurs only in the amorphous regions. Large-scale phase separation is frustrated by the crystalline boundaries if polymerization occurs below the depressed melting temperature of that polymer substrate,[106,107] allowing a simple method to directly prepare small-scale phase separated blends. The majority of polymer composites that we studied were prepared

using free radical polymerization.[99,106,108] Solid polymer substrates were soaked in a supercritical CO_2 solution of monomer and radical initiator at a temperature that the initiator decomposed very slowly. Then the system was heated up to rapidly decompose the initiator, starting the polymerization.

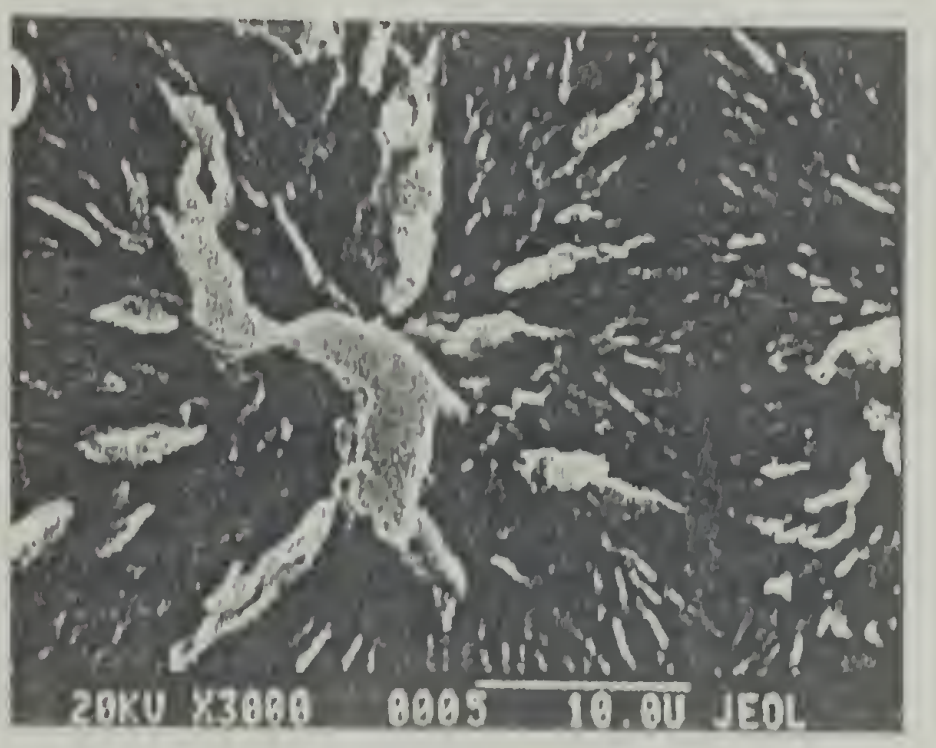

Figure 3.4: Secondary electron micrograph of a polystyrene/HDPE with 43 wt% of polystyrene.(etched in potassium permanganate/acid solution, polystyrene raised up.)[106]

Kung[106] used SEM to study the etched sample of polystyrene/high-density polyethylene (PS/HDPE) composites, and found out that polystyrene resided in the non-crystalline domains and permeated throughout the spherulitic structure of the HDPE substrates. The SEM micrograph of a typical sample is shown in Figure 3.4. However, he did not notice any separation from crystalline lamellae. Watkins[108] looked at polystyrene/poly(chlorotrifluoroethylene) (PS/PCTFE) by TEM, and did not specify if there is lamellae separated morphology. Arora polymerized styrene inside of CO_2-swollen poly(tetrafluoroethylene-co-hexafluoropropylene) (FEP)[109] as well as CO_2-

swollen poly(4-methyl-1-pentene) (PMP).[41] But the main focus there was to investigate composite foaming behavior. No transmission electron microscopic (TEM) study was reported. In fact, the first and also the only nanocomposites made by this method are platinum/poly(4-methyl-1-pentene) (Pt/PMP) and platinum / poly (tetrafluoroethylene) (Pt/PTFE).[94] Although TEM pictures of these nanocomposites (for example, Figure 3.5) show nanometer size metal clusters, there is no indication that metal is deposited in between crystalline lamellae.

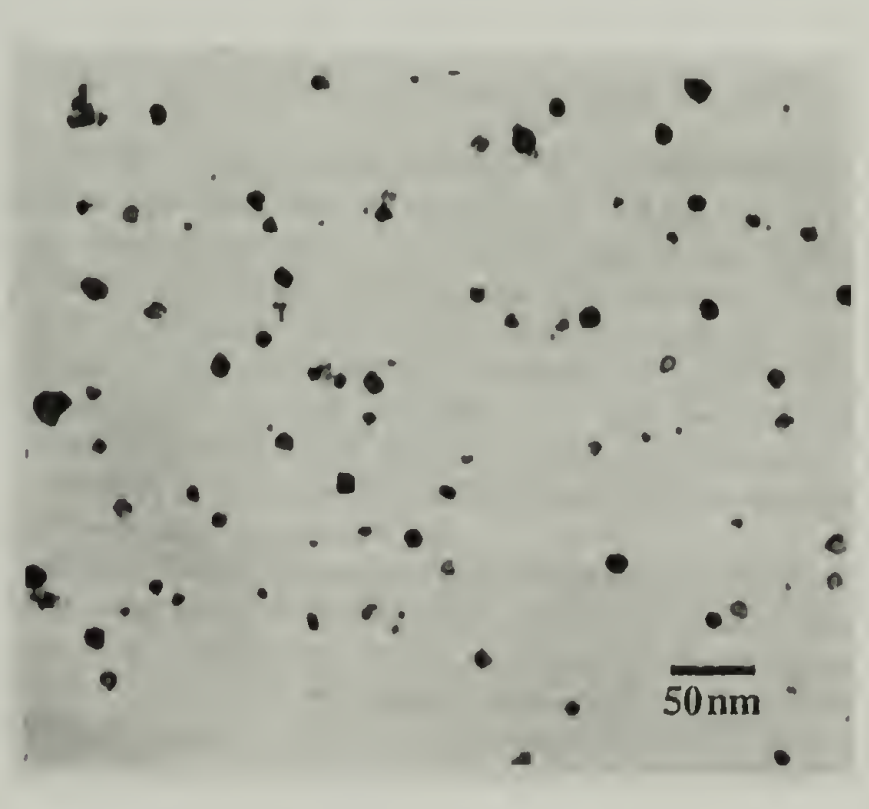

Figure 3.5: TEM image of Pt clusters in PMP using a CO_2 method.[94]

3.1.4 Interpenetrating polymer networks (IPNs)

When it comes to polymer blends, interpenetrating polymer networks (IPNs) have to be mentioned because of their unique structures and the resulting properties. Interpenetrating polymer networks, by definition,[110] are materials composed of two or more polymers in network form, with at least one such polymer synthesized and/or crosslinked in the immediate presence of the other(s). Interpenetrating polymer

networks belong to the broad polymer blend family. The final structure and morphology are mainly determined by thermodynamics, the free energy of mixing. However, due to the presence of crosslinking and also the synthetic procedure, the phase-separated domain size of IPNs is normally smaller and better-controlled than that of traditional polymer blends, plus, in many cases, dual phase continuity exists. Interpenetrating polymer networks have seen broader commercial applications, including but not limited to, ion exchange resins, sound and vibration dampening materials, automobile parts, and other outdoor appliances.

Different types of interpenetrating polymer networks can be produced from different procedures or different starting materials. Following are general definitions[110,111] of some important IPNs often seen in literatures. 1) **Sequential IPN:** Polymer network I is synthesized first. The second monomer with cross-linkers and activators are added to swell the network I, and polymerized in situ to form network II. 2) **Simultaneous interpenetrating network (SIN):** The monomers and/or prepolymers plus cross-linkers and activators of all networks are mixed, and polymerized simultaneously without interfering reactions. 3) **Latex IPN:** The polymers are in the form of latex. Each latex particle is a micro-IPN. 4) **Gradient IPN:** In this type of IPN, the overall composition or cross-link density of materials varies gradually from location to location macroscopically. 5) **Thermoplastic IPN:** The networks are cross-linked by physical means, like crystals or block copolymers, rather than chemical bonds. 6) **Semi-IPN:** One or more polymers are not cross-linked while at least one polymer is cross-linked.

3.1.5 Gradient polymer/polymer composites

Gradient composites are multi-component systems where the concentration of one component varies gradually through space on the macroscopic level. One significant feature of gradient composites is that, material properties change continuously along the gradient, with less (even no) sharp interface present. Because of this feature, gradient composites find applications in two main areas. One takes advantage of the gradually changing properties inside of one system, for example, the fabrication of gradient refractive index (GRIN) rod lenses for imaging and optical communication applications.[112] Another emphasizes their ability to bridge two different materials together smoothly. One example is to avoid delamination by creating a gradient structure between two layers. Gradient polymer/polymer composites are part of the big gradient composites family, where all components are made of polymers. They are gaining more attention because of the easy processing and low cost of polymers. To synthesize a gradient polymer/polymer composite, a common method involves establishing a concentration gradient profile of one monomer inside of another polymer matrix. The polymerization of the first monomer is followed to fix the gradient structure. Many techniques can produce a gradient profile, like diffusions,[113-116] centrifugation,[112,117] etc.

3.1.6 Ring-Opening Metathesis Polymerization (ROMP)

Equation 3.1:

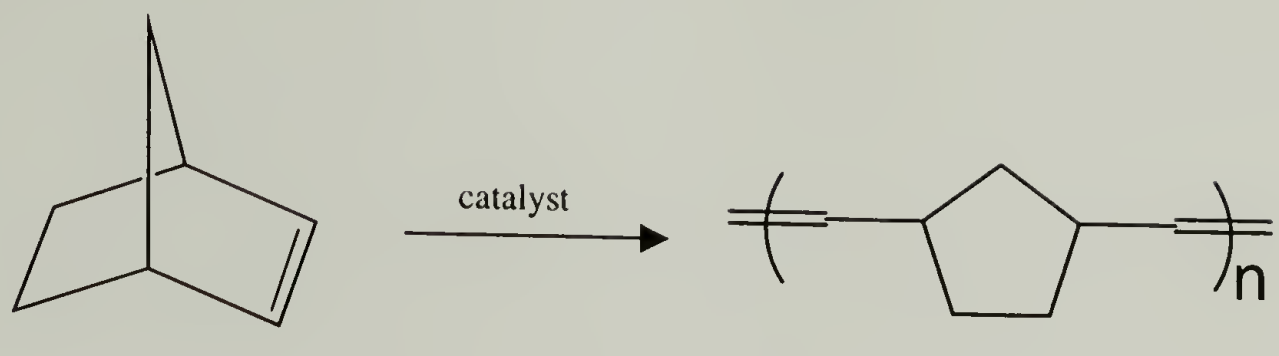

Ring-opening metathesis polymerization (ROMP) is a relatively old area.[118,119] The synthesis of polynorbornene (PN) by ROMP is shown in Equation 3.1 as an example. The catalysts used in early times were all ill-defined, and the mechanism was not clear. Tebbe and others[120] reported the first example of a well-defined carbene complex, the Tebbe reagent, as shown in Figure 3.6(I). The living polymerization of norbornene with related titanacyclobutane complexes (II and III in Figure 3.6) was

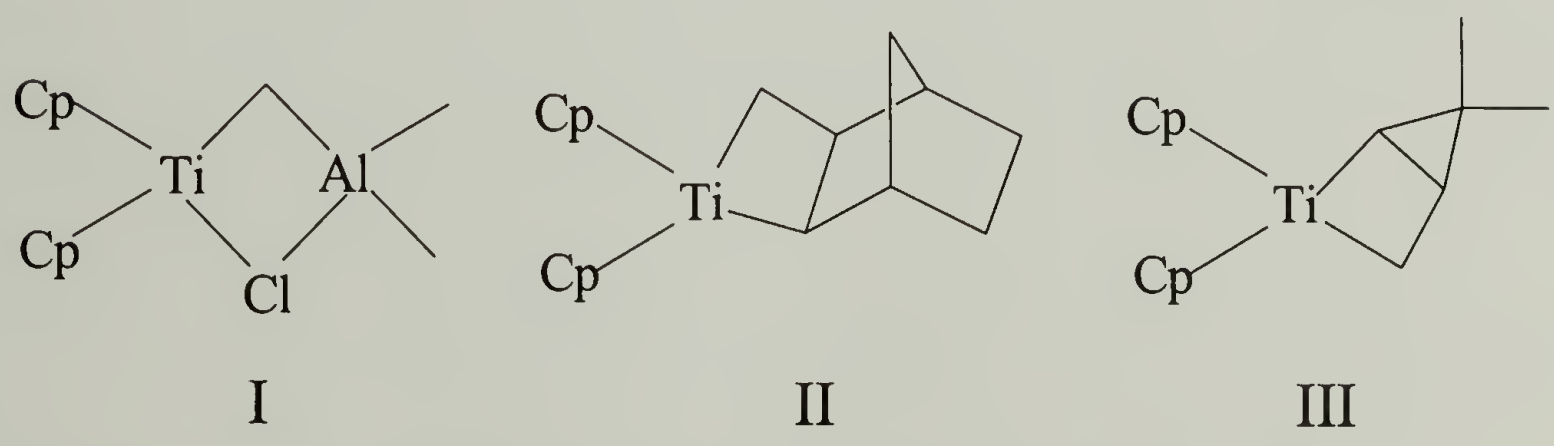

Figure 3.6: Carbene complex and titanacyclobutane complexes.

further illustrated by Gilliom and Grubbs.[121] However, it was not until Schrock[122,123] and Grubbs[124,125] developed their stable and well-defined transition metal carbene complexes did ROMP begin to receive the most attention. Two typical catalyst

examples are shown in Figure 3.7. They are relatively stable, highly active towards ROMP, and are tolerant to some functionalities.

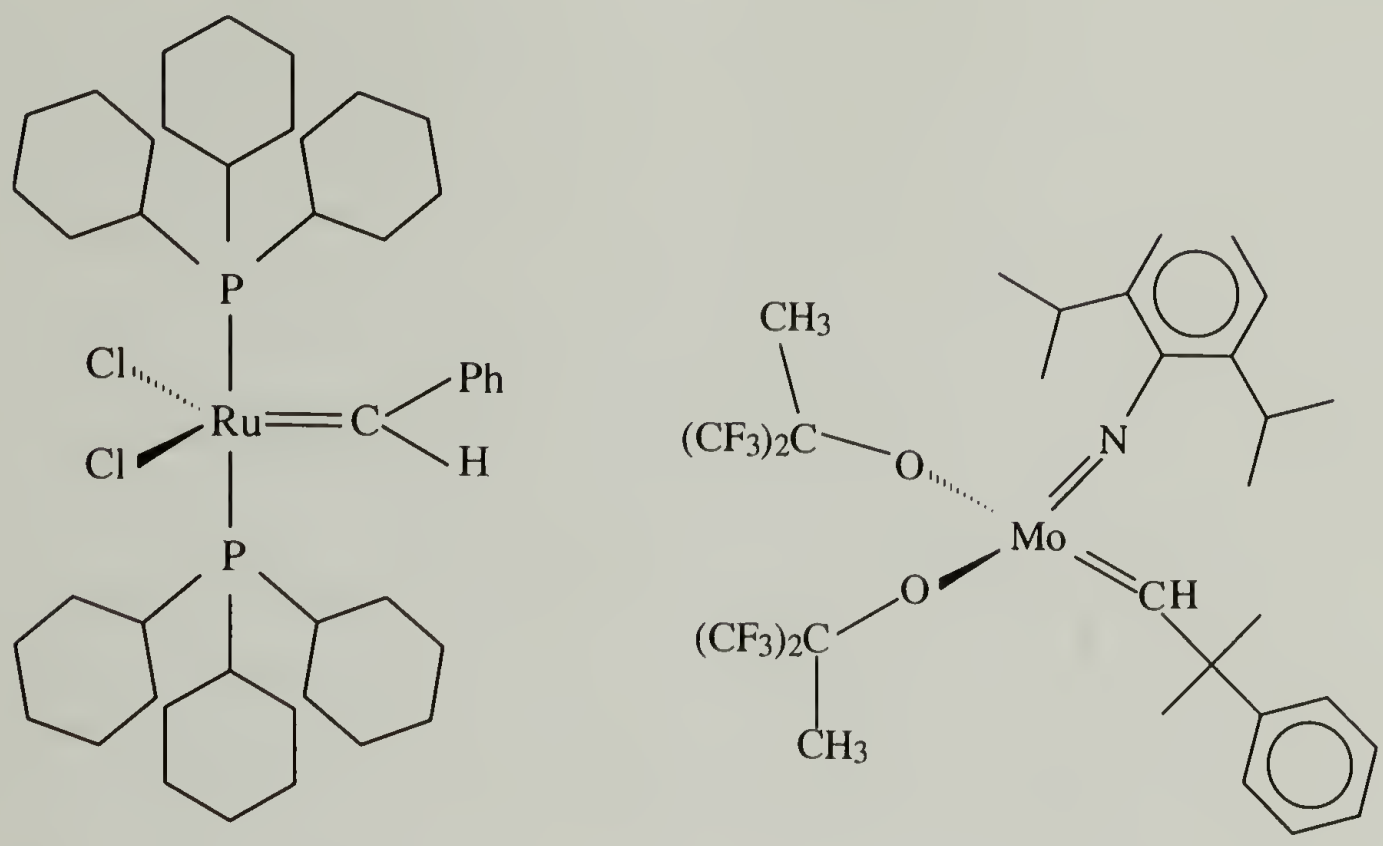

Figure 3.7: The structures of Grubbs' catalyst (Ruthenium based) and Schrock's catalyst (Molybdenum based).

A detailed study of ROMP is not the purpose of this research. The following paragraphs will show a few ROMP products with important industrial values.[126]

Polynorbornene from norbornene monomer. Norbornene is made by the Diels-Alder reaction of cyclopentadiene and ethene. Polymerization occurs as in Equation 3.1 and an $RuCl_3$/HCl catalyst is used in butanol. The highly trans (90%) polynorbornene was put on the market in 1976 by CdF Chimie in France, and in 1978 by companies in the USA and Japan. The polymer is sold as a molding powder under the trade name *Norsorex*, and contains a small amount of non-staining antioxidant. It has a high molecular weight (2×10^6), and can absorb up to seven parts of extending oils and ester plasticizers. The plasticized material has good green strength and is

highly compatible with fillers. It can be molded and cured in the common way at temperature up to 185 °C. The glass transition temperature of 35 °C is depressed to –60 °C by sufficient plasticization. The vulcanized product has important specialty applications, particularly for engine mountings, anti-vibration mounts, shock-proof bumpers, and flexible coatings.

Equation 3.2:

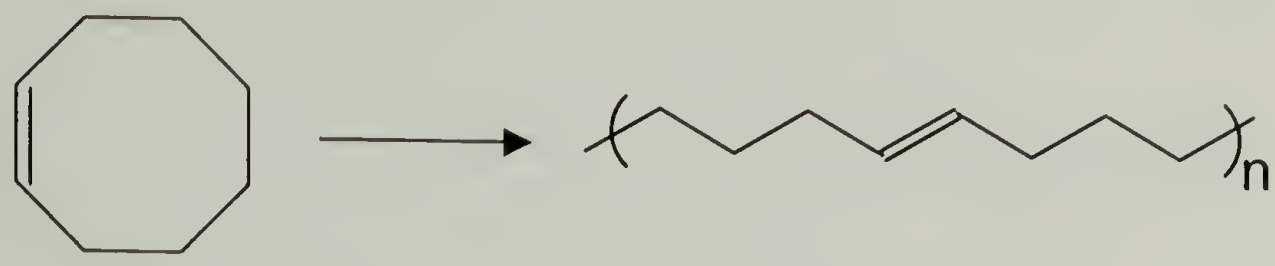

Poly(1-octenylene) (or polyoctenamer) from cis-cyclooctene. The polymerization of cis-cyclooctene proceeds as in Equation 3.2, and the product of polyoctenamer was first marked in 1980 by Chemische Werke Hüls in Germany, under the trade name Vestenamer 8012. The number 8012 denotes that the product contains 80% trans double bonds and has viscosity of 120 cm^3/g when measured in 0.1% toluene solution at 25 °C. Vestenamer 8012 possesses extremely unusual properties for an elastomer. It is hard and has an exceptionally high viscosity at 20 °C while above 60 °C it becomes a fluid with a honey-like consistency. The hardness of the polymer at low temperature is due to the cystallinity (33%). The melting temperature of the unvulcanized polymer is 55 °C. Low molecular weight (60,000) results in the fluidity at higher temperature. The Tg for the filler-free vulcanized polymer is –65 °C. It is especially suitable to be blended with other rubbers because it can carry this property into blends to some extent with moderate loading, about 10 to 30% of the whole blend.

The blends then have some technical advantages, like easier filler incorporation and distribution, higher green strength at room temperature, easier processing at high temperature. And they are highly stable against thermal, oxidative, and photochemical degradation.

Equation 3.3:

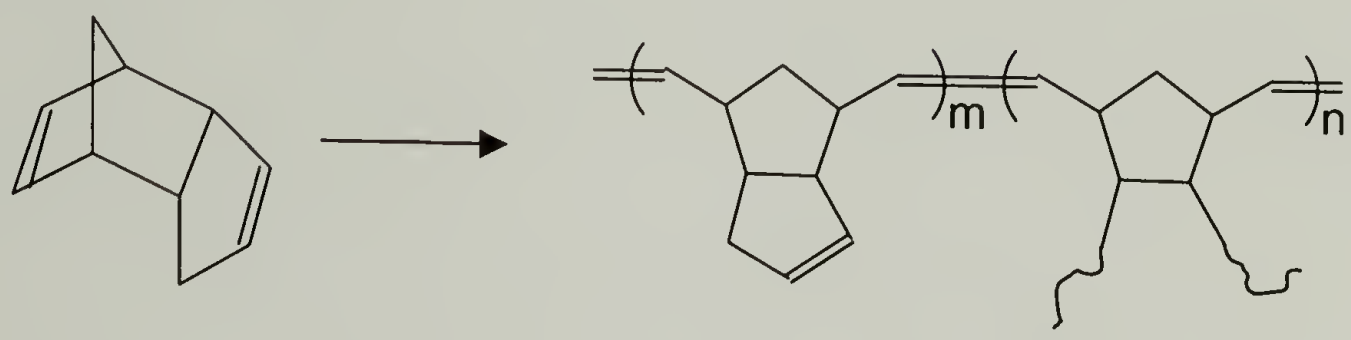

Poly(dicyclopentadiene) from endo-dicyclopentadiene. Endo-dicyclopentadiene (DCPD) is a cheap by-product from oil cracking, making it an attractive candidate for ROMP. Equation 3.3 shows the polymerization. Because DCPD has two cyclic olefin functionalities, the final product is a highly cross-linked thermoset as the less hindered cyclic olefin undergoes crosslinking by either radical or metathesis mechanisms following the ROMP of the norbornene-type double bond. Commercially, poly(dicyclopentadiene) is produced by the reaction injection molding (RIM) technique. There are two streams. One contains a catalyst, like WCl_6/ROH, and the other has a cocatalyst (activator), for example, Et_2AlCl. DCPD monomer and/or co-monomers can be put in one or both streams. The two streams pass into a mixing chamber first, and then the mixture is injected into the mold where the heat of reaction raises the temperature to about 150 °C within one minute. The whole reaction can be finished in two minutes. The final product is a tough, rigid thermoset with high modulus and excellent impact strength. Fillers can be added into the streams before

mixing. Two general problems associated with RIM should be addressed. First, premature reaction needs to be slowed down to avoid clogging between the mixing chamber and the mold. Normally, a less active cocatalyst, or a Lewis base (moderator) is added into the system to retard the acceleration. Second, the complete conversion of monomer is difficult to achieve as the whole process is fast, and the mixture becomes extremely viscous in a very short period. In the DCPD case, the presence of monomer not only affects the mechanical properties, the odor of DCPD is very unpleasant. That is why most of poly(dicyclopentadiene) products are for outdoor applications.

3.1.7 ROMP in CO_2

Ring-opening metathesis polymerization in CO_2 has been studies by a few groups. Mistele and coworkers[127] used $Ru(H_20)_6(tos)_2$ (tos = p-toluenesulfonate) as catalyst and norbornene as monomer. $Ru(H_20)_6(tos)_2$ is not soluble in CO_2. They got around by adding small portion of methanol as polar co-solvent. The effect of methanol on stereo-selectivity was also studied. Fürstner et. al.[128] looked at olefin metathesis, including ROMP, in both liquid and supercritical CO_2 using highly active and stable Grubbs' catalyst and Schrock's catalyst. They observed high polynorbornene yield and high molecular weight. Ruthenium-based Grubbs' catalyst also polymerizes cis-cyclooctene to high molecular weight polymers in good yield. The polymerizations are mostly heterogeneous although Schrock's catalyst was suspected to be partially soluble in CO_2. Unfortunately, there is no following publication to clear the questions in the paper, probably because the authors are more interested in organic synthesis than polymerization.

3.2 Research introduction

The purpose of this research is to test the concept of using semicrystalline polymers as nanotemplates. A semicrystalline polymer substrate was swollen by CO_2 first. Then a monomer was diffused into the amorphous and interlamellar regions with the help of CO_2. Polymerization of the monomer *in situ* produced a polymer/polymer composite. Due to the fact that polymer crystals are used as nanotemplates, high temperature processes should be avoided to preserve the crystalline structure.

In this study, highly crystalline poly(4-methyl-1-pentene) (PMP) was chosen as the nanosubstrate because it has high mass uptake of CO_2.[41,129] Ring-opening metathesis polymerization by carbene catalysts was used to produce the second polymer inside of PMP. The reasons for choosing ROMP are as following: (1) It expands the previous CO_2 methods of making polymer blends from radical polymerizations into metal-catalyzed polymerizations. (2) ROMP has been well-studied in the last two decades. (3) By applying ROMP, there is no chain transfer to the polymer substrate. Thus no grafting reaction occurs. (4) Polymerization can be carried out at room temperature. Supercritical state is not a necessary condition. (5) Osmium tetraoxide readily stains ROMP products that have double bonds on the backbone, leaving PMP intact. This strong contrast promises that Transmission Electron Microscopy (TEM) should give better results on morphology studies. Due to the solubility problems of those carbene catalysts in carbon dioxide, the synthesis was done in two steps, as illustrated in scheme 3.1. First, the diffusion of catalysts into PMP substrate was carried

out using organic solvents. Second, the monomer (norbornene) was infused into the PMP as a CO_2 solution, where it polymerized and precipitated out. Although the use of small amount of organic solvents shadowed our "green" method, homopolymer formation outside of the substrates was eliminated because CO_2 can't extract the catalysts out of substrate. Polymerization should occur only inside of PMP.

Scheme 3.1:

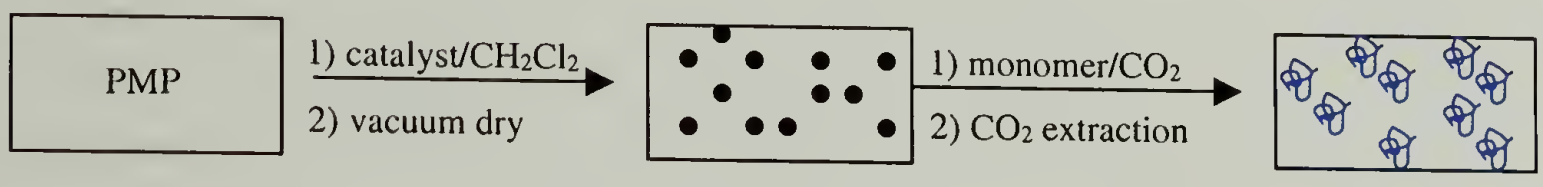

The fact of polymerizing one monomer inside of another polymer in this research makes it look similar to interpenetrating polymer networks (IPNs) synthesis. The main difference between the system here and IPNs is that, neither polymer is crosslinked in this system. Plus, very diluted CO_2 solution (< 10 wt% regarding to CO_2) is used to carry out monomer diffusion. Thus, monomer self-diffusion into substrate can be neglected. And carbon dioxide is the carrier to put materials in place. Furthermore, because the specific monomer chosen in this chapter (norbornene in this case) can be polymerized in seconds by those carbene catalysts, there is almost no monomer-soaking period. The polymerization occurs as soon as the monomer diffuses into PMP and reaches the catalyst. No diffusion equilibrium is reached before polymerization is done. It is expected that polynorbornene concentrations gradually change along the diffusion direction.

3.3 Experimental section

3.3.1 Materials

Commercially available poly(4-methyl-1-pentene) (PMP) (Scientific Polymer Products Inc., melt index: 26) pellets were melt-pressed into 0.8 mm thick plaques at 260 °C and 25,000 psi. The temperature was then lowered to 100 °C in air while maintaining the same pressure. When the temperature reached 100 °C, cool water was used to increase the cooling rate. After this process, the final PMP sample had a crystallinity of about 70% by DSC (Differential scanning calorimetry). These plaques were subsequently cut into appropriate sized specimens, usually 20 mm × 8 mm. PMP has a unique property: at ambient conditions, the density of its crystalline phase is slighter lower than that of its amorphous phase (0.828 g/cm^3 and 0.838 g/cm^3, respectively). For its Heat of fusion (ΔH_f), 61.9 J/g is chosen according to the literature.[130,131] Rybnikar and Geil[132] reported the lamellar thickness of PMP to be about 35 nm for a sample crystallized from the melt at 201-235 °C.

Bis-(tricyclohexylphosphine)-benzylidineruthenium(IV) dichloride (Grubbs' catalyst) and 2,6-Diisopropylphenylimido-neophylidenemolybdenum(VI) bis(hexafluoro-t-butoxide) (Schrock's catalyst) (structures are shown in Figure 3.7) were obtained from Strem Chemical Inc. Norbornene (Aldrich) was distilled from sodium under nitrogen atmosphere. Methylene chloride was purified following a reported procedure,[133] and stored under nitrogen in a dark and cold area. Ethyl vinyl ether, tetrahydrofuran (THF), and methanol were obtained from Aldrich and used as received. Carbon dioxide (Coleman grade 99.99 %, Merriam Graves) was passed

through activated alumina and Q-5 catalyst (Englehard Industries) to remove water and oxygen, respectively. A 100DM high-pressure syringe pump (Isco Inc.) fitted with a heating/cooling jacket was used to deliver CO_2 at the required pressure and temperature.

3.3.2 ROMP of norbornene in liquid carbon dioxide

In a nitrogen-purged glove bag, norbornene and a tiny vial containing ROMP catalyst were sealed in a stainless steel high-pressure view cell equipped with sapphire windows. The view cell was then sealed and taken out of the glove bag. CO_2 was introduced into the view cell at room temperature and 2000 psi. The CO_2 solution turned cloudy in seconds. After a certain reaction period, CO_2 was vented into ethanol. The polynorbornene was recovered as white, sometimes yellow, material. Large catalyst particles were visible in the polymer, indicating a heterogeneous polymerization. The polymer was dissolved in THF along with two drops of ethyl vinyl ether to deactivate the remaining catalyst (for Grubbs' catalyst). The solution was filtered through a layer of silica gel and recovered by filtration to remove the catalyst and the polymer was precipitated in rapidly stirred methanol. The product was dried under vacuum to constant mass.

3.3.3 CO_2 and norbornene diffusion experiments in PMP

The method described here was originally explained by Berens,[134] and used by a lot of former McCarthy group members[41,106-108,129] to obtain mass uptakes and diffusion coefficients of CO_2 and other additives in varies of polymers. The method assumes a Fickian diffusion in an indefinitely wide planar sheet. Pieces of PMP films with a thickness of 0.8 mm were tared (about 0.3 g each), and placed in high-pressure vessels

individually. CO_2 was then filled at room temperature and about 4000 psi. After a certain soaking period, CO_2 was quickly vented, and the PMP sample was quickly transferred to a balance interfaced to a computer. The mass loss was recorded as a function of time. Plotting mass uptake vs the square root of desorption time gave a linear curve in the early stage, indicating a Fickian diffusion kinetics in that stage. Total mass uptake at the end of the absorption period was obtained by linear extrapolation to zero desorption time. A series of absorption times were studied until final equilibrium was reached. The mass uptake values at different absorption times should fit into the equation derived by Crank.[135] (Equation 3.4)

Equation 3.4:

$$\frac{M_t}{M_\infty} = 1 - \sum_{n=0}^{\infty} \left[\frac{8}{(2n+1)^2 \pi^2} e^{\left(\frac{-D(2n+1)^2 t}{4l^2} \right)} \right]$$

Here, M_t is the mass uptake at time t, M_∞ is the equilibrium mass uptake, D is the diffusion coefficient, and l is the half thickness of the original sample. The diffusion coefficient D can be easily calculated through either curve fitting, or zero order approximation.

The diffusion of norbornene along with CO_2 in PMP was attempted following similar procedures presented in literatures.[106,108,134] It failed due to the quick sublimation of norbornene.

3.3.4 Composite synthesis

PMP specimens were immersed in Grubbs' catalyst/CH_2Cl_2 solution at a given concentration for a period of time. After soaking, they were rinsed with CH_2Cl_2 to remove any surface-adsorbed catalyst, and dried under vacuum to remove the solvent inside. The samples showed a little purple color, indicating some purple Grubbs' catalyst did get inside. These catalyst-embedded specimens were then sealed in stainless steel high-pressure vessels with norbornene solid. CO_2 was introduced to the vessels at desired temperature and pressure. Under the conditions used here, norbornene and CO_2 mixed in seconds upon shaking, and remained as one phase. After a certain reaction period, CO_2 was vented into ethanol, and the specimens were extracted by fresh CO_2 several times to remove all unreacted norbornene. (Many ROMP products have odor due to the unreacted monomers. CO_2 extraction may be a way to remove the odor.) Ethyl vinyl ether was added at the same time to deactivate the remaining catalyst. The finally products were opaque because of a small amount of CO_2-induced foaming or crazing, sometimes also yellowish. It still kept the original geometry. There was no polymer stuck on surface. (Schrock's catalyst was also tested with no success. Apparently no active Schrock' catalyst was left inside of PMP.)

3.3.5 Characterization

Polynorbornene synthesized in carbon dioxide was characterized using classical techniques. Molecular weight measurements were made by gel permeation chromatography with THF as the mobile phase and narrow molecular weight distribution polystyrenes as calibration standards. A Bio-Rad 175C FTIR was used to

record transmission infrared spectra. Nuclear magnetic resonance (NMR) spectra were recorded using a Bruker 300 MHz NMR and $CDCl_3$ as solvent.

Polynorbornene/poly(4-methyl-1-pentene) (PN/PMP) composites were characterized by a variety of different techniques. Mass gain gave the average composition of the composites. Differential scanning calorimetry (DSC) measurements were carried out with a DuPont 2000 DSC under nitrogen flow at a heating rate of 10 °C/min. For the Heat of fusion (ΔH_f) of PMP, 61.9 J/g was chosen according to the literature.[130,131] Thermal gravimetric analysis (TGA) was conducted on a DuPont Instruments TGA 2950 at a heating rate of 10 °C/min to 600 °C under nitrogen. Wide angle X-ray diffraction (WAXD) was performed on a Siemens D500 diffractometer. Attenuated total reflectance (ATR) infrared spectra were recorded for both surfaces and intersections of samples. Transmission electron microscopy (TEM) was performed on a JEOL 100CX. Thin sections were obtained by cryomicrotoming samples at –50 °C, and stained subsequently by OsO_4 vapor for 4 hours. Infrared-microscopy was performed at Markem Inc., Keene, NH. The instrument is a Mattson Galaxy 7020 with a Mattson Quantum IR microscope, and the transmission IR spectra can be recorded from a rectangular window of 120 × 90 μm or less. Again, cryomicrotoming was used to provide ultra-thin sample sections of about 1 μm thickness for good transmission IR studies.

3.4 Results and Discussion

3.4.1 ROMP in liquid CO_2

As mentioned in Section 3.1.7, ring-opening metathesis polymerization in CO_2 has been studies by a few groups.[127,128] The study performed here is actually a reproduction of Fürstner's work in 1997 using different conditions, and similar phenomena were observed. Reactions for both Grubbs' catalyst and Schrock's catalyst were repeated in liquid CO_2. Polymerizations using Grubbs' catalyst are heterogeneous because of the insolubility of Grubbs' catalyst in CO_2. Although Shrock's catalyst did show some solubility (the CO_2 solution turned yellow), it is still unclear if the reaction is indeed homogeneous or not. Due to the high reactivity of both catalysts, very high molecular weight polymers were formed in seconds. Polynorbornene obtained after releasing CO_2 was a white soft solid. Figure 3.8 and Figure 3.9 show spectra (NMR and IR) for polynorborene synthesized by Schrock's catalyst and Grubbs' catalyst, respectively. Both methods can be used to easily measure the cis and trans configurations of polynorbornene chains. Schrock's catalyst gives polymers with more cis content while Grubbs' catalyst produces more trans. Since Schrock's catalyst did not show reactivity in the following composite synthesis, it was dropped, and most of the following study was conducted using Grubbs' catalyst. Table 3.1 compared the ROMP of norbornene in CO_2 with that in methylene chloride, both using Grubbs' catalyst. In both solvents, Grubbs' catalyst has similar activity and stereo-selectivity. Because Grubbs' catalyst is not soluble in CO_2, the polymerization is heterogeneous. The molecular weight of

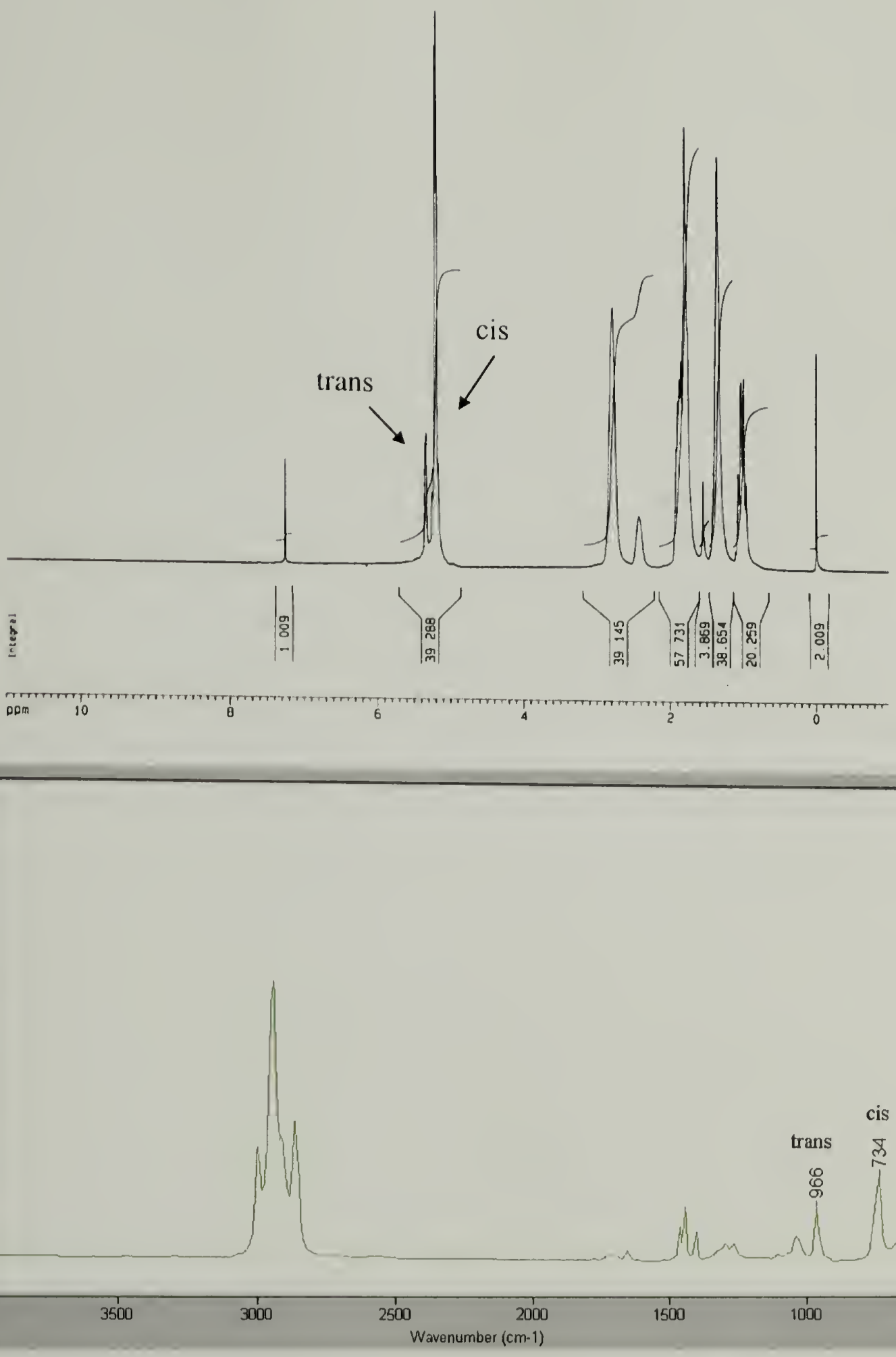

Figure 3.8: NMR and IR spectra of polynorbornene made by Schrock's catalyst in CO_2.

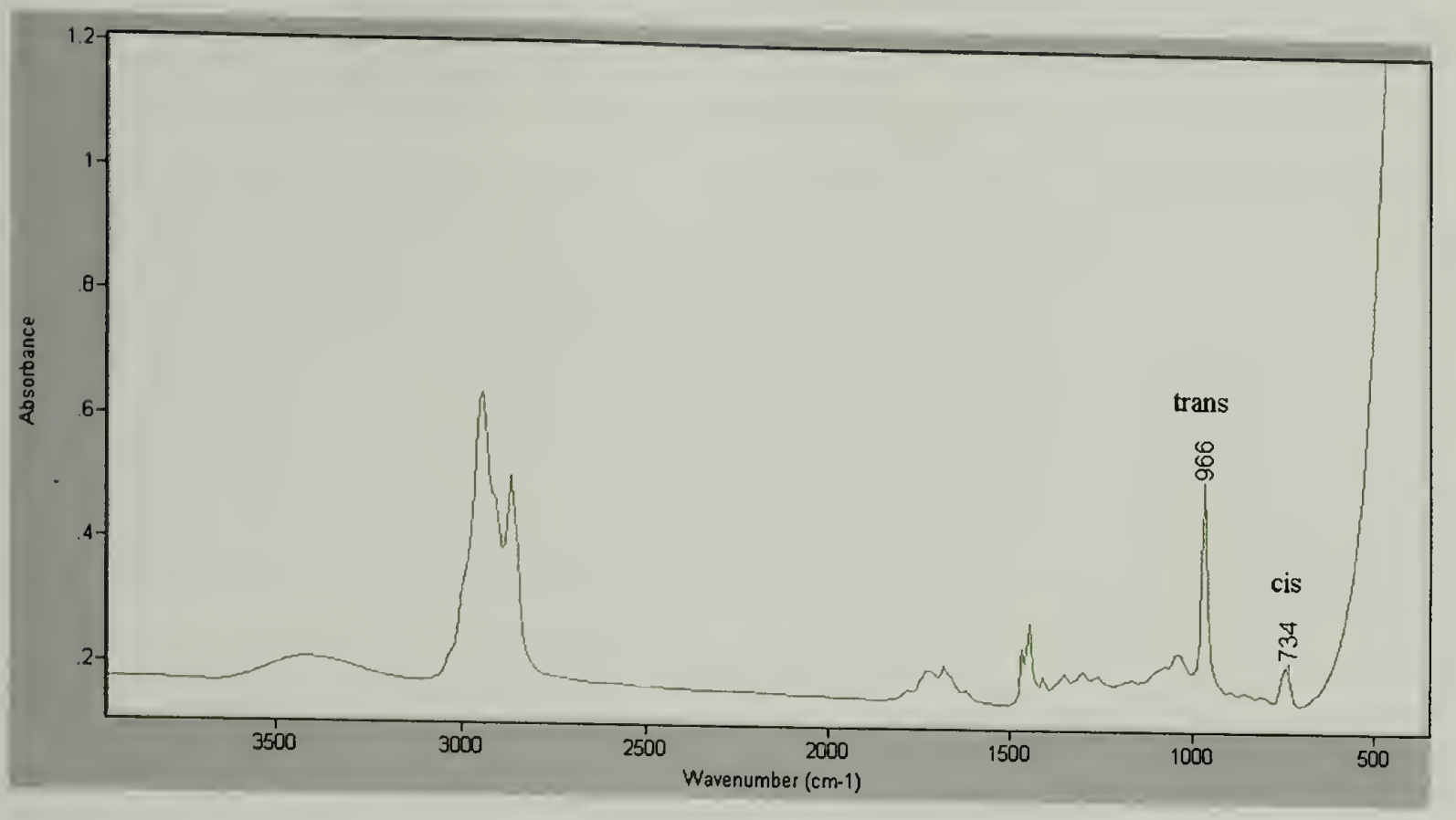

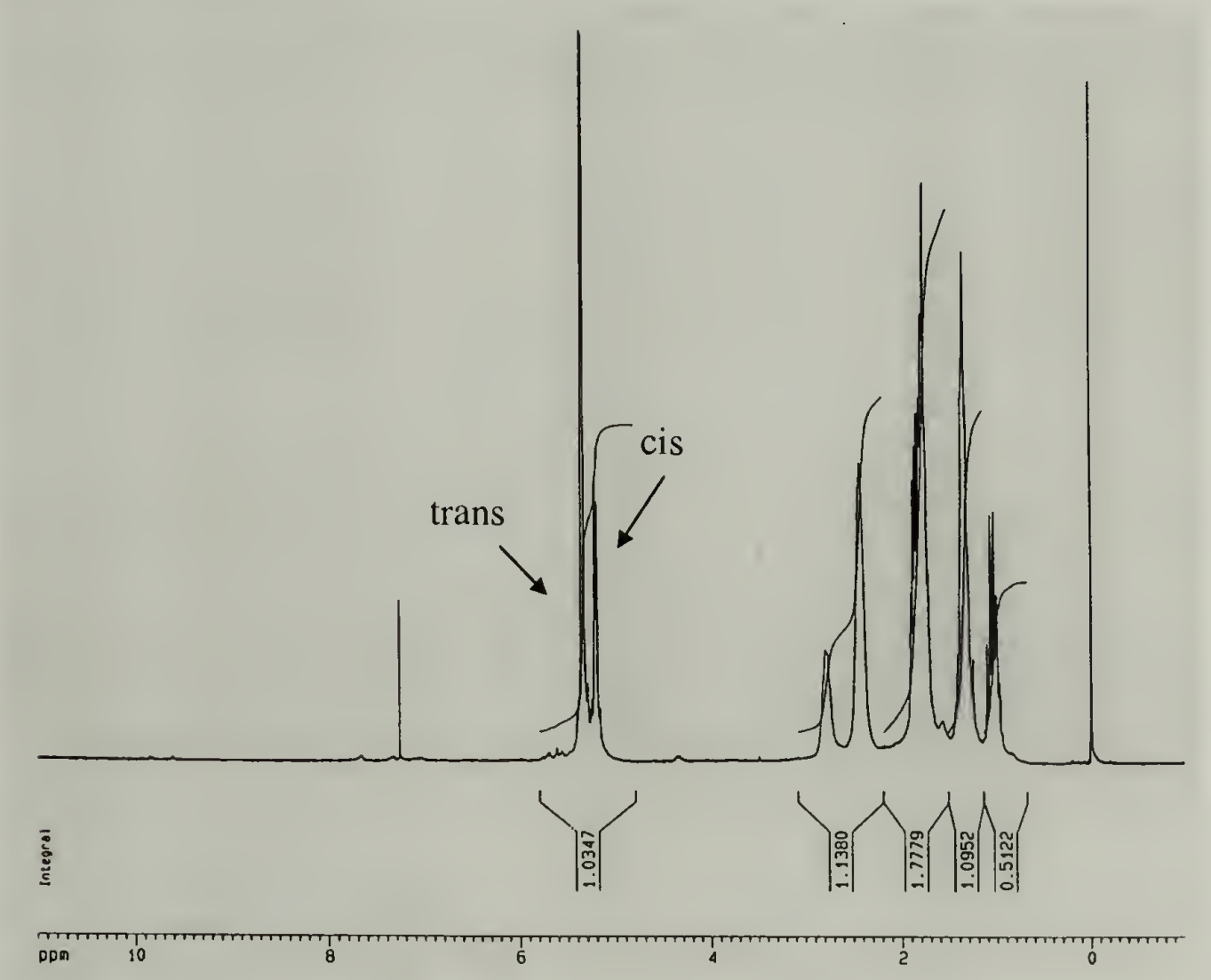

Figure 3.9: IR and NMR spectra of polynorbornene made by Grubbs' catalyst in CO_2.

polynorbornene is difficult to control, and easily reaches the million level. This also hinders efforts to extract polynorbornene out of the composites synthesized in CO_2. Another feature worth mention is that, polymerization of norbornene using Grubbs' catalyst is not living, probably due to back-biting or some other transfer reactions.[136]

Table 3.1: Polynorbornene synthesized using Grubbs' catalyst in CO_2 and in CH_2Cl_2.

	in CO_2	in CH_2Cl_2
M_w	4M[a]	[b]
PDI	3.0	2.6
cis content (%)	30	21
yield (%)	90	80

[a] Polystyrene standards are used for calibration. The solution has to be very dilute to pass the filter.

[b] Molecular weight is controlled by the ratio of catalyst and monomer.

3.4.2 CO_2 and norbornene diffusions in PMP

Hayes in the McCarthy group[129] has previously determined that the equilibrium mass uptake of carbon dioxide in PMP is 17.6 % at 60 ºC and 2600 psi. And the diffusion coefficient at this condition was reported to be 4.5×10^{-6} cm^2/s. PMP can swell quickly and significantly with supercritical carbon dioxide because its bulky side groups provide loose chain packing, which gives PMP a very low density (crystalline: ~ 0.828, amorphous: ~0.838). Carbon dioxide has a critical point of 31.1 °C and 1070 psi (73.8 bar). As most of reactions in this research were performed at room temperature, it is necessary to have a look at liquid CO_2 (subcritical) diffusion in PMP. An absorption-desorption method was used as described in the literature.[108,134] Figure 3.10 is a typical

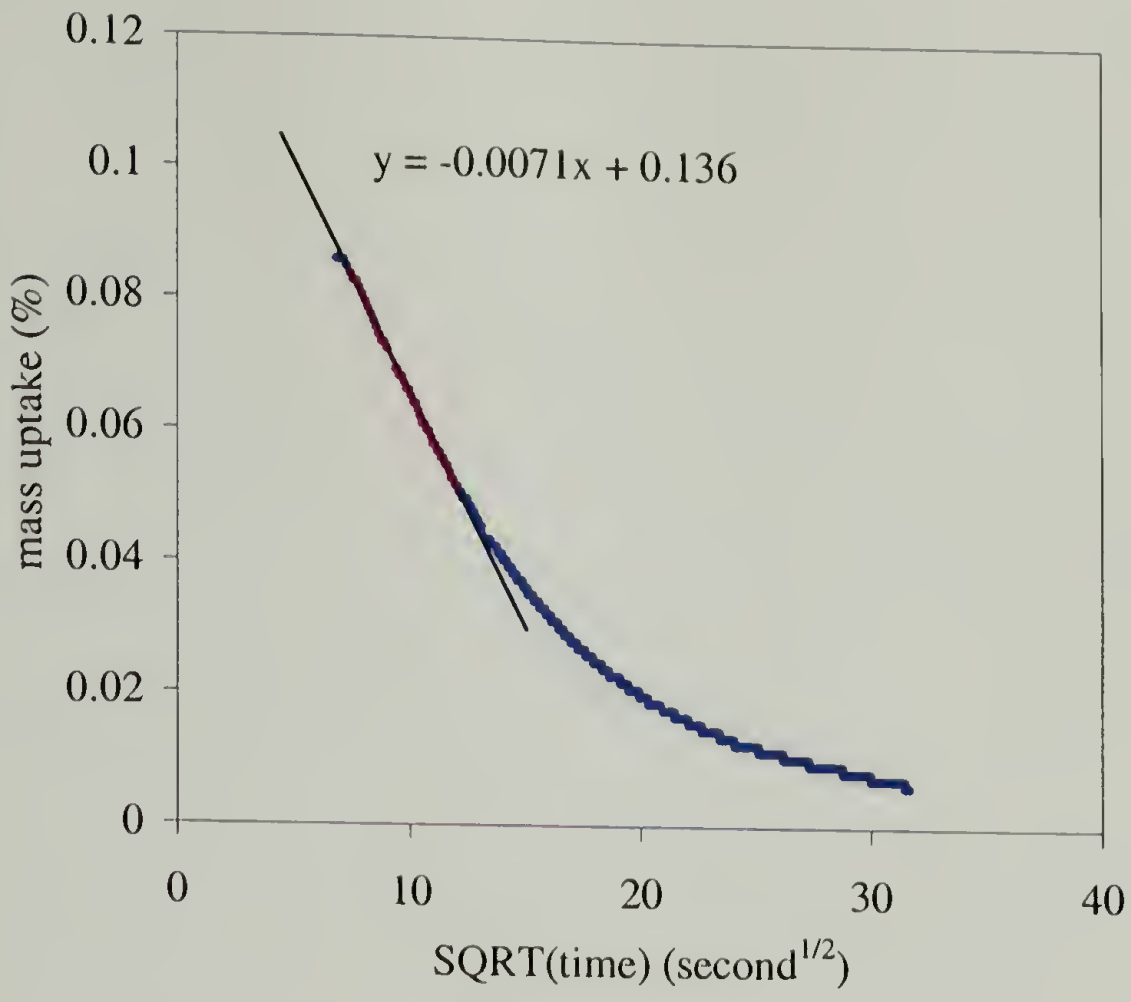

Figure 3.10: The desorption curve for a 0.8 mm thick PMP sample soaked in CO_2 for about 30 minutes at 23 °C and 4000 psi.

desorption curve for a 0.8 mm thick PMP sample soaked in CO_2 for about 30 minutes at 23 °C and 4000 psi. It is shown in the curve that the early stage of desorption is linear, indicating a Fickian diffusion behavior. Extrapolating to zero time gives the CO_2 mass uptake at the end of the soaking period of 30 minutes. The CO_2 diffusion kinetics in PMP at 23 °C and 4000 psi was obtained as shown in Figure 3.11. For 0.8 mm thick PMP films, it takes about 30 min to reach equilibrium mass uptake of 13%. Later decreasing of mass uptake is probably due to a small degree of crystallization of PMP induced by CO_2, as illustrated in the literature for poly(ethylene terephthalate) (PET)[137,138] and poly(chlorotrifluoroethylene) (PCTFE).[106] The following DSC study also confirmed it. The diffusion coefficient of CO_2 in PMP at this condition is

calculated to be about 1.36×10^{-6} cm^2/s. The value is close to that of supercritical CO_2 referred above. No sharp change occurs regarding the CO_2 diffusion coefficient in PMP when it goes from subcritical state to supercritical state. There is not always a magic line between supercritical and subcritical state. In some cases, subcritical (liquid) CO_2 can do just as well.

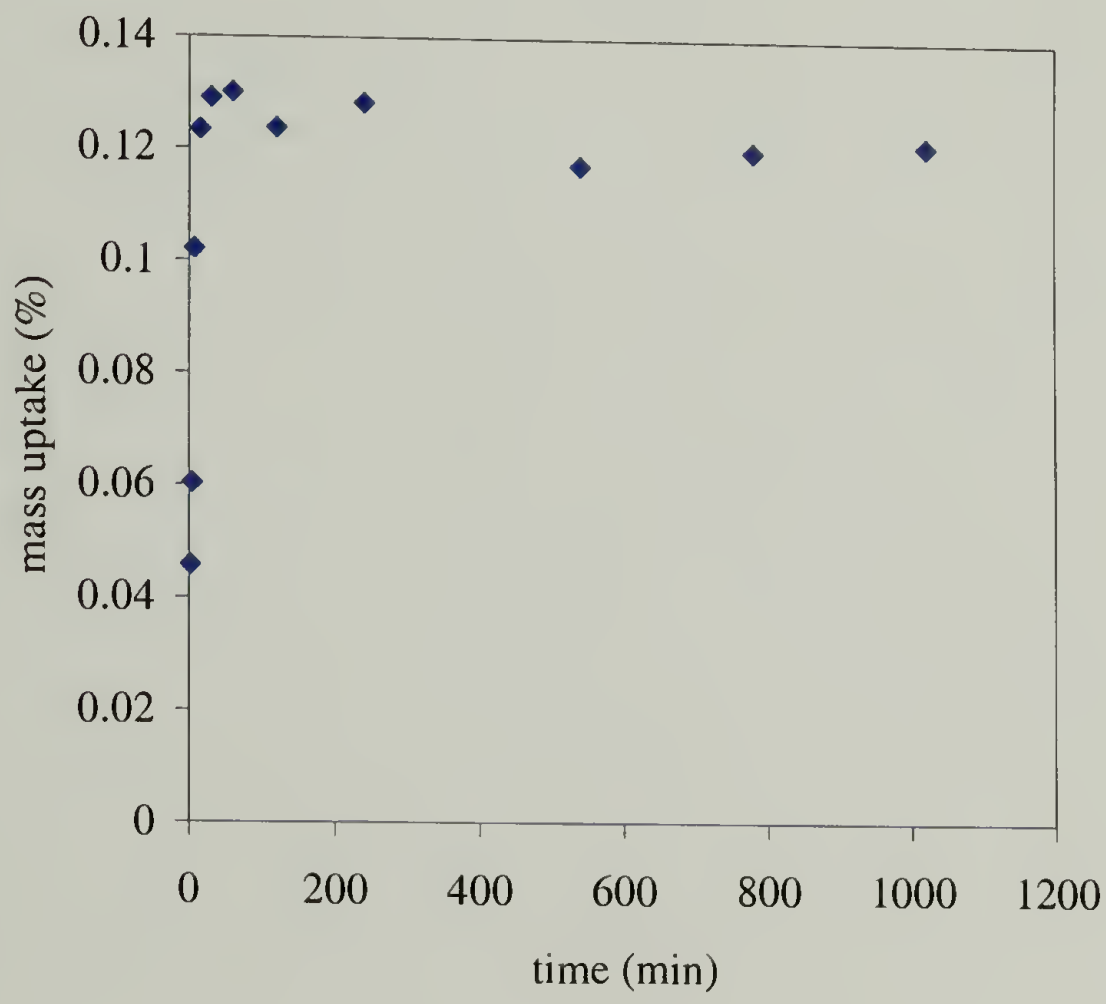

Figure 3.11: Absorption kinetics of CO_2 in PMP of 0.8 mm thickness at 23 °C, 4000 psi. (The diffusion coefficient at this condition is calculated to be about 1.36×10^{-6} cm^2/s.)

The attempt of trying to determine norbornene diffusion kinetics in PMP/Norbornene/CO_2 ternary system failed because of the fast sublimation of norbornene at room temperature. Berens' method[134] assumes that CO_2 will quickly leave the substrate while the additive diffuses out slowly. Thus the weight gain after CO_2 is diffused out can be considered as a close approximation of the amount of

additive at the end of absorption period. However, in the case of norbornene, it is questionable to take the weight gain of the polymer substrate after most of CO_2 has escaped as a close approximation of the amount of norbornene present at the end of adsorption. Nonetheless, some desorption studies of the norbornene/CO_2/PMP ternary system were performed. For 0.8 mm thick PMP films, the equilibrium norbornene uptake is about 7 – 8 wt% at the conditions mentioned above. Diffusion of norbornene through PMP without the help of CO_2 is slow, while there is still 3 – 4 wt% of monomer left after drying norbornene/PMP under vacuum for two weeks. However, the amount of norbornene inside of PMP decreases sharply upon CO_2 extraction, and becomes negligible after two cycles of CO_2 extraction. This control experiment gives us confidence in the weight-gain measurements described below. No norbornene monomer is left in those composites after CO_2 extractions. It again proves that CO_2 is a good extracting solvent, just as illustrated by its popular decaffeination application.

3.4.3 Weight-gain measurement of PN/PMP composites

Because CO_2 can extract almost all unreacted monomer from the composites and leaves polynorbornene untouched, weight gain is purely due to the polynorbornene incorporation. Although the equilibrium mass uptake of norbornene is only about 7-8 wt%, the final composites can have as high as 40 wt% of polynorbornene. This phenomenon has been explained by Watkins.[108] The polymerization of norbornene inside of PMP decreases the concentration of norbornene in PMP. It induces the repartition of norbornene between PMP/CO_2 mixture and CO_2 outside of PMP, which effectively drives more norbornene into PMP, continuing the polymerization.

Attenuated total reflectance (ATR) infrared spectra were recorded for the surfaces of PN/PMP composites. No signal corresponding to polynorbornene was detected, which means that in the composites there is a skin layer of at least 1 μm thickness without polynorbornene. It is probably because the rinse process after the catalyst soaking period effectively removes all catalyst on the surface and those immediate underneath the surface. Attempts of extracting polynorbornene out to measure molecular weight failed. The molecular weight of polynorbornene made in CO_2 is above one million, according to the study of ROMP in CO_2 shown above. It is conceivable that the M_w of polynorbornene inside of the composites is at least in that range, if not more. Previous work[106,108] on composites synthesis using radical polymerizations in CO_2 showed that polymers made inside of the substrate have much higher molecular weight that those synthesized outside, mainly due to less termination inside of the substrate.

3.4.4 Effect of reaction conditions on PN/PMP composition

As mentioned in the experimental section, the synthesis of PN/PMP was performed in two steps. First, PMP films were soaked in Grubbs' catalyst/CH_2Cl_2 solution to incorporate the catalyst into PMP substrate. Then they were rinsed, dried, and sealed in a norbornene/CO_2 solution to form composites. During this process, catalyst concentration in CH_2Cl_2 solution, soaking time, monomer concentration in CO_2, polymerization time, reaction temperature and pressure all have effects on the final composition of PN/PMP. To illustrate these effects, systematic studies on most of these parameters were performed, which is summarized in Figure 3.12.

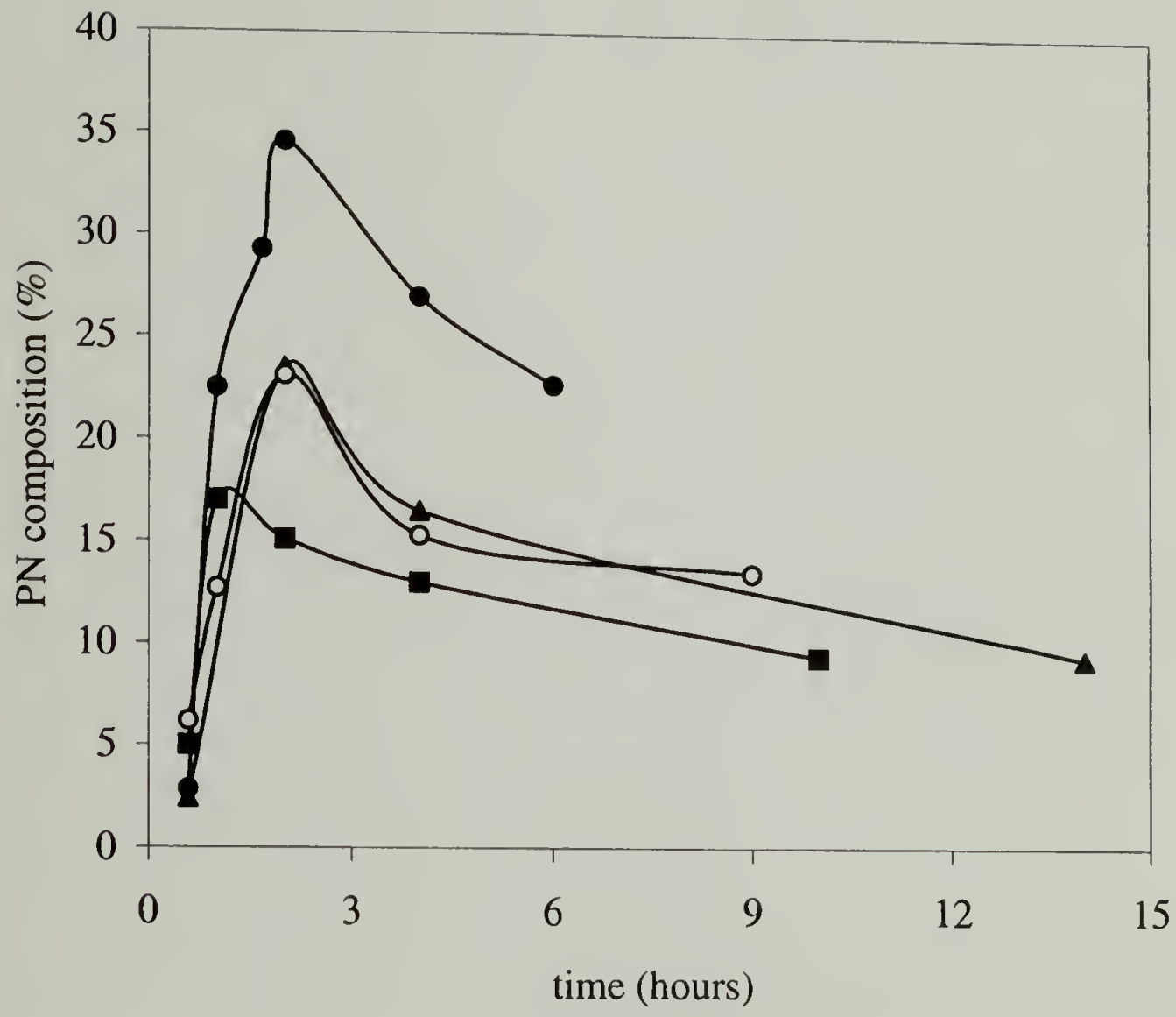

Figure 3.12: Composition changes of PN/PMP according to different conditions.

▲ : catalyst: 4mg/ml; norbornene: 0.059g/ml; CO_2: 23 °C, 4000 psi; 1 day.
○ : catalyst: 8mg/ml; norbornene: 0.059g/ml; CO_2: 23 °C, 4000 psi; 1 day.
■ : catalyst: 4mg/ml; norbornene: 0.059g/ml; CO_2: 40 °C, 5600 psi; 1 day.
● : catalyst: 4mg/ml; norbornene: 0.1g/ml; CO_2: 23 °C, 4000 psi; 1 day.

From the diagram, it is clear that two parameters, soaking time in the catalyst solution and norbornene concentration in CO_2, play the most important roles in PN/PMP composition. The effect of norbornene concentration looks obvious. Larger monomer input normally means more polymer produced. However, the effect of soaking time in catalyst solution is somewhat complicated. Two hours of soaking gave the highest percentage of polynorbornene in PMP. It is thought that, at first, the catalyst/CH_2Cl_2 solution has to diffuse into PMP substrate, which takes time. The catalyst concentration inside of PMP thus increases with time during the early soaking period. It reaches the maximum in two hours. In fact, the study of pure CH_2Cl_2 diffusion into PMP showed that the amount of CH_2Cl_2 in PMP reached a plateau after two hours. The decreasing of polynorbornene composition in PMP at longer soaking time is due to catalyst decomposition. Although we distilled CH_2Cl_2, degassed it before use, and tried to keep PMP clean, Grubbs' catalyst still decomposes slowly in CH_2Cl_2, and it became worse with time. Thus, a one-day soaking period transports less active catalyst into polymer substrates than a two-hour period does.

Increasing catalyst concentration from 4 mg/ml to 8 mg/ml apparently has little effect on PN/PMP composition, which may suggest that the absolute catalyst amount in PMP does not affect final composition too much. The polymerization of norbornene using Grubbs' catalyst in CO_2 is heterogeneous. Thus changing the absolute amount of catalyst does not make much difference. It is probably the distribution of catalyst inside of PMP which is more important. The catalyst needs to be distributed all the way through PMP substrate to get high polynorbornene incorporation, while the exact amount of catalyst can be very little. This statement is also supported by the fact that

Grubbs' catalyst has extremely high activity for ROMP of norbornene. Very little catalyst is needed to perform the polymerization. However, there is no handy tool available to probe the catalyst distribution inside of PMP substrate because the concentration was extremely low. Another possible explanation is that higher catalyst concentration gives lower molecular weight polymers. This hypothesis is not tested either, due to the failure of solvent extraction of polynorbornene from PN/PMP composites. Polynorbornene in PMP either has very high molecular weight, or is slightly cross-linked.

The temperature effect study was compromised by the instability of Grubbs' catalyst at high temperature. Thus the polymerization in supercritical CO_2 gave lower yield than in subcritical CO_2. No kinetics study of norbornene polymerization inside of CO_2-swollen PMP was performed. The CO_2 venting process after the reaction period weas usually slow to avoid destruction of the PMP susbtrate, and several CO_2 extractions were used to remove the unreacted monomer. All of these facts make the determination of the real reaction time difficult. Extending the reaction time to two days gave almost the same yield. It is comfortable to say that the reaction is complete within one day, due to the fast polymerization of norbornene by Grubbs' catalyst.

3.4.5 Nano-structure of PN/PMP composites

Figure 3.13 shows a series of TEM micrographs of PN/PMP composites with 22 wt% of PN at different magnifications, all stained by OsO_4 vapor. The morphology is much different from that of conventional blends. Instead of spherical domains of the minor component dispersed in the matrix of the major component, regular white lines

are observed here with a width of 20 – 40 nm. Amazingly, these images look more like those of micro-phase separated diblock copolymers while the samples are really just mixtures of two different homopolymers without any grafting. Rybnikar and Geil[132] reported the lamellae thickness of PMP as about 35 nm for a sample crystallized from the melt at 201 – 235 °C. In this research, the PMP sample preparation induced a similar condition. The line width shown in these micrographs is very close to Geil's value, which suggests that the white lines are probably PMP crystalline lamellae, showing up because of the contrast from neighboring dark polynorbornene regions.

To confirm that the white lines are actually crystalline lamellae, several tests were performed. First, pure PMP samples were studied using TEM, both OsO_4 stained and non-stained. This blank test should reveal if PMP itself contributes to the contrast. Neither case gave the same contrast as PN/PMP composite samples do. In fact, there was almost no contrast. This observation rules out the possibility that OsO_4 may diffuse into PMP amorphous regions and provide contrast even without polynorbornene presence. F. S. Bates and colleagues stated that they did not find OsO_4 could stain amorphous phases of polyolefins.[139]

The second test was an annealing study. The PMP sample used here has a melting temperature of 235 °C. If these white lines are crystalline lamellae of PMP, annealing the PN/PMP composites above T_m should melt all crystalline phases. Upon cooling, the melt has no memory to return into perfect lamellae in the same position, so the lines should disappear. On the other hand, annealing under T_m should make no change on the white lines. Figure 3.14 shows the results of annealing. Annealing at 270 °C under nitrogen for 1000 minutes totally destroyed the fine structures, and larger scale

phase separation can be seen. Annealing at 160 °C gave almost the same pictures as unannealed. These observations are strong evidence that the white lines are indeed PMP crystalline lamellae.

Following is a short comment on electron diffraction experiment. Although it is relatively satisfactory that the white lines are crystalline lamellae, final proof relies on electron diffraction from selected area, as suggested by TEM expert Dr. Gido. The goal is to obtain electron diffraction pictures from a selected area where only crystals present, in this case, about one micron in diameter. Due to the quick melt of crystals under electron beam, the electron microscope is set in diffraction mode first. A selective aperture is applied to expose electron beam to the selected area. After an electron diffraction is captured, the mode is switched to imaging while the aperture is still in place. In our PN/PMP composite case, this method proved extremely difficult. The electron diffraction comes from PMP crystals. In the PN/PMP composites, some crystalline regions have polynorbornene. Some do not. While only the region with polynorbornene shows imaging contrast, both regions give electron diffraction. If diffraction is performed before imaging, the selected area is mostly pure PMP crystalline domain with no imaging contrast. If imaging is performed before diffraction, the PMP crystalline region with polynorbornene is easily selected. But the crystals are already melted, and no electron diffraction can be detected. Eventually we gave up selected electron diffraction due to these difficulties.

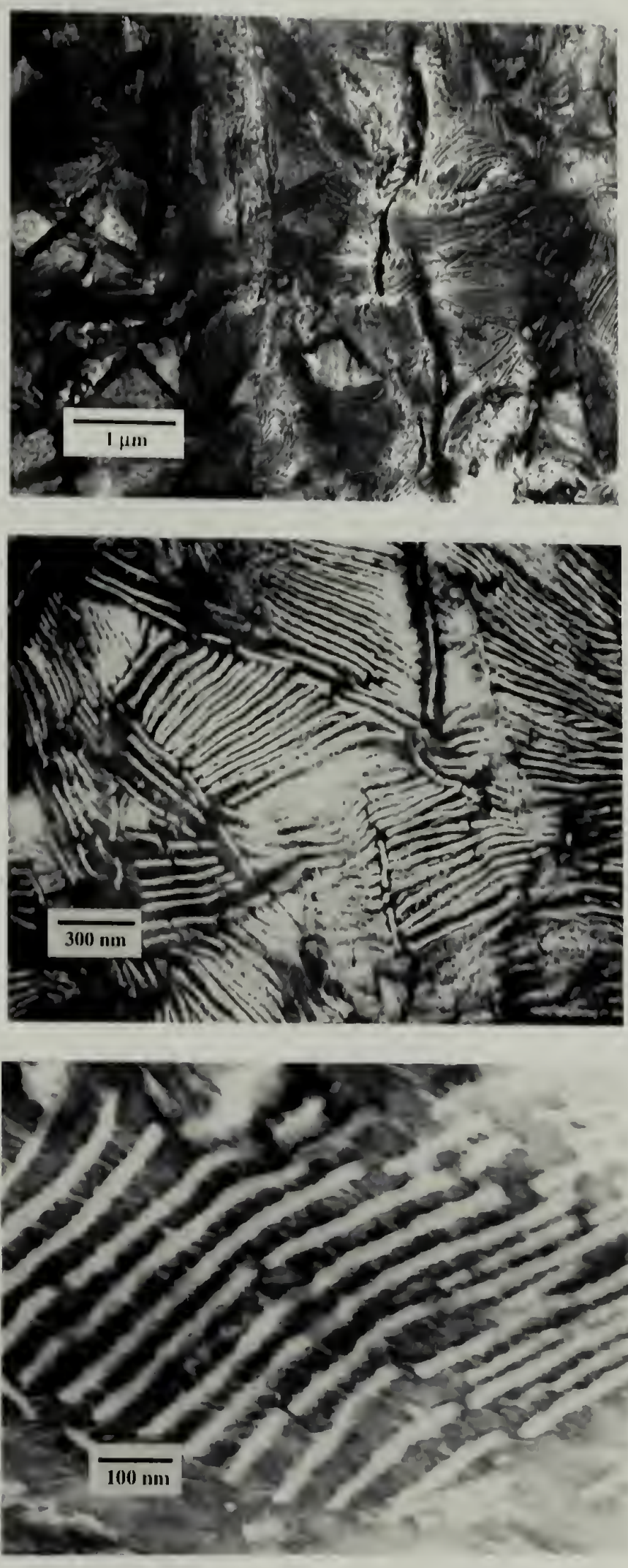

Figure 3.13: TEM micrographs of a PN/PMP composite containing 22 wt% polynorbornene. (OsO_4 vapor stained)

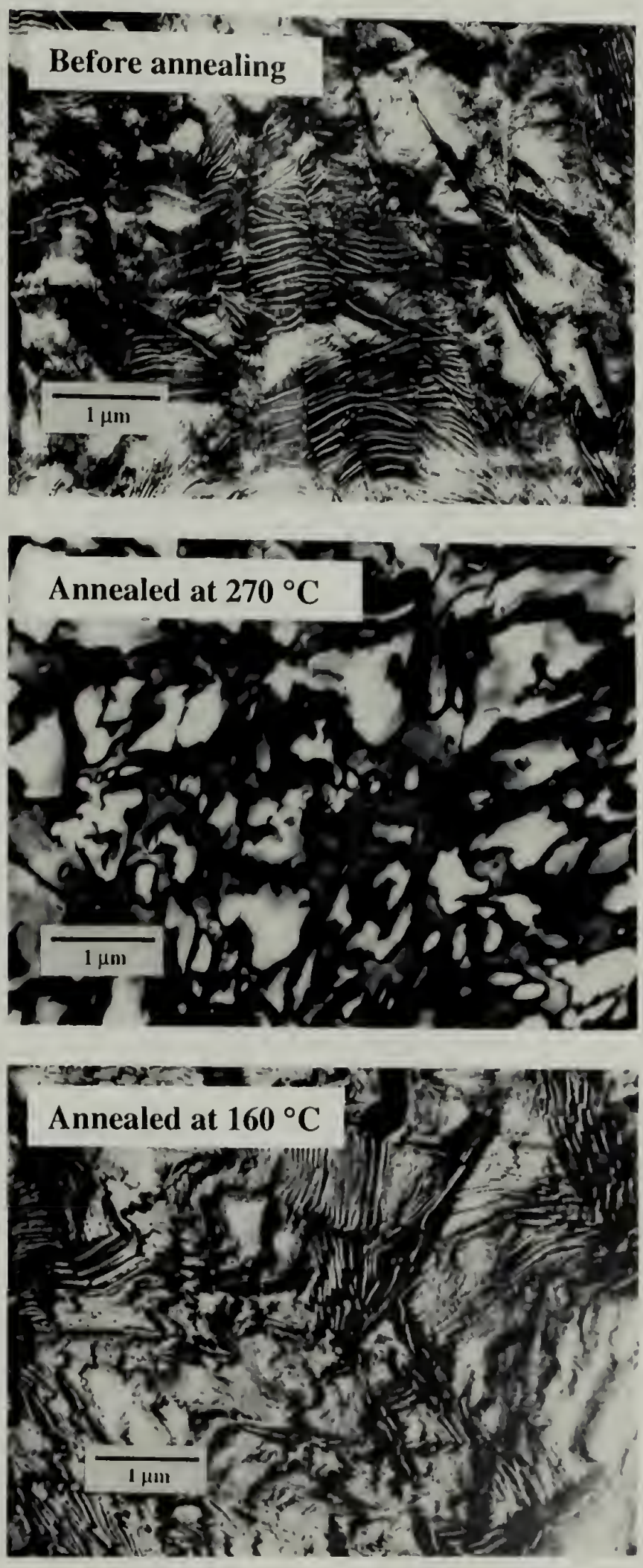

Figure 3.14: Annealing study of a PN/PMP composite with 17 wt% polynorbornene.

It was mentioned above that the polymerization of norbornene is expected to occur only in the amorphous and interlamellar regions of PMP. These TEM images are highly consistent with the previous expectation. Norbornene, in a CO_2 solution, enters into the amorphous domains as well as interlamellar regions. Upon meeting with the catalyst already deposited there during soaking, it polymerizes and precipitates in these regions. OsO_4 stains polynorbornene and renders these regions black. The white lines in the TEM images are of uniform thickness, both in cumulated regions and in separated regions, which indicates again the regular lamellar structure. The thinner white lines connecting two neighboring PMP lamellae are interlamellar fibrils (tie links).[140] Because there is no chemical grafting between polynorbornene and PMP, the composites are indeed polymer blends. However, the diblock-like morphology can never realized by simple mixing. The structure illustrated here is not thermodynamically stable, but kinetically trapped. These polymer/polymer composites achieve nanometer-scale phase separation not by thermodynamic process or by chemical linking, but rather by a "templating" process. It is similar to the templating works for polymer/silicate composites.[79,141] The difference is that in this research the templates are polymer crystalline lamellae instead of silicate nanolayers. Tie chains hold individual lamellae together so that it is impossible to form exfoliated (delaminated) structures without breaking the tie molecules. The structures are mostly "intercalated". The TEM images in Figure 3.15 were taken from the near surface region, where polynorbornene may have the highest concentration (due to gradient structure, explained in the following section.). The lamellae are still parallel even when they are well separated. In some areas,

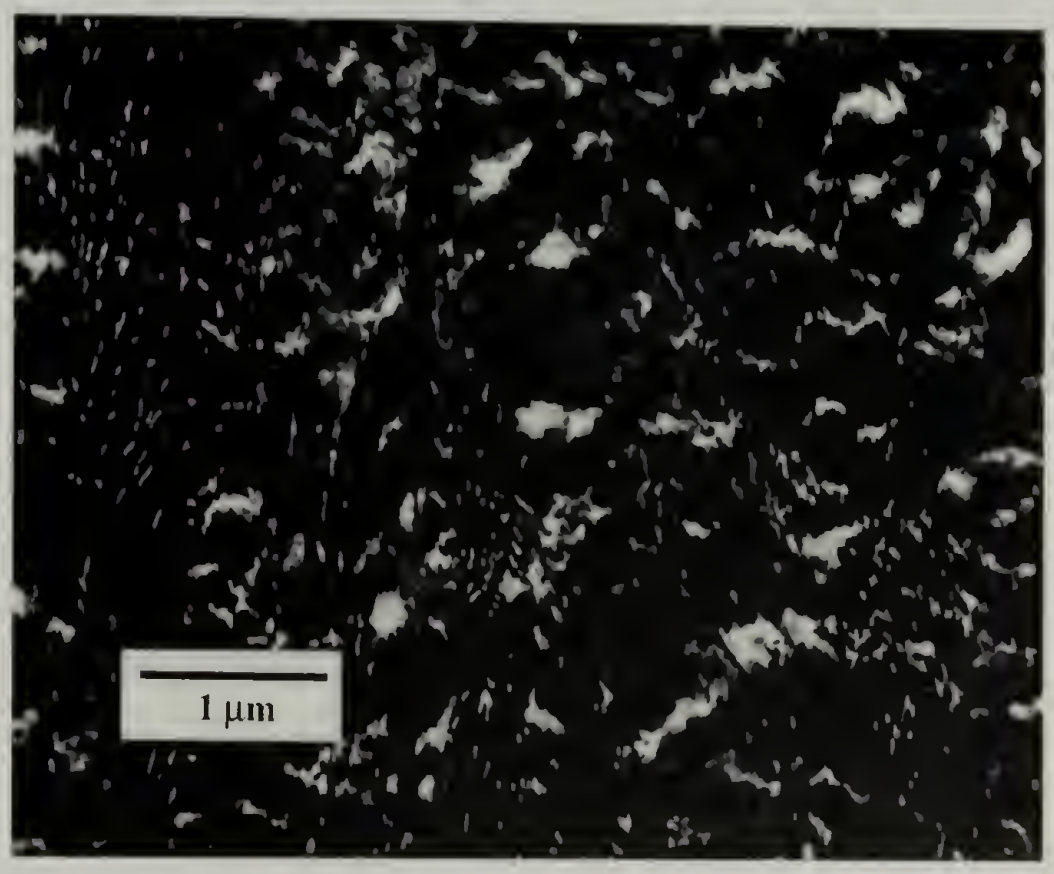

Figure 3.15: TEM images from the near surface region of a PN/PMP composite with 17 wt% polynorbornene.

polynorbornene concentration is so high that lamellae are probably damaged by the expansion of polynorbornene.

Not only is the formation of nanometer-scale polymer/polymer mixtures quite unique, the way we observed the PMP crystalline phase is also worthy of mention. Because the amorphous phase and crystalline phase of PMP have almost same density, there is little contrast under TEM without staining. There are literature reports[130,140] of using swelling and fracture surface replicas to explore the structure of PMP. This method is an indirect observation and time-consuming. RuO_4 staining of the amorphous phase has also been reported,[130] which is not easy either. Control of staining time is crucial to get good images. Shorter time gives little or no contrast while longer time resulted in the formation of ruthenium agglomerates on the sample.[139] Plus, the staining mechanism is also complicated.[139] However, polynorbornene in these PN/PMP blends is easily stained by conventional technique — OsO_4 vapor staining, providing excellent contrast to distinguish PMP crystalline lamellae from PMP amorphous area where polynorbornene resides. It even shows the 4 – 7 nm thick interlamellar fibrils in between two lamellae. If polynorbornene is considered as a staining agent, the whole process of nanocomposite synthesis described above, in the eyes of polymer physicists, is merely revealing the morphology of semicrystalline PMP by a special staining technique. This concept of incorporating a staining "primer" (polynorbornene) to enhance staining may be applicable for morphology studies of some "hard to stain" materials.

3.4.6 Gradient structure of PN/PMP composites

Since this method can provide PN/PMP nanocomposites with polynorbornene composition ranging from 5 wt% to 40 wt%, a TEM survey was conducted on most of the samples. The original purpose was to understand the relation between composite composition and morphology. However, this attempt failed. Although the overall trend is that higher polynorbornene concentration gives more dark areas in TEM images, even 5 wt% polynorbornene sample has certain areas that look just like those containing 30 wt% polynorbornene. This phenomenon suggests that the composites are not homogeneous. Recall that, at the beginning, it was predicted that the composites might have some gradient structures due to simultaneous polymerization along with diffusion. The controversy between morphology and composition may be a proof of that prediction.

To assess the distribution of polynorbornene along the diffusion direction, attenuated total reflectance infrared (ATR-IR) on intersections cut from the composite samples was conducted. Although ATR-IR is a nice tool to probe surface functionality, it can not measure the interface directly. The simplest way is to cut the sample open, turning the interface into surface. Polynorbornene has vinylene groups along backbone. The cis sp^2-carbon hydrogen bending shows up at 966 cm^{-1}, while PMP has no absorption in this region. Thus this specific peak is a good reference to monitor the change of polynorbornene concentration. Figure 3.16 shows three PN/PMP intersection spectra with one pure polynorbornene spectrum and one pure PMP spectrum. The first spectrum is for polynorbornene, and the last one is for PMP. The second spectrum was recorded on a complete intersection of about 0.1 mm thickness. The third and fourth

spectra were recorded on the same section, but the edges of that section were sequentially removed. These edges are actually surfaces of the composite samples, which are supposed to contain more polynorbornene if there is gradient along the diffusion lines. It is obvious from these IR spectra that the concentration of polynorbornene is highest near the surface of the PN/PMP composite and lowest in the interior, indicating a gradient blend structure.

The ATR-IR technique mentioned above can only give a rough picture of the gradient structure because of sample preparation. Sequentially removing the edges of a small sample is extremely difficult when its width is reduced to only a few tenths of millimeter. However, IR-microscopy should solve this problem and give detailed information about local functional group concentration. Figure 3.17 is a series of IR spectra from a microscopy study on a thin section of PN/PMP sample with 23 wt% of polynorbornene. Each spectrum was recorded from a 120 × 90 μm window. The original thickness of PMP substrates is 0.8 mm. After norbornene polymerization, it increases to 0.9 – 1 mm. So the middle part of the sample should be in between number 5 and number 6. The spectra clearly show that polynorbornene concentration gradually decreases along the diffusion direction. The spectrum of edges does not fit well because of the bad baseline. Plus, recall that the samples were rinsed after catalyst embedding period. Thus near surface areas may have less catalyst left. To further reveal the gradient details, the window for IR measurement was reduced to 900 × 60 μm. Figure 3.18 shows a total of eighteen spectra on a complete thin sample section. Again, the gradient distribution of polynorbornene following diffusion direction is clearly observed.

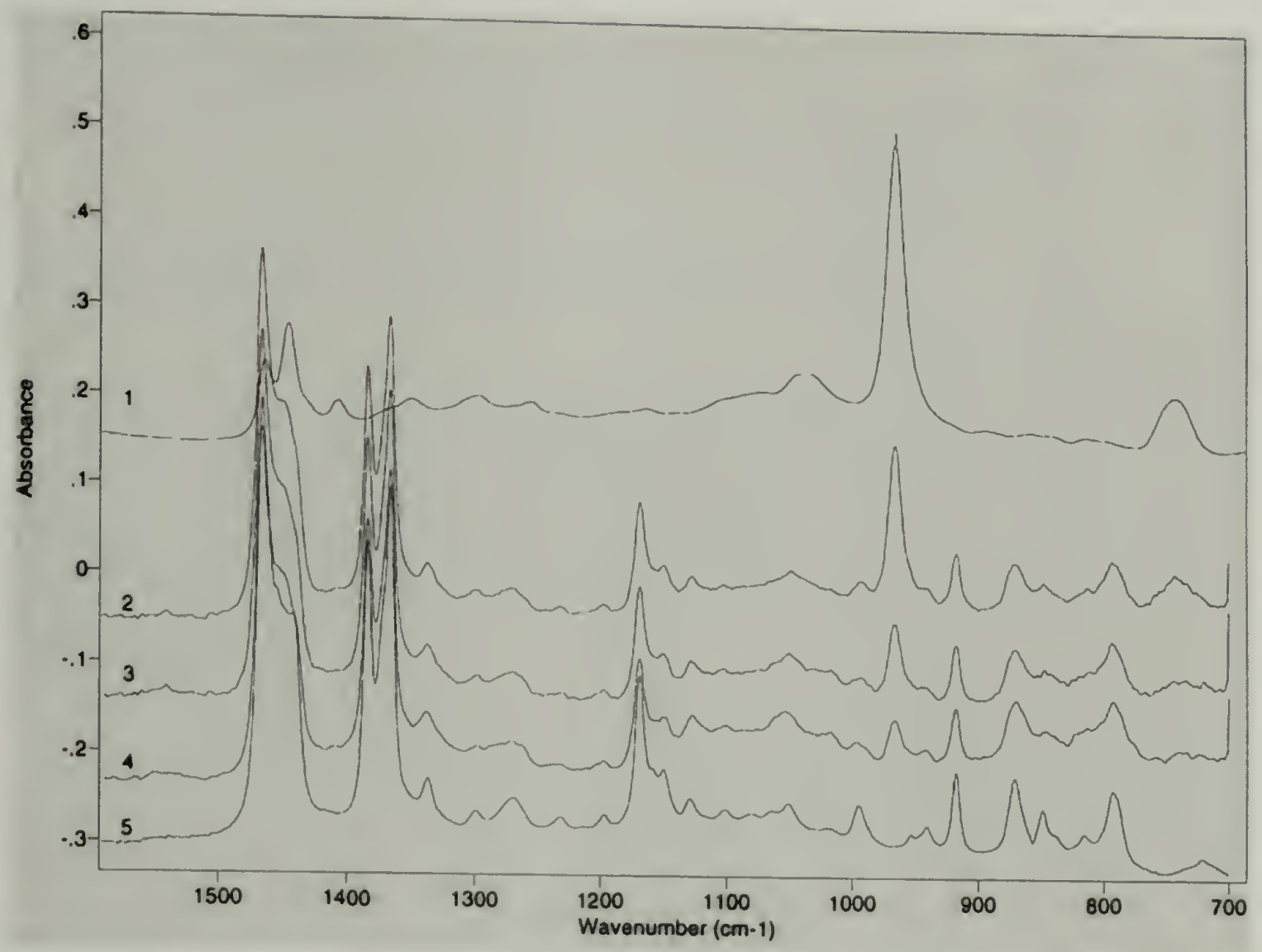

Figure 3.16: ATR-IR spectra of polynorbornene, PMP and the intersections of a PN/PMP composite containing 22 wt% polynorbornene. (1: polynorbornene; 2-4:shrinking intersections of PN/PMP; 5: PMP.)

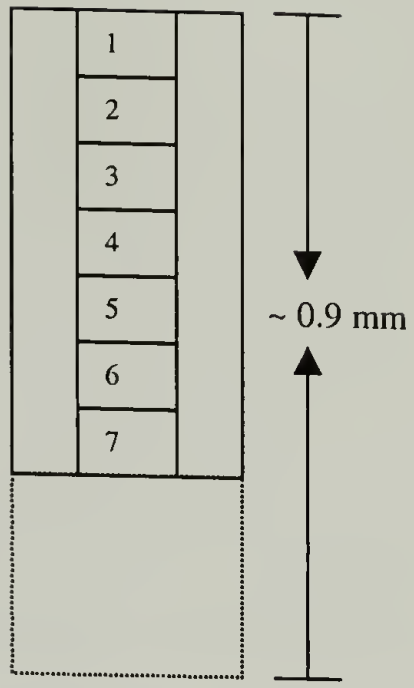

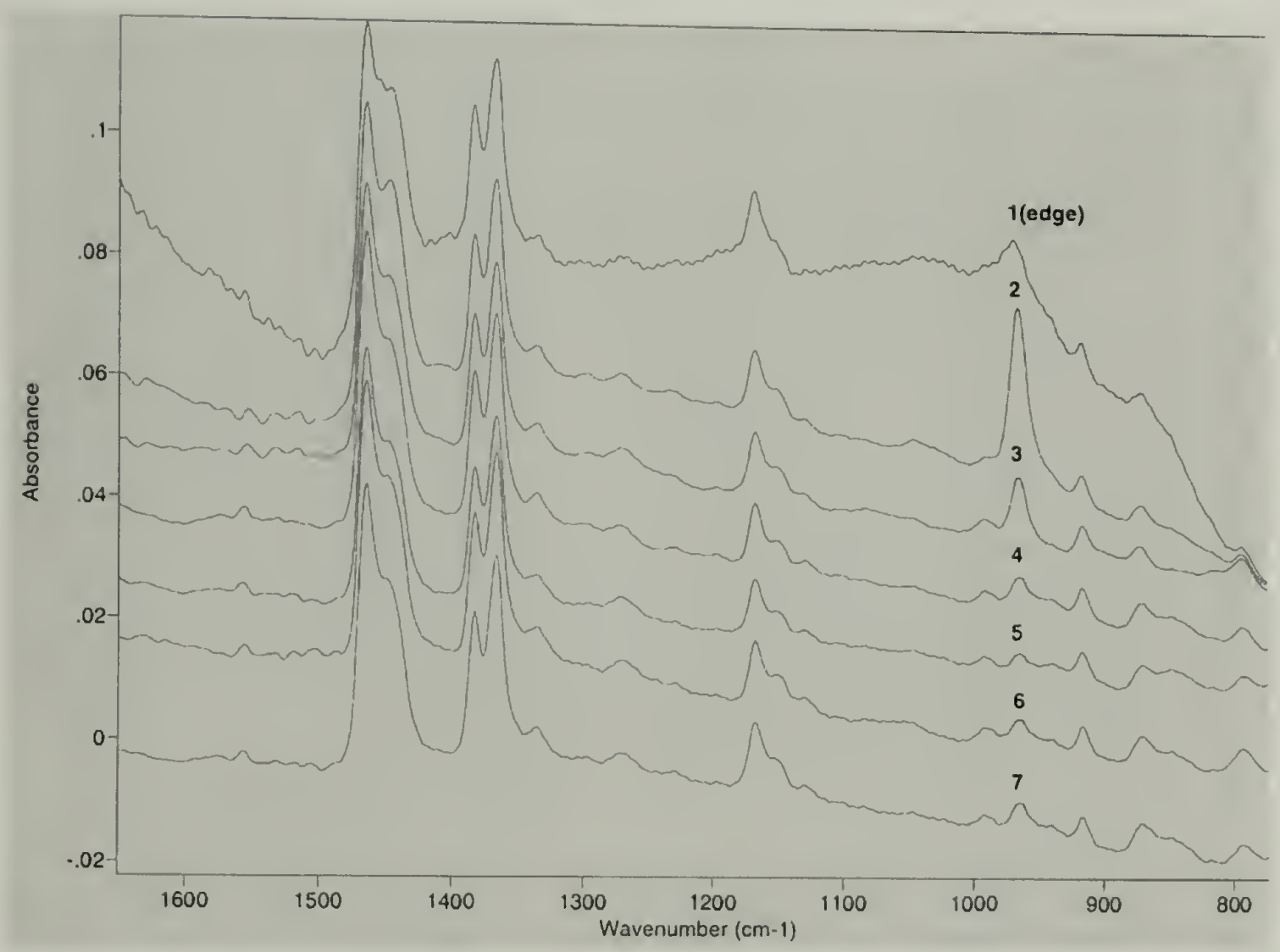

Figure 3.17: Microscopic-IR spectra of a PN/PMP composite containing 23 wt% polynorbornene. (IR window: 120 × 90 μm The image of sample section is shown on top.)

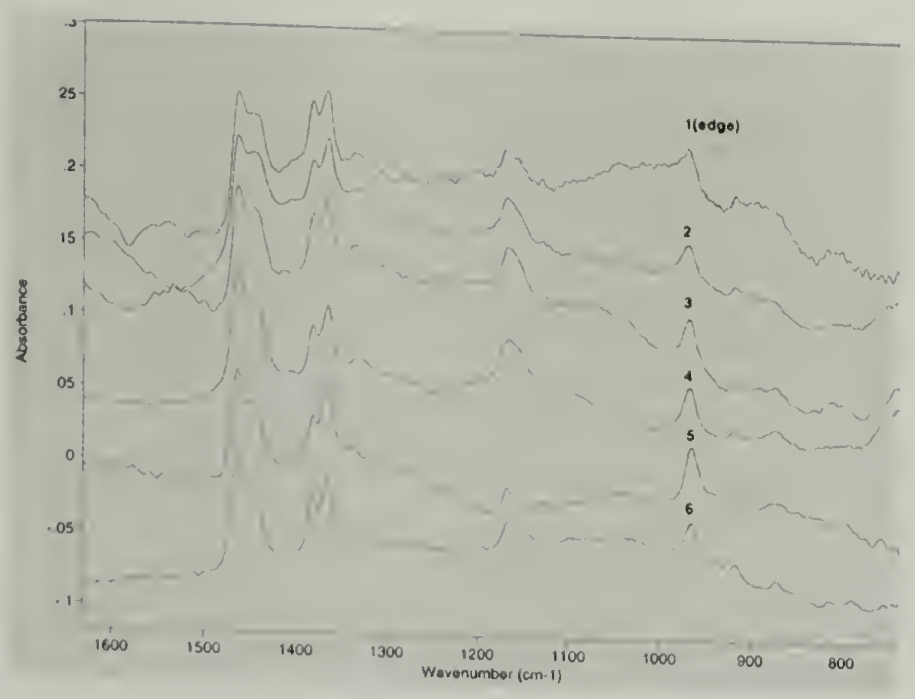

Figure 3.18: Microscopic-IR spectra of a PN/PMP composite containing 34.6 wt% polynorbornene. (IR window: 90 × 60 μm)

In spite of being a tool for local morphology study, TEM can also provide convincing evidence about gradient structures if the sample is prepared carefully. Using the cryomicrotoming technique, we successfully prepared an ultra-thin section about 400 μm long that was thin enough to get clear TEM images. Figure 3.19 to3.21 illustrate the morphologic changes along the diffusion direction. Overall, this sample contains 34.6 wt% of polynorbornene. In the areas close to surface, polynorbornene domains (dark areas) are more than expected from overall concentration, and most of them are distributed inside of interlamellar regions, forming sheet-like nanostrucutres. As diffusion goes further, dark areas decrease accompanied by decreasing of sheet-like structures and appearance of some hundreds-of-nanometer size dark domains. These big domains normally contain one crystal plane in the middle. In the areas close to center, polynorbornene concentration is much less than overall value. Sheet-like structures almost disappear, replaced by small dark spots and a few big dark domains.

What contributes to these gradient structures? First of all, diffusion has to be a key factor. From the procedure of making these samples, two diffusion processes are present. In the catalyst-embedding process, Grubbs' catalyst has to diffuse into PMP's amorphous region. That can cause a gradient distribution of catalyst. In the later polymerization process, norbornene has to diffuse into PMP to meet the catalyst. This is another gradient source. Trying to single out either one and rule out another proves to be difficult. As to the catalyst distribution, we can measure the average catalyst concentration for the whole sample using elemental analysis for ruthenium. It is in the range of 100 – 200 ppm with huge uncertainties, ± 100 %. Even if the instrument errors

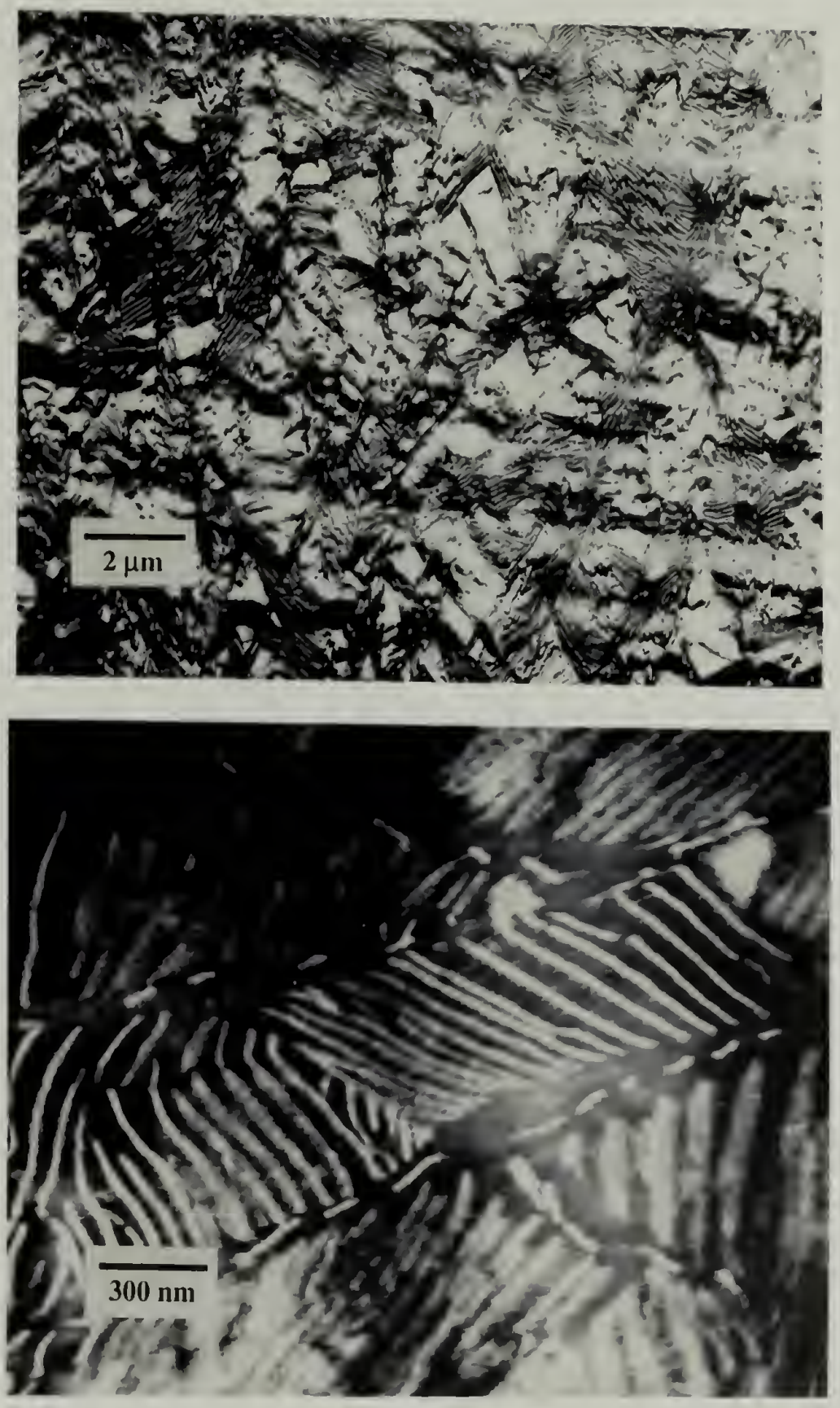

Figure 3.19: Gradient morphology of a PN/PMP composite with 34.6 wt% polynorbornene. A: close to surface.

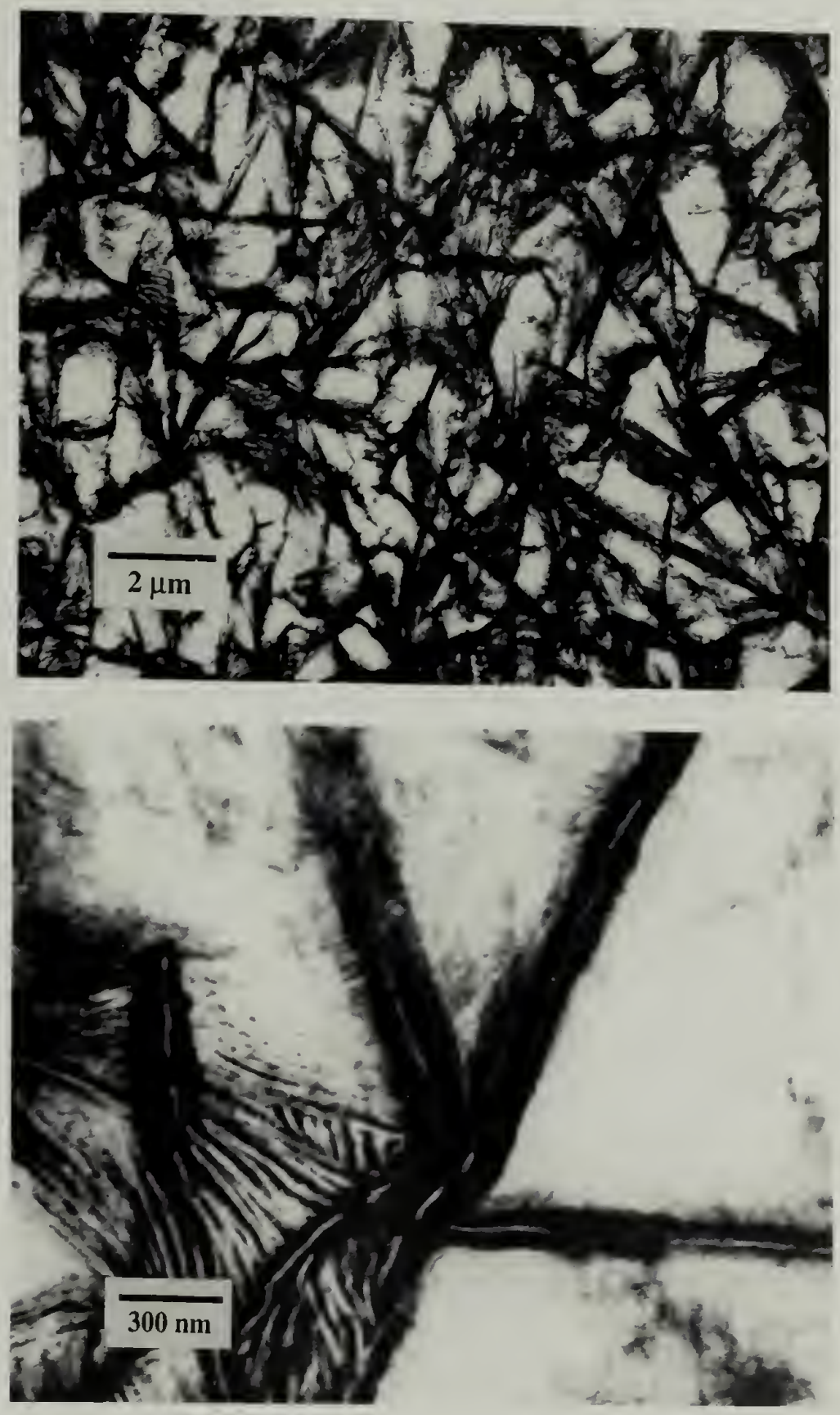

Figure 3.20: Gradient morphology of a PN/PMP composite with 34.6 wt% polynorbornene. B: between surface and center.

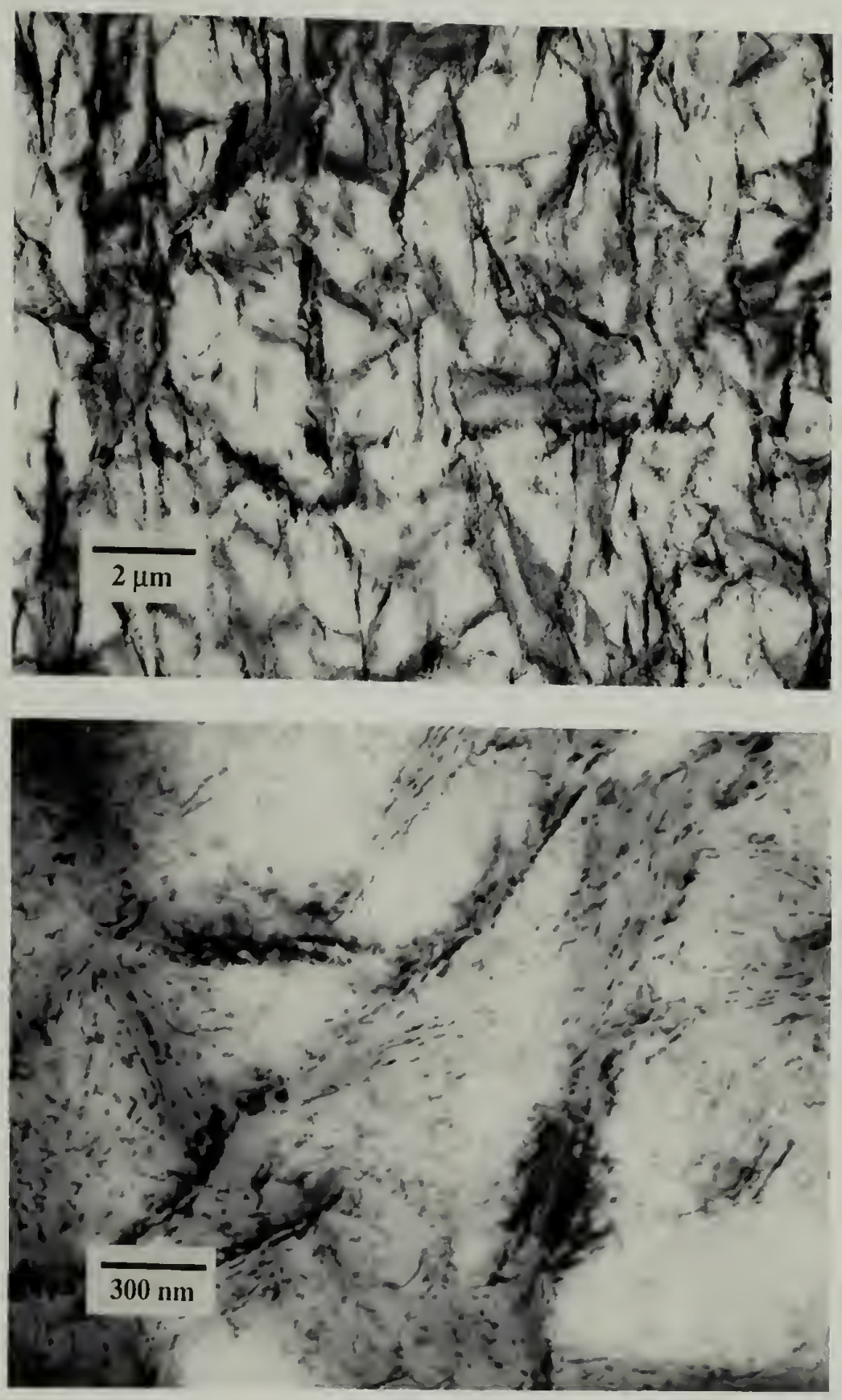

Figure 3.21: Gradient morphology of a PN/PMP composite with 34.6 wt% polynorbornene. C: close to center.

are disregarded, the local concentration is still undetectable. We can't perform local analysis because neither concentration nor absolute amount of catalyst satisfies the limitation of our instrument. Because of catalyst decomposition, removing catalyst effect by saturating the substrate with catalyst solution for long soaking period also failed. On the other hand, we can not equilibrate norbornene CO_2 solution in PMP before polymerization to remove the monomer diffusion effect. Norbornene polymerizes extremely fast with the Grubbs' catalyst. This problem will be solved in the next chapter when monomers other than norbornene are used in the study. At this stage, we have to say that catalyst distribution and monomer diffusion may both help to form gradient structure. Secondly, these diffusions are the essential requirement for gradient formation, but not the only requirement. The barrier property of the newly-formed polymer is also important. Only surface composites can be formed if the newly-formed polymer acts as a good barrier for further monomer diffusion, while a homogeneous composite is the final product if the newly-formed polymer has no barrier effect towards the monomer.

Here we should mention another unique aspect of our approach. Instead of trying to make polymers soluble in CO_2 like many other research groups do,[86,142] synthesizing CO_2-insoluble polymers are a key to get gradient nanostructures or any thermodynamically unstable structures. During diffusion and polymerization, new polymer has to precipitate to preserve the diffusion gradient. Otherwise, thermodynamic driving forces will result in homogeneous blends eventually.

3.4.7 WAXD and DSC studies of PN/PMP composites

Wide angle X-ray diffraction (WAXD) and Differential scanning calorimetry (DSC) experiments were conducted on virgin PMP samples and PMP samples after swollen in pure solvents (both methylene chloride and carbon dioxide) and dried. Both WAXD patterns and T_m are almost unchanged, which indicates that neither solvent gives irreversible changes on crystalline structure of PMP. Crystallinity of CO_2-swollen PMP increases slightly, which is due to some kind of annealing effect by CO_2.[41,108,137]

The WAXD and DSC studies on PN/PMP composites are shown in Figure 3.22 and Figure 3.23, respectively. Again, the diffraction pattern does not change. Peak position and width are the same for both pure PMP and PN/PMP composites, which means there is no polynorbornene deposited inside of PMP crystals. Crystallinity decreases solely because of the incorporation of fully amorphous polynorbornene. The glass-transition temperature for polynornornene is about 46 °C. However, DSC hardly detects it from a PN/PMP composite with 22 wt% polynorbornene. One possible reason is that, the chain mobility decreases due to the confinement of polynorbornene from PMP lamellae. We have not got into this issue deep enough to give a conclusive explanation.

3.4.8 Thermal behavior of PN/PMP composites

The thermal degradation of these PN/PMP composites is also interesting. Figure 3.24 shows thermal gravimetric analysis (TGA) results for PMP, PN and a PN/PMP composite. The curve for PN/PMP composite is not like a combination of the two individual polymers. Instead, it shifts to be almost the same as polynorbornene. To find

out reasons, we performed a TGA study on both catalyst-embedded PMP and a PN/PMP melt-extruded mixture (home-made samples), shown in Figure 3.25. Putting catalyst inside of PMP actually increases the onset temperature. Some kind of Ruthenium metal complex may stabilize PMP at early degradation stage, just like adding stabilizers to polymers to enhance thermal properties. This also explains why the onset temperature for PN/PMP composites is even higher than polynorbornene. Beyond this metal effect, we proposed another possible mechanism to account for the interesting thermal degradation behavior of our PN/PMP composites. Polynorbornene has double bonds alone backbone. When the temperature reaches the decomposition temperature of PMP, thermal induced homolytic cleavage of C-C bonds happens.[143] Instead of attacking PMP chains to degrade the polymer, the radicals easily abstract hydrogen from tertiary carbon atoms on the backbone of polynorbornene, forming more stable allylic radicals. Here polynorbornene acts as a radical stabilizer. In the melt-extruded blends case, polynorbornene and PMP do not mix well. The stabilization effect from polynorbornene is largely depressed. However, for our composites, these two polymers can reach tens of nanometer scale mixing. The chance for radicals to find polynorbornene is much greater. Someone may argue that conventional blends and our composites will become essentially the same above melting temperature of PMP because all the fine structures melt. From previous annealing studies, we did see the disappearance of tens-of-nanometer scale fine structures above melting temperature. However, the phase separation is still in the sub-micron scale, which is much smaller

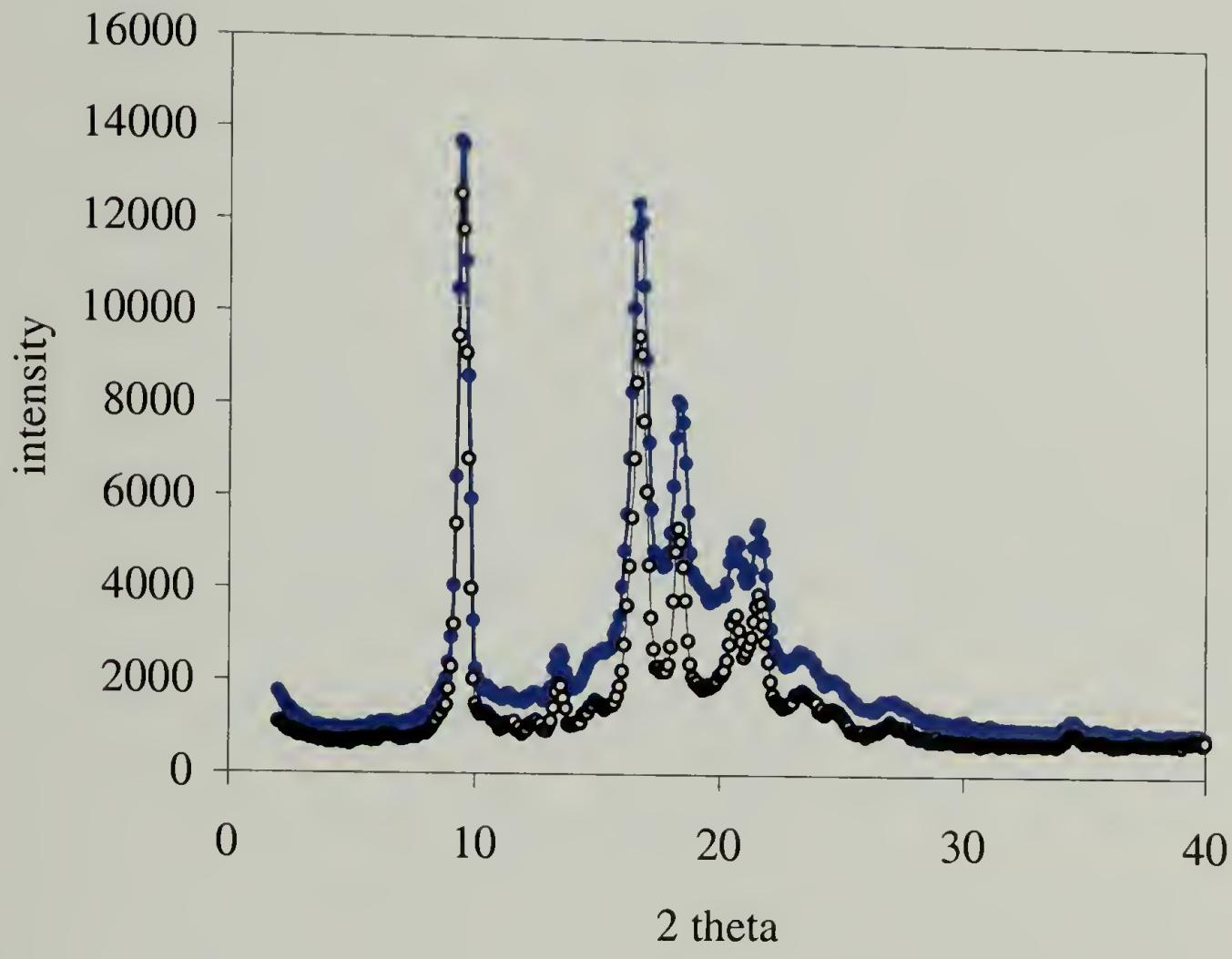

Figure 3.22: WAXD curves for PMP substrate (o), and a PN/PMP composite with 22 wt% polynorbornene (•).

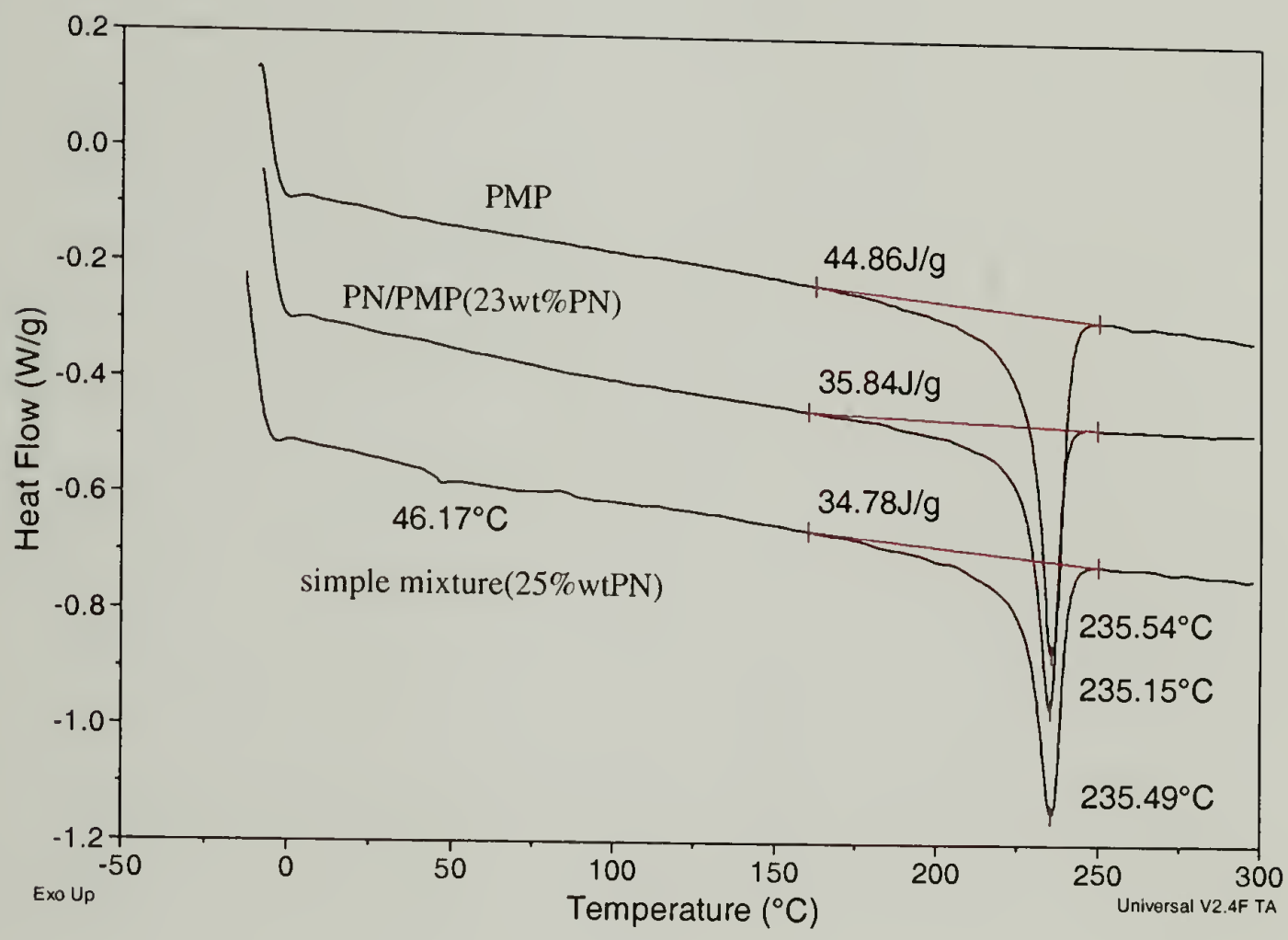

Figure 3.23: DSC diagrams for PMP, a PN/PMP composite with 23 wt% polynorbornene and a PN/PMP simple mixture with 25 wt% polynorbornene.

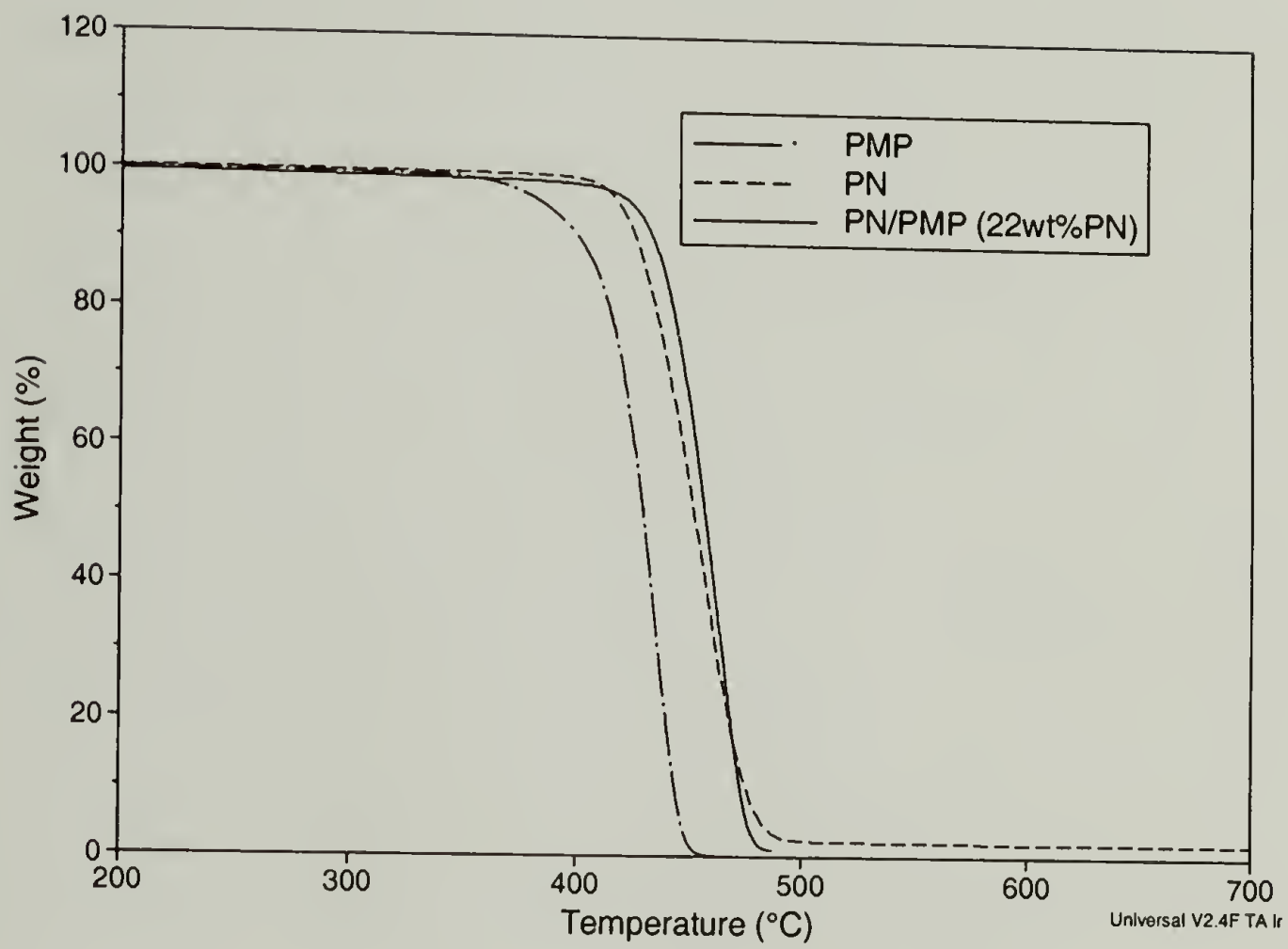

Figure 3.24: Thermal degradation behavior for PMP, PN, and a PN/PMP nanocomposite with 22 wt% polynorbornene.

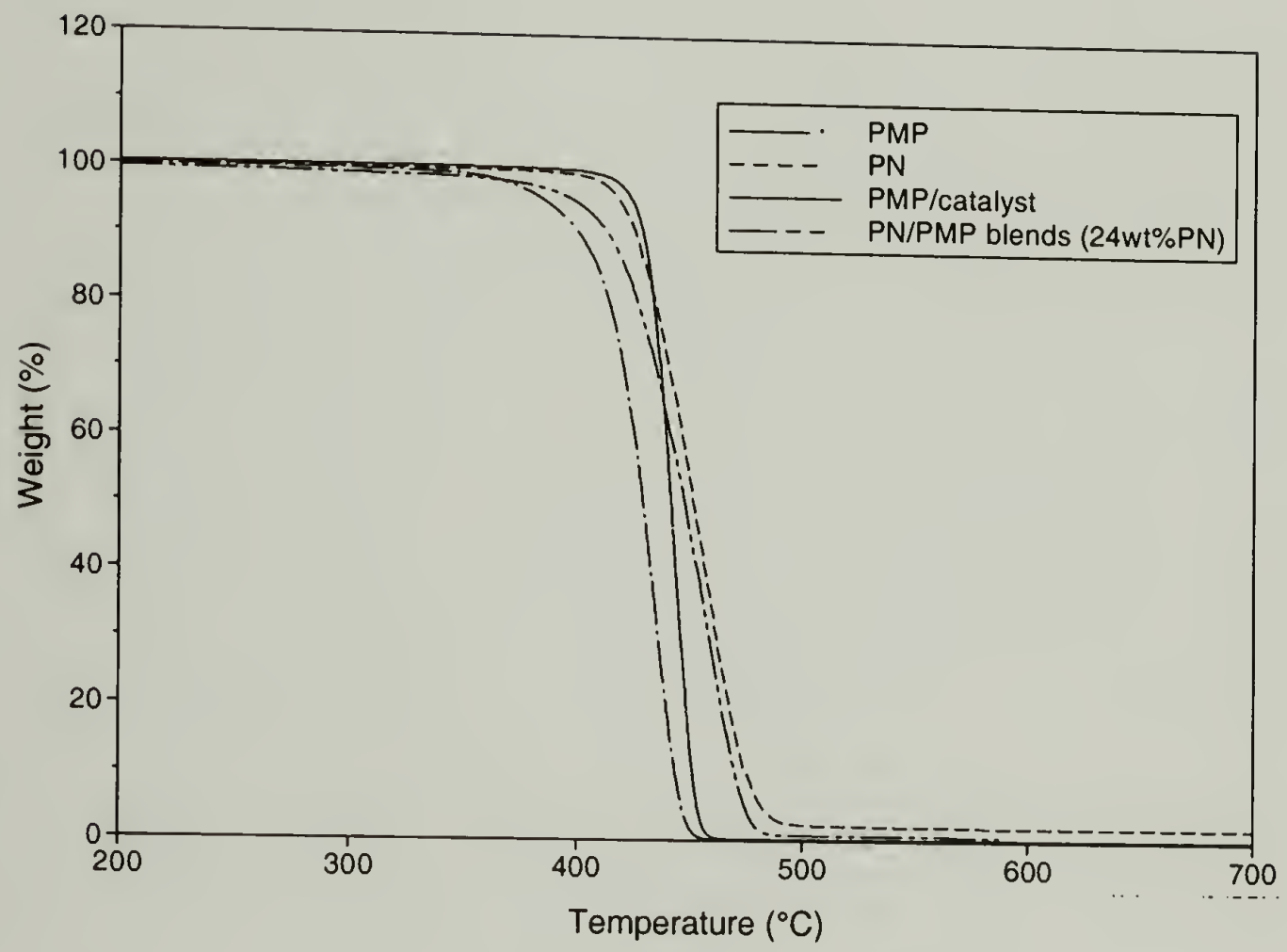

Figure 3.25: Thermal degradation behavior for PMP, PN, PMP with Grubbs' catalyst and a PN/PMP blend with 24 wt% polynorbornene.

than that of conventional blends. Plus, we noticed that the annealed samples still kept the original geometry, which means that the polynorbornene phase is probably continuous and has very high molecular weight (or is possibly crosslinked). It holds the structure even after PMP – the major component melts to liquid. Some TEM results from annealed sample show that even the gradient is preserved to certain degree. When PMP starts to degrade into volatile products, polynorbornene may still preserve the structure and retard the release of those gases. Polymer/clay nanocomposites show remarkable decrease of flammability due to this retardation effect.[144] Although they are inorganic/organic composites, and the length scale is much smaller, the size and geometry may have the similar effects on our system. To prove this proposed mechanism, more research need to be done.

3.5 Conclusions

Unique polymer/polymer composites were synthesized by performing ring-opening metathesis polymerizations inside of CO_2-swollen semicrystalline polymer substrates. At first glance, these are simple polymer blends because there is no covalent bond between the two polymers. Closer look shows that one polymer component is physically trapped in another's amorphous domains. Apparently, macro-phase separation gives up to micro-phase separation. Confinement from crystalline lamellae results in tens of nanometer-scale separation. In another word, semicrystalline PMP now acts as a nanotemplate. The whole process is to turn a nanocomposite of crystalline PMP with amorphous PMP into another nanocomposite of crystalline PMP

with polynorbornene and amorphous PMP mixture. We believe it is the first observation that one polymer's crystalline lamellae can be mixed with another polymer to get nano-blends. Both Infrared spectroscopy and TEM reveal the gradient structure of these nanocomposites. The polynorbornene concentration is the highest near the surface, and gradually decreases along the diffusion direction. Because the reactions were done in two steps, Either catalyst diffusion or monomer diffusion or both affect the gradient formation. It is better understood in the next chapter.

This new class of polymer/polymer composites may have interesting properties due to their unique structures. We already illustrated their unusual thermal degradation behaviors. The composites that contain only about 20 wt% of polynorbornene degrade at a temperature slightly higher than polynorbornene's degradation temperature, which is about 20 °C higher than PMP's. Not only for application purposes, these polymer/polymer nanocomposites are of interest for some fundamental problems too, such as confinement effects on glass-transition temperature, on polymer mixing and thermodynamics of polymer binary system. Furthermore, if we choose proper agents and reaction conditions, inorganic/polymer and metal/polymer nanocomposites can be synthesized as well using the same concept.

CHAPTER 4

SYNTHESIS AND CHARACTERIZATION OF POLYOCTENAMER/POLY(4-METHYL-1-PENTENE) AND POLY(DICYCLOPENTADIENE) NANOCOMPOSITES IN CARBON DIOXIDE

4.1 Introduction

In Chapter 3, we proved that semicrystalline polymers can be used as nanotemplates because CO_2 selectively transports materials into the amorphous and interlamellar domains while leaving crystalline domains free. It was presented in the case of ring-opening metathesis polymerization of norbornene inside of catalyst-embedded, CO_2-swollen poly(4-methyl-1-pentene) (PMP). Remarkably, the newly-formed polynorbornene (PN) was indeed deposited only in PMP's amorphous and interlamellar regions, forming PN/PMP nanocomposites with tens of nanometer thick PMP crystalline lamellae dispersed inside of a polynorbornene/amorphous PMP mixture. Naturally, the next question is if it is a general method, or, how to expand this method to other systems. In the end of Chapter 3, it was envisioned that inorganic/polymer and metal/polymer nanocomposites can be synthesized by applying the same concept. In fact, even inside of the ROMP family, there are numerous monomers to choose to give a variety of products with different properties. In this study, we selected two different cycloolefin monomers, namely cis-cyclooctene and endo-dicyclopentadiene (DCPD), to perform the same ROMP reactions inside of CO_2-swollen PMP.

Other than exploring the scope of this approach, one reason for choosing these two is to study the mechanical behavior of this type of nanocomposites. Recently, there

are huge interests on the mechanical properties of block copolymers.[145,146] The main reason behind that is, block copolymers can undergo micro-phase separation, forming well-ordered nanostructure, such as, BCC spheres, hexagonally packed cylinders, gyroid, and lamellar structures. The equilibrium structure depends precisely on the ratio of molecular weights of the two polymer blocks. Because two polymer blocks are connected through covalent bonding, the interfacial adhesion is strong. Very promising mechanical properties have been reported for diblock copolymers.[147] Our composites have similar nanomter-scale phase separations through a totally different mechanism. The structures are similar to lamellar or gyroid type. It is interesting to see how it affects the mechanical behaviors of these nano-blends.

The polynorbornene/PMP nanocomposites studied in Chapter 3 do not show improved mechanical properties, possibly due to their close glass transition temperatures. The amorphous phase of PMP has a glass transition temperature of 35 °C while polynorbornene synthesized here is around 46 °C. By squeezing polynorbornene into PMP, the total free volume is reduced, and the materials become more brittle. Polyoctenamer (common name for the ROMP product of cis-cyclooctene) (PCO) with a T_g of –100 °C is an elastomer at room temperature. Poly(dicyclopentadiene) (PDCPD) is a highly-crosslinked thermoset. By incorporating these two materials into PMP using the same method, rubber/plastic and thermoset/thermoplastic blends were obtained, respectively. These are two big industrial polymer families with thousands of products and all kinds of applications.[102,148-151] Most of them are produced using blending methods, and their structure and morphology follow thermodynamic rules. The materials synthesized using our method are non-classic polymer blends with kinetically

trapped morphologies. Both polyoctenamer and poly(dicyclopentadiene) are present in the amorphous and interlamellar regions, forming diblock copolymer-like blends.

A detailed illustration of synthesis and industrial applications of polymer products from both cis-cyclooctene and endo-dicyclopentadiene[126] was presented in Chapter 3. Ring-opening metathesis polymerization of cis-cyclooctene in CO_2 using Grubbs' catalyst was studied by Fürstner and coworkers.[128] They found that the polymerization gave moderate molecular weight polymers with a PDI of 2.0. There was no report about ROMP of endo-dicyclopentadiene in CO_2 using Grubbs' catalyst.

4.2 Experimental section

4.2.1 Materials

Cis-cyclooctene from Aldrich was distilled from calcium hydride under nitrogen atmosphere. Endo-dicyclopentadiene was obtained from Aldrich, and used as received. Bis-(tricyclohexylphosphine)-benzylidineruthenium(IV) dichloride (Grubbs' catalyst) was obtained from Strem Chemical Inc. Methylene chloride was purified following a reported procedure,[133] and stored under nitrogen in a dark and cold area. Ethyl vinyl ether, tetrahydrofuran (THF), and methanol were obtained from Aldrich and used as received. Carbon dioxide (Coleman grade 99.99 %, Merriam Graves) was passed through activated alumina and Q-5 catalyst (Englehard Industries) to remove water and oxygen, respectively. A 100DM high-pressure syringe pump (Isco Inc.) fitted with a heating/cooling jacket was used to deliver CO_2 at the required pressure and temperature. Commercially available poly(4-methyl-1-pentene) (PMP) (Scientific Polymer Products

Inc., melt index: 26) pellets were melt-pressed into 0.8 mm thick plaques at 260 °C and 25,000 psi. The temperature was then lowered to 100 °C in air while maintaining the same pressure. When the temperature reached 100 °C, cool water was used to increase the cooling rate. After this process, the final PMP sample has a crystallinity about 70% by DSC (Differential scanning calorimetry). These plaques were subsequently cut into appropriate sized specimens, usually 20 mm × 8 mm. For those samples used later for tensile testing, the original size followed an ASTM type V geometry.

4.2.2 Composite synthesis

Scheme 4.1:

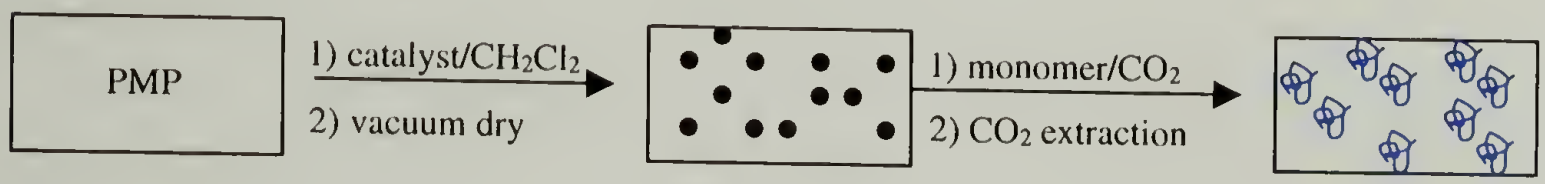

The synthetic procedure followed the one used in Chapter 3, as repeated in Scheme 4.1. PMP specimens were immersed in Grubbs' catalyst/CH_2Cl_2 solution at a given concentration for a period of time. After soaking, they were rinsed with CH_2Cl_2 to remove any surface adsorbed catalyst, and dried under vacuum to remove all solvent. These catalyst-embedded specimens were then sealed into stainless steel high-pressure vessels with ROMP monomers (cis-cyclooctene or endo-dicyclopentadiene). CO_2 was introduced to the vessels at desired temperature and pressure. Under the conditions used here, monomers and CO_2 mixed in seconds upon shaking, and remained as one phase. After a certain reaction period, CO_2 was slowly vented into ethanol, and the

specimens were extracted with CO_2 several times to remove all unreacted monomer. Ethyl vinyl ether was added at the same time to deactivate the remaining catalyst.

4.2.3 Characterization

Molecular weight measurements were made by gel permeation chromatography (GPC) with THF as the mobile phase and narrow molecular weight distribution polystyrenes as calibration standards. A Bio-Rad 175C FTIR was used to record transmission infrared spectra. Nuclear magnetic resonance (NMR) spectra were recorded using a Bruker 300 MHz NMR and $CDCl_3$ as solvent. Mass gain gave the average composition of the composites. Differential scanning calorimetry (DSC) measurements were carried out with a DuPont 2000 DSC under nitrogen flow at a heating rate of 10 °C/min. 61.9 J/g was chosen as the Heat of fusion (ΔH_f) of PMP, according to the literature.[130,131] Thermal gravimetric analysis (TGA) was conducted on a DuPont Instruments TGA 2950 at a heating rate of 10 °C/min to 600 °C under nitrogen. Wide angle X-ray diffraction (WAXD) was performed on a Siemens D500 diffractometer. Attenuated total reflectance (ATR) infrared spectra were recorded for both surfaces and intersections of samples. Transmission electron microscopy (TEM) was performed on a JEOL 100CX. Thin sections were obtained by cryomicrotoming samples at low temperatures, and stained using OsO_4 vapor for 4 hours. Scanning electron microscopy (SEM) was performed on a field emission JSM 6320F. Samples were coated with a thin layer of gold. IR-microscopy was performed at Markem Inc., Keene, NH. The instrument is a Mattson Galaxy 7020 with a Mattson Quantum IR microscope, and the transmission IR spectra were recorded from a rectangular window

of 120 × 90 μm. Tensile tests were performed at room temperature on an Instron 1123 operated at a crosshead speed of 5 mm/min. Tensile specimens were cut before the composites were produced with an approximate thickness of 0.8 mm in an ASTM type V geometry. The width and gauge length were re-measured due to the changing of specimen dimensions after reaction. Crosshead displacement was used for strain calculation.

4.3 Results and Discussion

4.3.1 General discussion about composite synthesis

As stated in Chapter 3, many reaction conditions have effects on the final composition of the composites. Among them, soaking time in the catalyst solution and monomer concentration in CO_2 are two most important factors. To simplify the study, all parameters in this study were kept unchanged except monomer concentration in CO_2. The soaking time in the catalyst solution was two hours, which gave the best result for the norbornene case in Chapter 3. Polymerization time was one day to ensure the reaction was complete. The catalyst concentration was usually about 11.5 mg/ml. Although it showed no sensitive effect on the final composition of PN/PMP composites, as illustrated in Chapter 3, it seemed that the catalyst concentration did affect the composition of polyoctenamer/PMP composites to certain degree. We did not perform a systematic study on this issue. Instead, we just kept the catalyst concentration constant for each batch.

Generally, increasing monomer concentration gave higher ROMP polymer content in the final composites. Figure 4.1 is a plot of final compositions of polyoctenamer (PCO) in the composites versus cis-cyclooctene monomer concentrations in CO_2. Obviously, a linear relationship is followed. In the experiments, the absolute

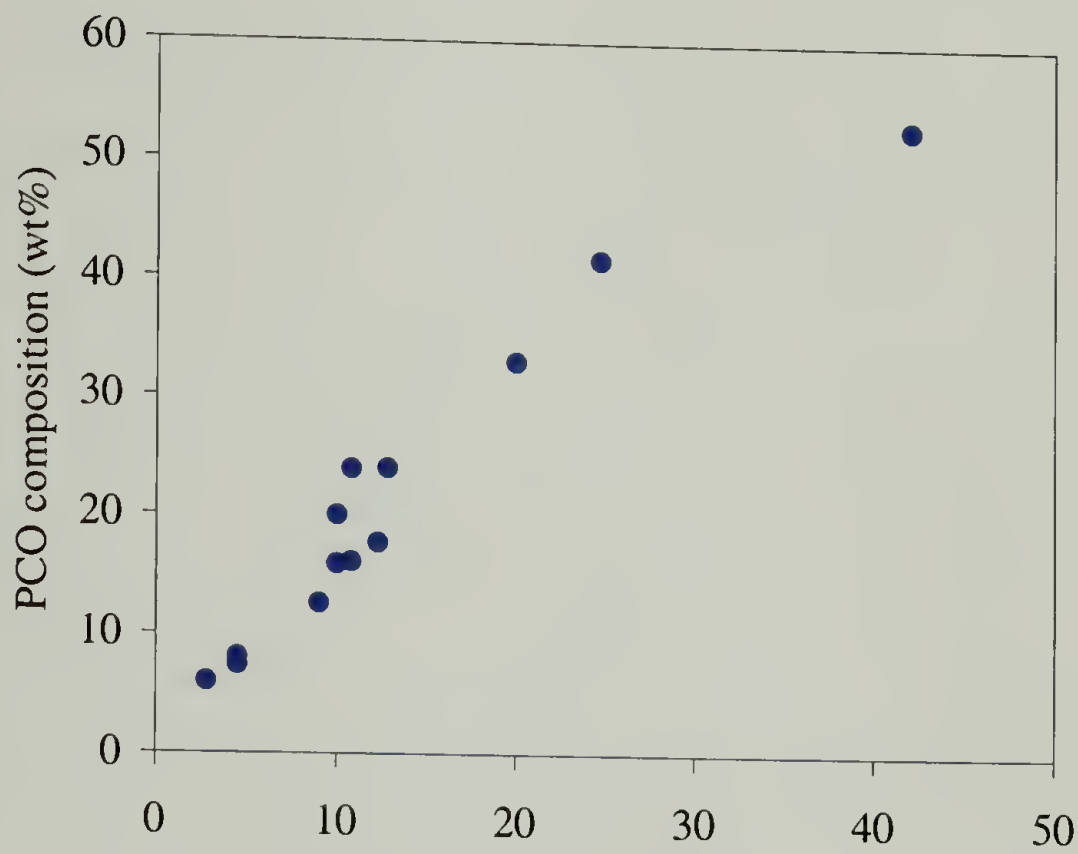

Figure 4.1: Polyoctenamer (PCO) composition in the final composites and cyclooctene concentration in CO_2. (Catalyst concentration is about 11.5 mg/ml.)

amount of monomer in the vessel was normally in excess to ensure enough monomer supply. Recall the difference between our approach and the IPN approach discussed in section 3.2. In our approach, CO_2 is the tool to carry materials into substrates. Monomer self-diffusion is negligible. As the concentration of cyclooctene increases, the self-diffusion of cyclooctene becomes more important. To distance us away from IPNs, most of the studies were carried out with a monomer concentration less than 20

wt%. In fact, the final composites often were distorted when the monomer concentration went too high.

Unfortunately, the experiments with endo-dicyclopentadiene(DCPD) met some difficulties. It appears that, for DCPD there is no good relationship between monomer concentration and final poly(dicyclopentadiene) (PDCPD) composition, which undermined the effort of a systematic study. Plus, it always needs a large excess of DCPD monomer to get a decent amount of PDCPD incorporation in PMP. Due to this fact, the major part of the following discussion is about polyoctenamer/PMP composites.

The appearance of these composites is also interesting. PDCPD/PMP is opaque, due to either crosslinked PDCPD or small cracking induced by CO_2 venting. Polyoctenamer/PMP (PCO/PMP) composites are still translucent. (PMP itself is transparent.) They have rubber-like appearance. The surface of PCO/PMP composites is covered by a thin layer of elastic polymer when the cis-cyclooctene monomer concentration is high. This polymer layer proved to be polyoctenamer by IR and NMR. In this case, cis-cyclooctene acts as a cosolvent. When the concentration of cis-cyclooctene in CO_2 is high, it can actually extract some catalyst out before high molecular weight polymer is formed because the ROMP of cis-cyclooctene by Grubbs' catalyst is slow. However, it is only a thin layer. After peeling off this layer, ATR-IR did not detect polyoctenamer signals on the surface, which means that there is no PCO chains penetrate the PMP surface. The skin layer of PMP with no second polymer still exists, as illustrated in section 3.4.3. ATR-IR studies on PDCPD/PMP also show no PDCPD near the surface.

The attempt of extracting out polyoctenamer from composites to study the molecular weight and its distribution failed again. It means that the molecular weight of polyoctenamer in the PCO/PMP composites is very high. It may be even slightly crosslinked.

4.3.2 Homogeneous composites

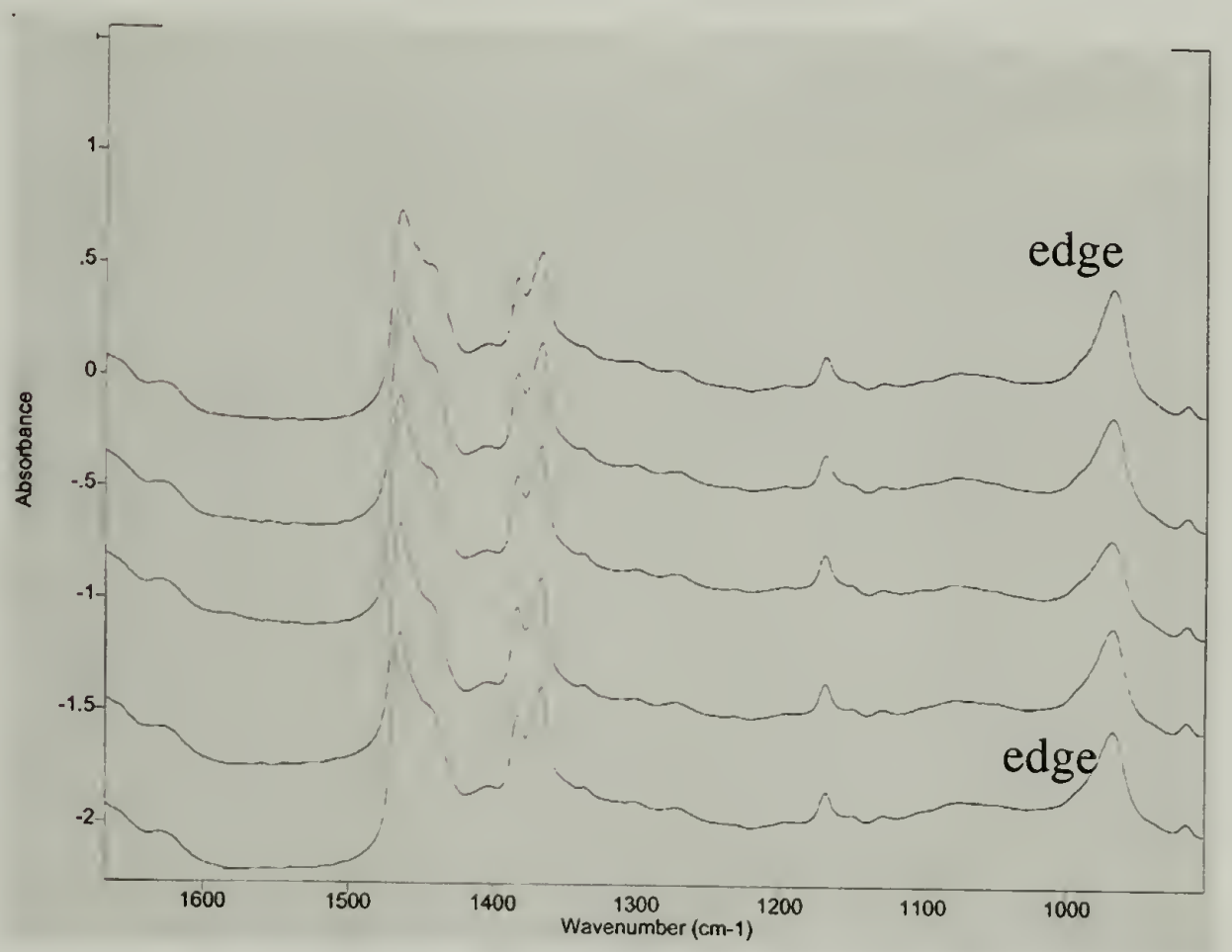

Figure 4.2: IR microscopy spectra of a PCO/PMP composite containing 53 wt% PCO.

Using the same method as in Chapter 3, IR Microscopy studies were conducted on polyoctenamer/PMP composites, as shown in Figure 4.2. The reference peak is still the absorbence of carbon hydrogen bending for the vinylene groups along the polymer backbond. Amazingly, there is no gradient detected. The distribution of polyoctenamer appears homogeneous. In the polynorbornene/PMP case, the distribution of polynorbornene shows a nice gradient along the diffusion direction. Why does the same

method give different results? We propose a mechanism to explain these observations. The final distribution of the second polymer inside of the substrate is controlled by three factors — monomer diffusion, polymerization rate, and the barrier effect of the new polymer. In the norbornene case, polymerization rate is very high. Grubbs; catalyst can polymerize norbornene in seconds. Thus, whenever norbornene meets the catalyst, high molecular weight polynorbornene is formed. And the polynorbornene hinders the further diffusion of norbornene to some degree, but does not totally block the diffusion. The result is a gradient distribution of polynorbornene along diffusion direction. On the

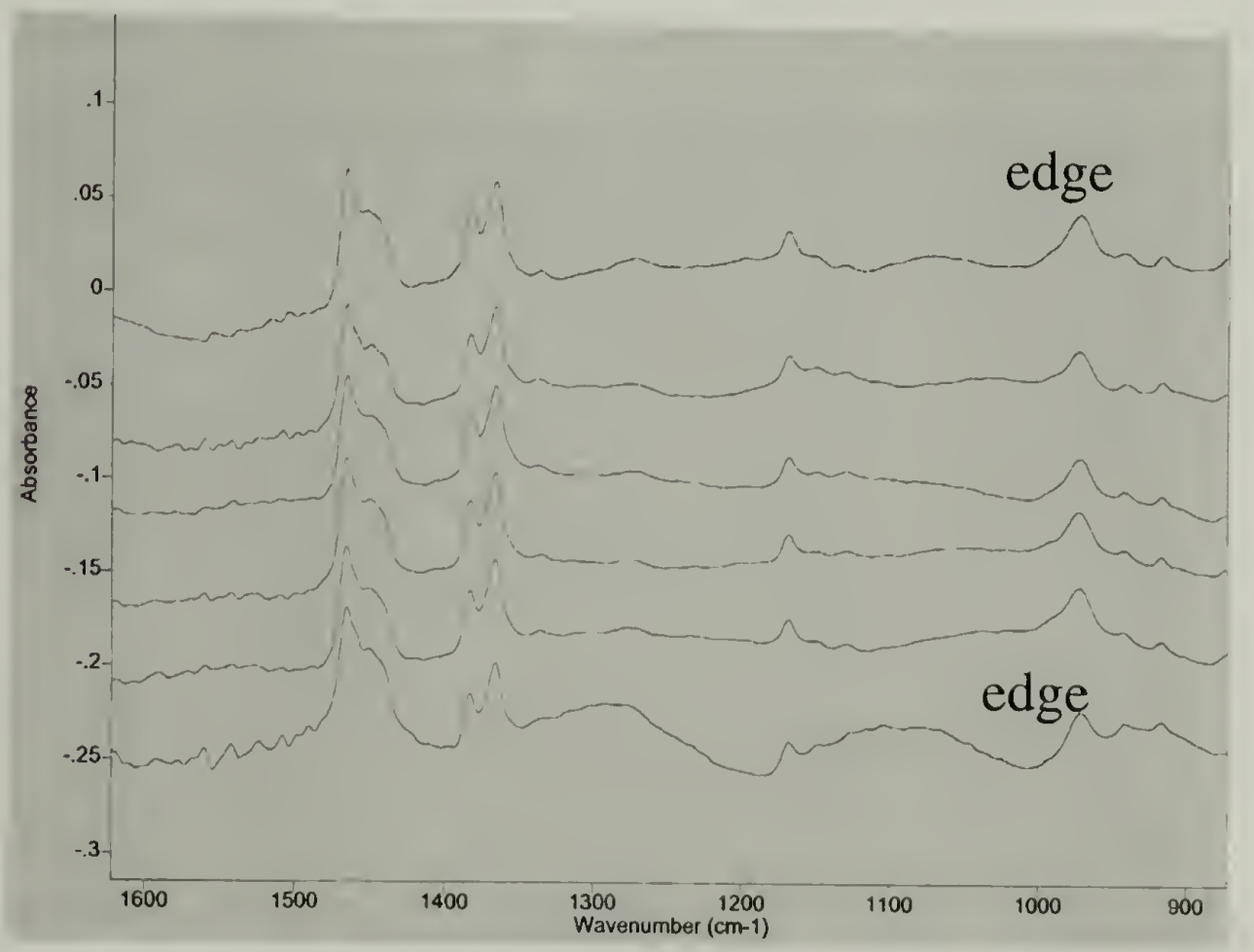

Figure 4.3: IR microscopy spectra of a PDCPD/PMP composite containing 30 wt% PDCPD.

other hand, the rate of cis-cyclooctene polymerization is slow, which means that the diffusion of monomer becomes relatively fast. High molecular weight polymer will not

form until most monomers diffuse into PMP. Plus, polyoctenamer is not a barrier for cis-cyclooctene molecules. Eventually, homogeneous composites are formed.

Additional crosslinking during polymerization makes the explanation for poly(dicyclopentadien)/PMP composites more complicated. Firgure 4.3 is the microscopic IR study. The sample appears homogeneous, no apparent gradient.

4.3.3 Nano-structure of PCO/PMP composites

Just like the polynorbornene/PMP case, ring-opening metathesis polymerization of cis-cyclooctene inside of CO_2-swollen PMP also gives tens-of-nanometer scale polymer blends due to the templating process. Figure 4.4 shows a series of TEM micrographs of PCO/PMP composites with 14.4 wt% of PN at different magnifications, all stained by OsO_4 vapor. The dark PCO domains and the white tens-of-nanometer thick PMP crystals are clearly seen in the pictures. Tie fibrils connecting two adjacent PMP lamellae are also visible at high magnification.

There are two unique features about the PCO/PMP nanocomposites. First, both PMP and polyoctenamer appear continuous. Remember this sample only contains 14.4 wt% of PCO. For a traditional polymer/polymer mixture, the minor component with 14.4 wt% composition always exists as separated phase. Our templating method provides a way to make non-classic materials. It is arguable that continuous morphology can be determined solely by TEM. A TEM image is a two-dimensional projection of a three-dimensional object. Other techniques are needed to reveal the true three-dimension structure. In the following discussions, more and more experiments,

nanocomposites, such as mechanical testing and annealing studies, confirmed the con-continuous nature of PCO/PMP.

Secondly, a hierarchical structure is present in the composites, which means mixing in several length scales. Figure 4.4 clearly shows that, on the micrometer scale, a picture of polyoctenamer in the PMP matrix says that it is a rubber-toughing system. When we focus on the polyoctenamer domains, there are many tens-of-nanometer thick PMP crystalline lamellae dispersed inside of polyoctenamer, which can be considered a crystal-reinforced rubber system. On the nanometer scale, there are tie-fibrils mixed with polyoctenamer in interlamellar regions. This kind of system should provide improved mechanical properties just as HIPS (high impact polystyrene) does. HIPS is synthesized by polymerizing styrene inside of lightly crosslinked polybutadiene. It involves grafting. The final morphology is spherical rubber domains dispersed inside of polystyrene matrix, while inside of each rubber domain, there are many small polystyrene microdomains. Upon damaging, this system generates huge numbers of crazes, and blocks the crack-growth. Figure 4.5 is a TEM image on a deformed HIPS sample.[152] As our PCO/PMP composites have similar dual-mixing morphology, we expect that they also will show interesting mechanical properties.

Since PCO/PMP composites are homogeneous, it is possible to compare different morphologies at different compositions. Figure 4.6 shows two TEM pictures for two composites containing 8 wt% and 24 wt% polyoctenamer, respectively. It is clear that there are more dark domains in the latter, and more PMP crystalline lamellae inside of the dark domains. Interestingly, the sample with 8 wt% polyoctenamer already

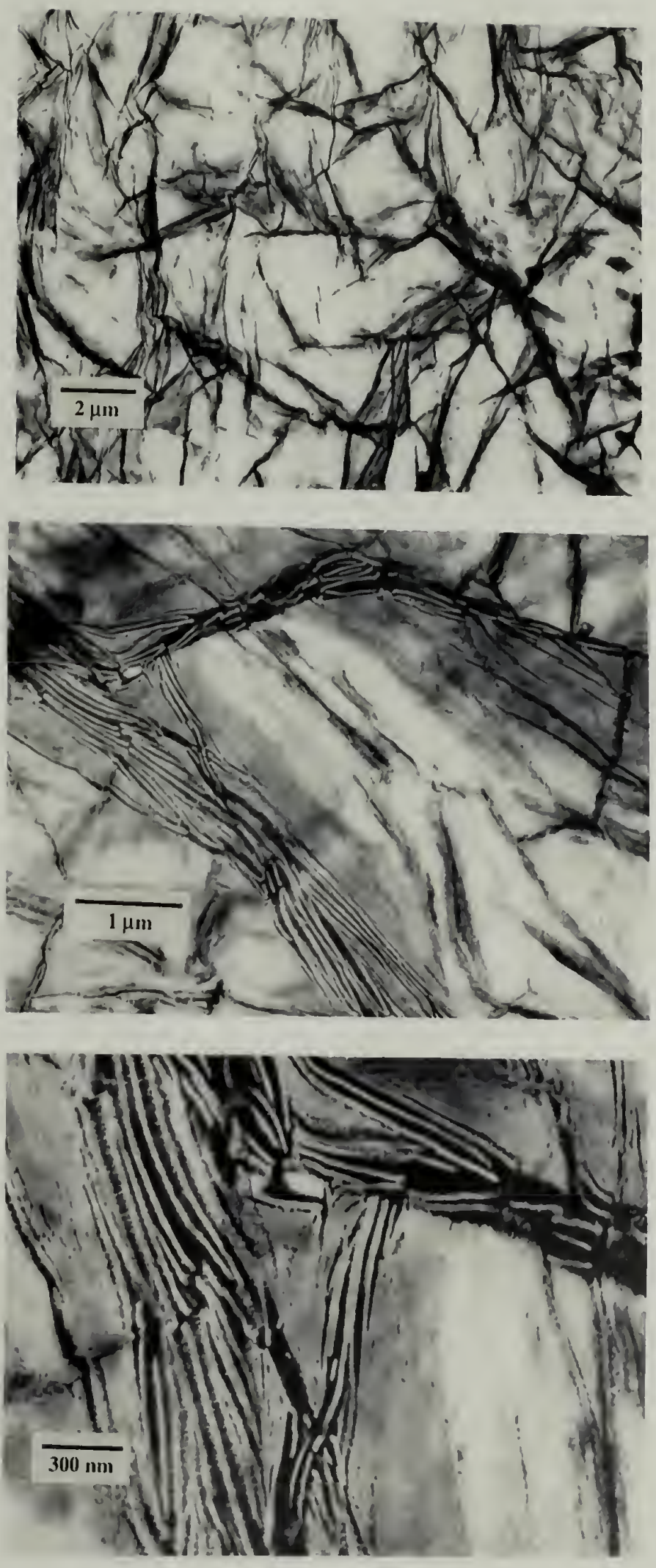

Figure 4.4: A series of TEM micrographs of a PCO/PMP nanocomposites with 14.4 wt% PCO.

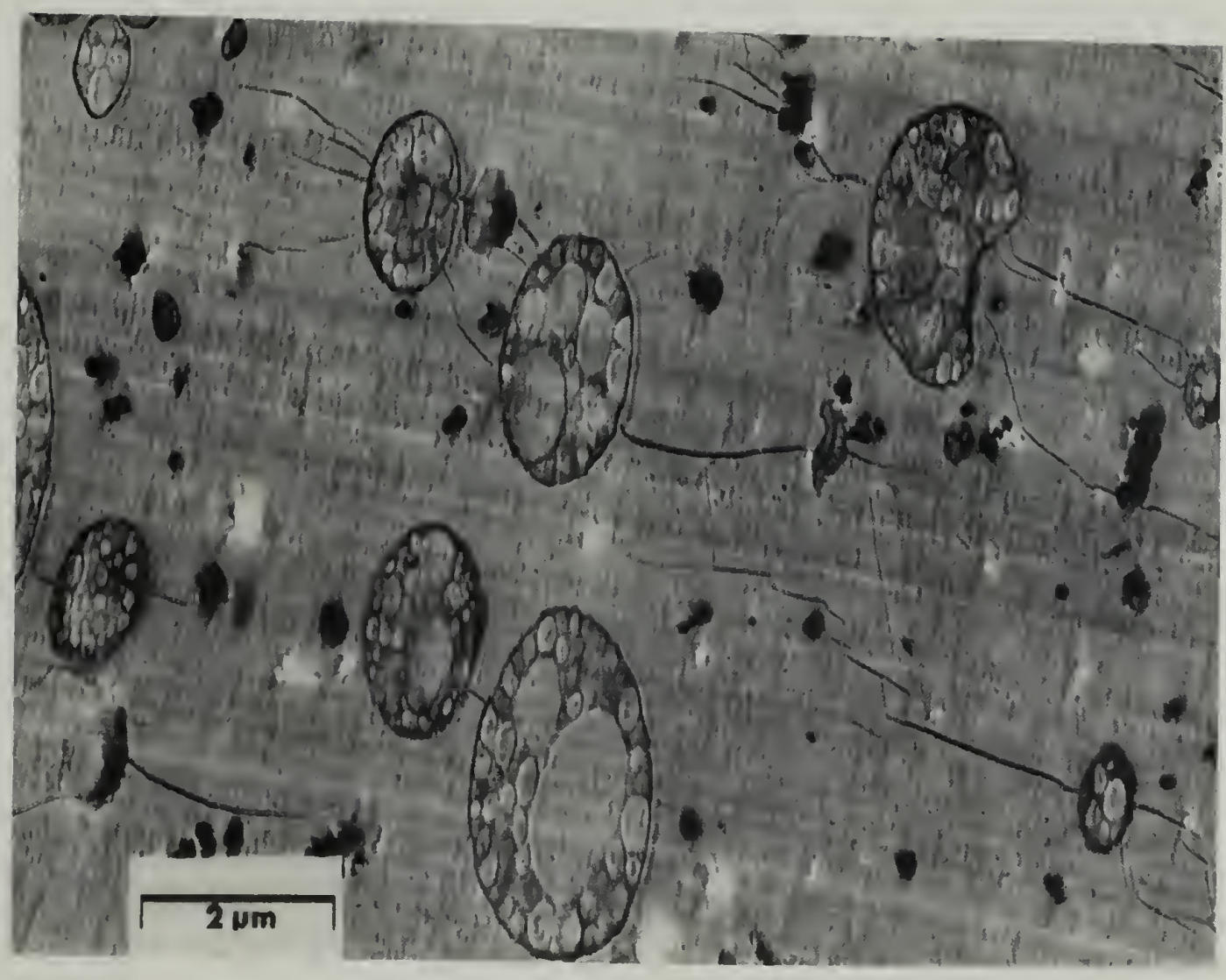

Figure 4.5: TEM micrograph of a deformed HIPS sample. (Black lines are crazes.)[152]

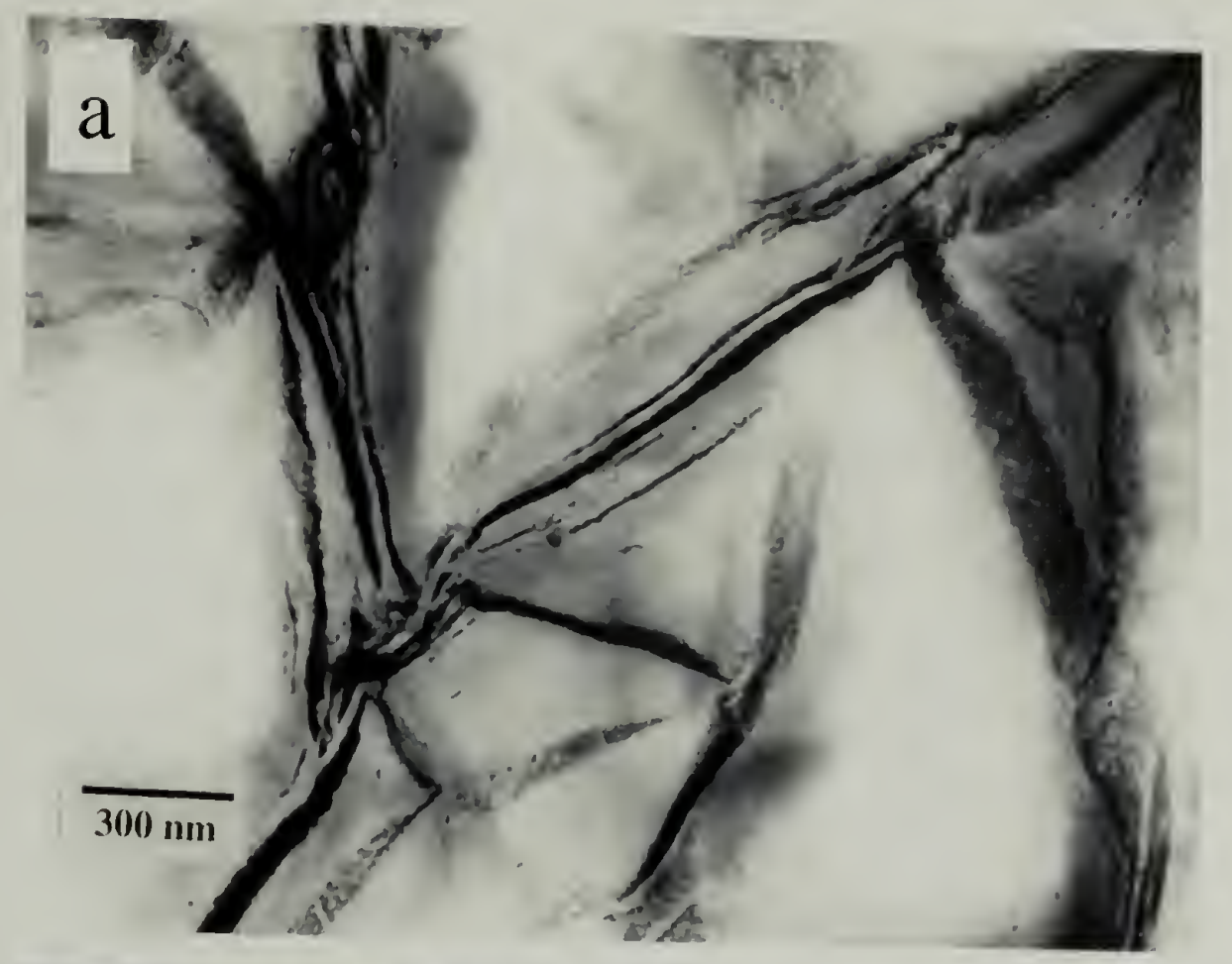

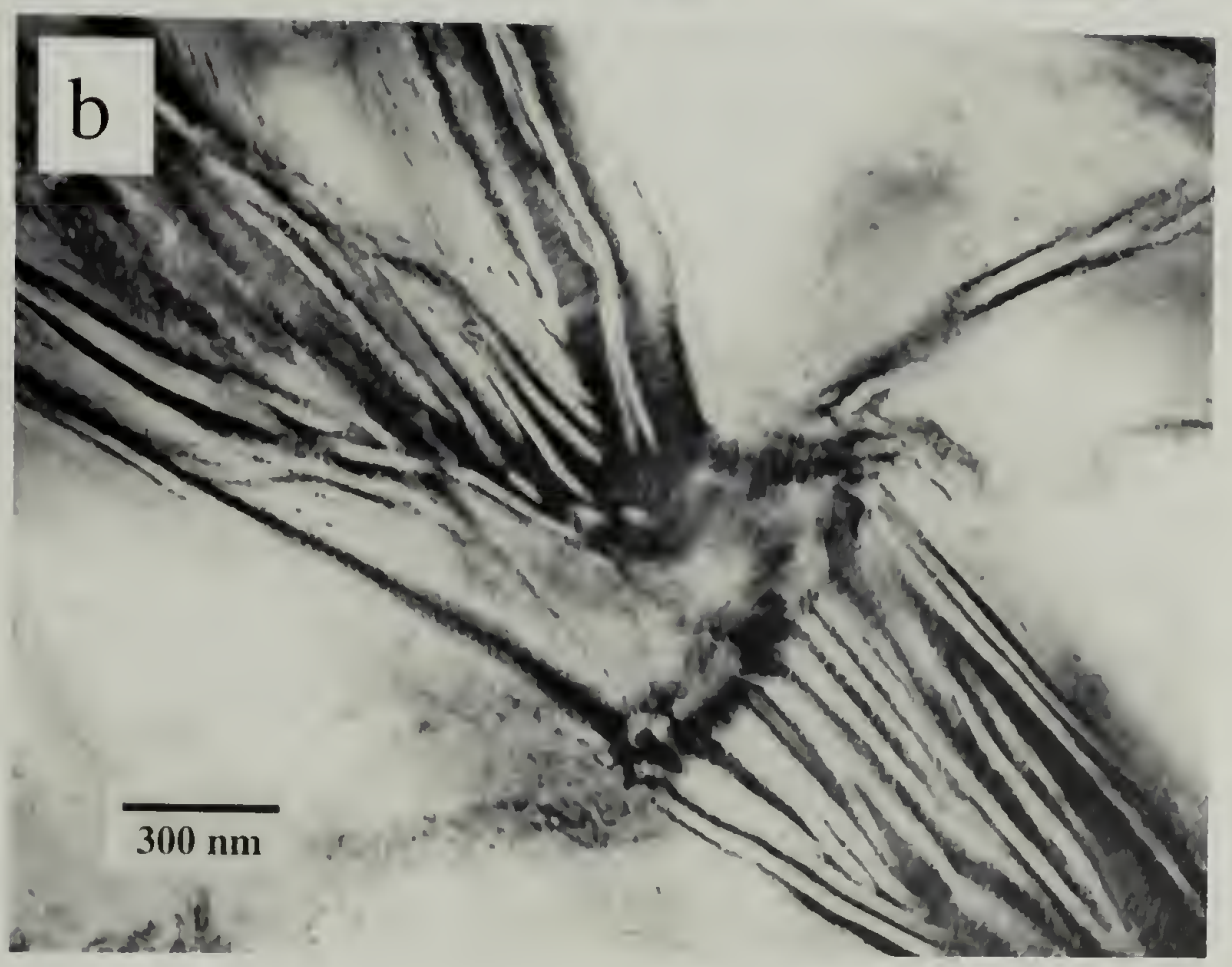

Figure 4.6: TEM micrographs of PCO/PMP nanocomposites with different composition. (a: 8 wt%; b: 24 wt%)

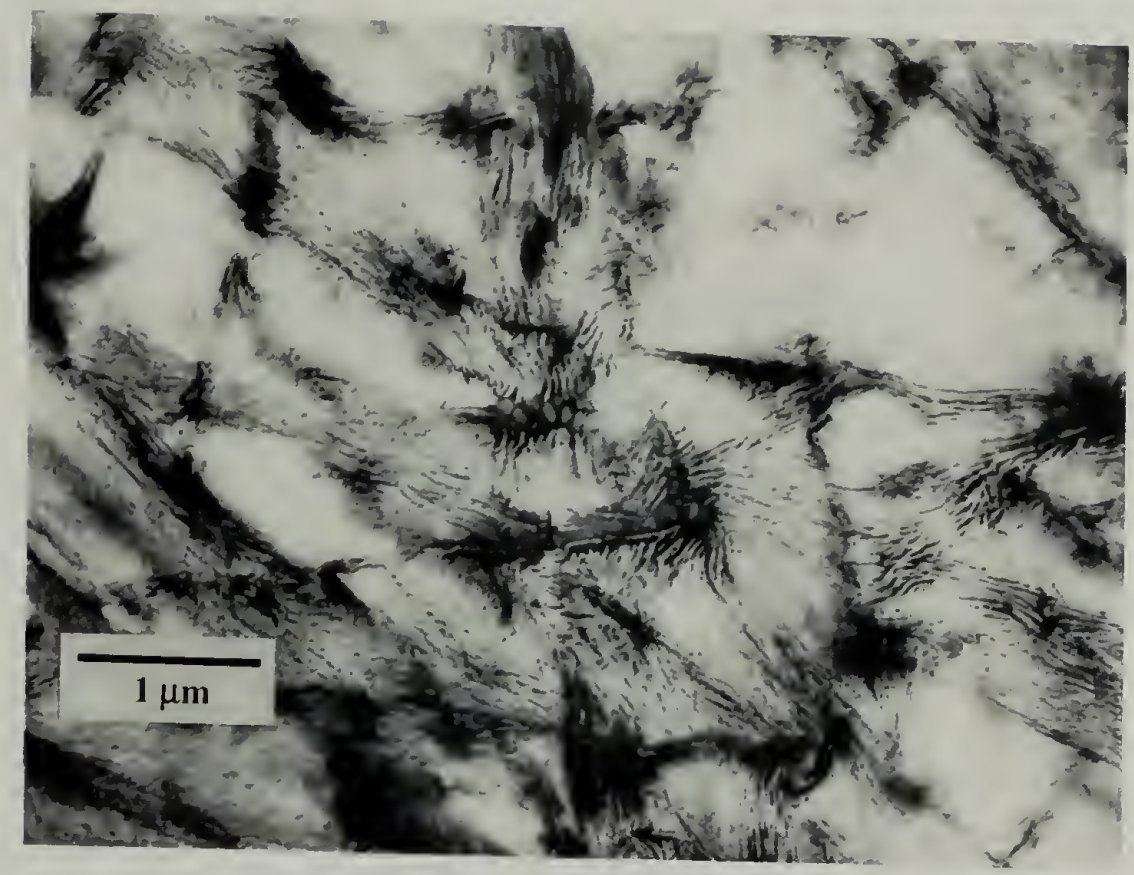

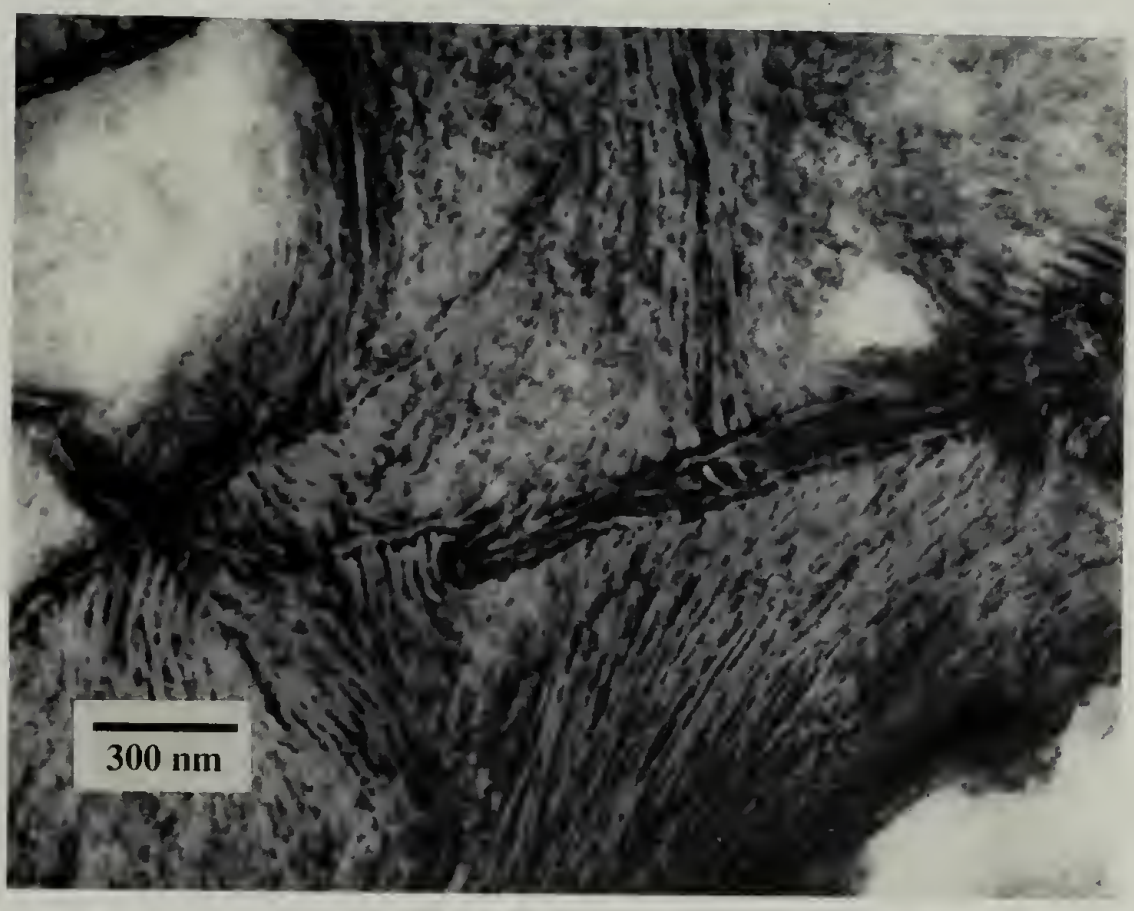

Figure 4.7: TEM micrographs of a PDCPD/PMP nanocomposite with 15.9 wt% PDCPD.

looks co-continuous. Because of the synthetic method, polyoctenamer precipitates in between lamellae, making it look as though growth occurs along the lamellae, forming the hyper-branched morphology.

4.3.4 Nano-structure of PDCPD/PMP composites

Poly(dicyclopentadiene) (PDCPD) also has double bonds along polymer chains. OsO_4 vapor will stain it to dark under electron beam while PMP is white. Figure 4.7 shows two TEM micrographs of a PDCPD/PMP composite with 15.9 wt% of PDCPD at different magnifications. The morphology is very similar to that of polynorbornene/PMP nanocomposites. All the PDCPD is deposited in the amorphous and inerlamellar regions. We believe it is the first example that a thermoset polymer can get into interlamellar areas, forming tens nanometer phase-separated blends.

4.3.5 Mechanical properties of PCO/PMP composites

4.3.5.1 Tensile testing

Figure 4.8 shows stress-strain curves of pure PMP and a polyoctenamer/PMP (PCO/PMP) composite with 24 wt% of PCO under tensile condition. It is surprising to observe that the strain at break increased from 100% to more than 500% with only 24 wt% of PCO incorporated, and the energy at break (toughness) increases about five times. The PCO phase has to be continuous to support this huge increase on maximum elongation. Wide angle X-ray scattering was performed on this damaged sample. There is no sign of drawing PMP during the tensile test. PMP itself should begin crazing in the early strain stage. However, due to the unique structure of the nanocomposites, the crazes in PMP are restricted locally by PCO rubbery phase, the catastrophic crack-

growth does not happen. The morphology studies in the following section provide us more evidences. Weidisch and coworkers studied the tensile properties of poly(styrene-b-butyl methacrylate) with different morphologies.[153] They observed higher tensile strength for co-continuous phase and much higher strain at break for perforated lamellar phase. Our PCO/PMP composites apparently are more close to perforated lamellae. Figure 4.9 showed the tensile modulus as well as the maximum strain vs. PCO composition. With the increase of PCO content in the composites, the maximum has a sharp increase, then reaches a plateau, while the tensile modulus decreases steadily. It fits into a rubber-toughening mechanism: Toughness increases with the trade-off of modulus.

We have a few comments on our tensile testing conditions. Because of the difficulty of the synthesis, it is difficult to get the exact same composition between batches. The values used in the analysis were from single measurements. There is no way to draw error bars, while the error may be big. Thus, the absolute value is not very trustable. However, qualitatively, the overall trend is very clear. The study did not go beyond 50 wt% of PCO. As we mentioned above, higher PCO incorporation needs higher monomer concentration. At a certain point, the monomer/CO_2 mixed solution began to have significant effect on substrate structure and catalyst extraction. That is where the study stopped.

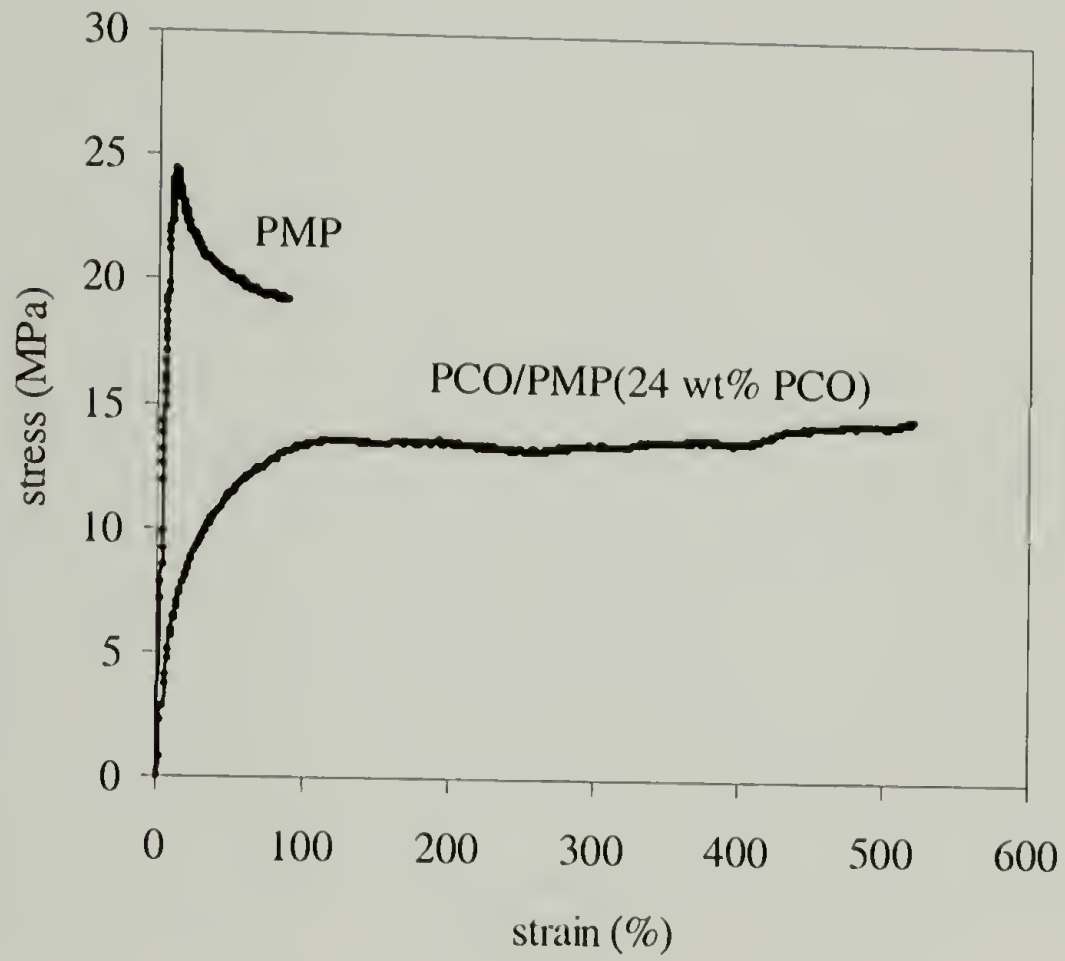

Figure 4.8: Strain-stress curves of pure PMP and a PCO/PMP composite containing 24 wt% of PCO under tensile condition.

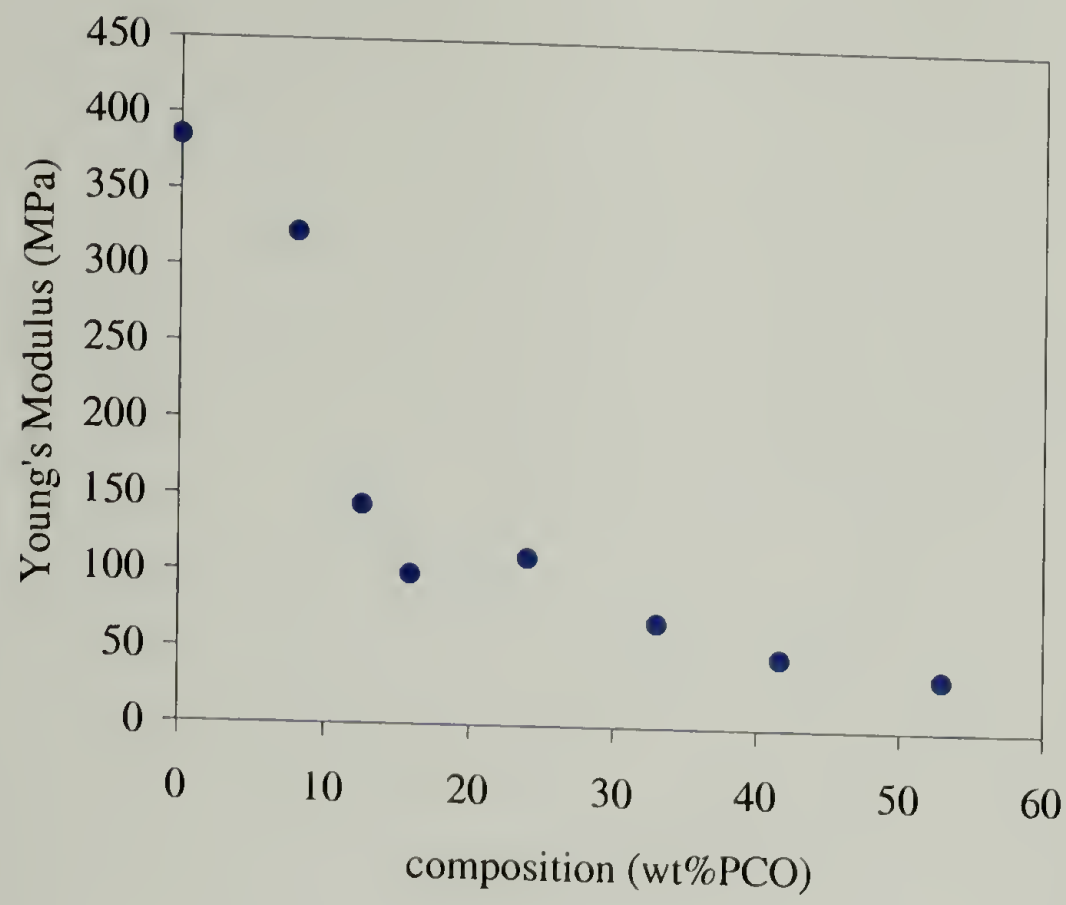

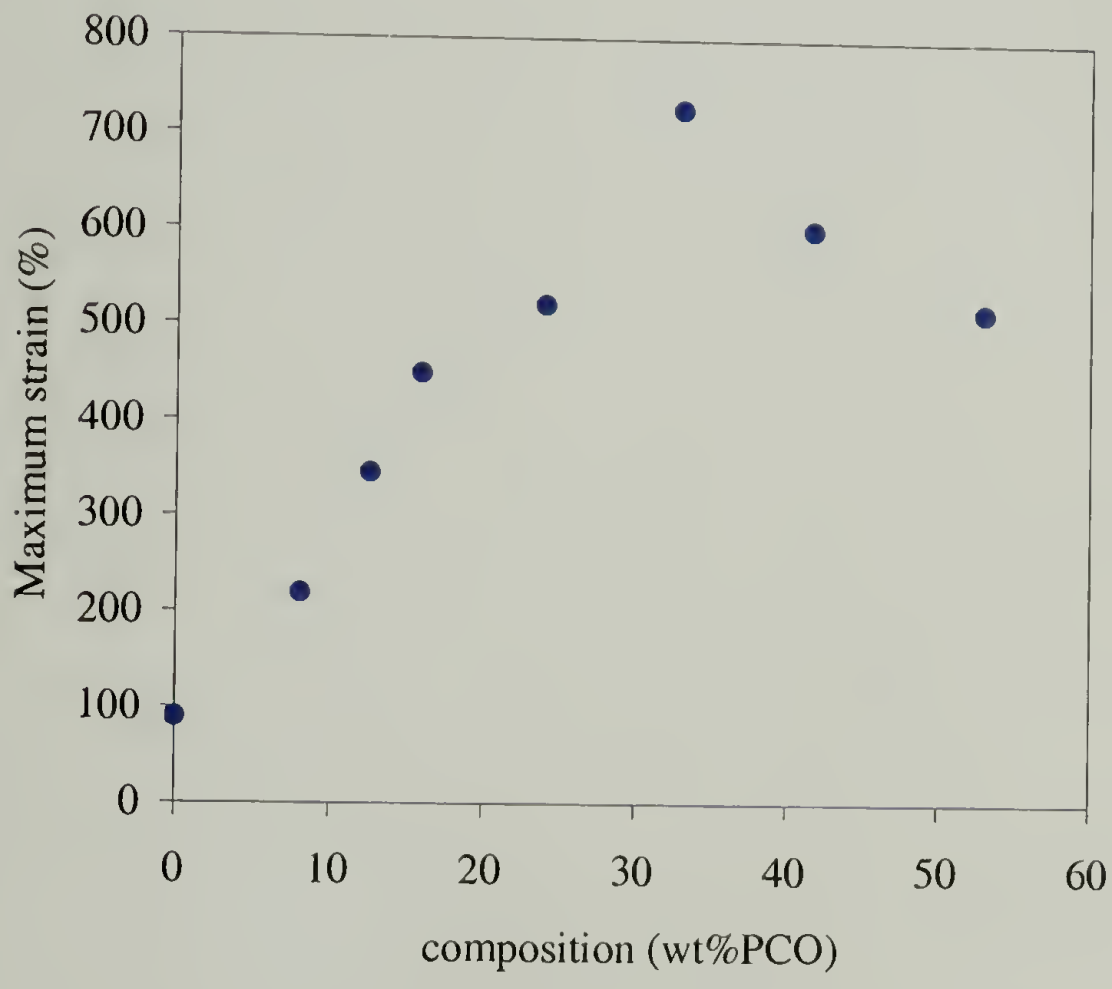

Figure 4.9: Plots of tensile modulus and maximum strain versus PCO composition in PCO/PMP composites.

4.3.5.2 Morphology study

Along with the mechanical testing, it is also important to look at the structure change during testing. Both transmission electron microscopy (TEM) and scanning electron microscopy (SEM) were used to study the deformed samples. Figure 4.10 shows TEM micrographs of a PCO/PMP composite containing 14.4 wt% PCO after it was broken at about 560% strain. Microtoming was performed along two directions, parallel to the tensile direction and perpendicular to it. From the "parallel-cut" picture, we can see that PCO phase became thinner and elongated along the tensile direction with a lot of micro-voids. Figure 4.11 is a high magnification image of the section. It is clear that the PCO elongated phase still contains PMP crystalline lamellae and some of the lamellae are actually broken. We also see black damage zones in the interface between the PCO phase and the PMP matrix. The "perpendicular-cut" also shows the thinned PCO phase, but the orientation is random worm-like. It also indicates that each PCO elongated phase is not like a fiber, but a twisted sheet.

After the samples were broken under tensile testing, we study the fractured surface using SEM. Figure 4.12 are SEM images of the fractured surface of both pure PMP and a PCO/PMP composite with 14.4 wt% PCO. PMP was stretched to 100% before break while the composite was stretched to about 560% before break. The fracture of PMP follows the typical crack-growth mechanism while with 14.4 wt% of PCO incorporated, the fracture mechanism changes to microshearing.[154] It is largely due to the presence of low modulus PCO in a continuous (or semi-continuous) fashion.

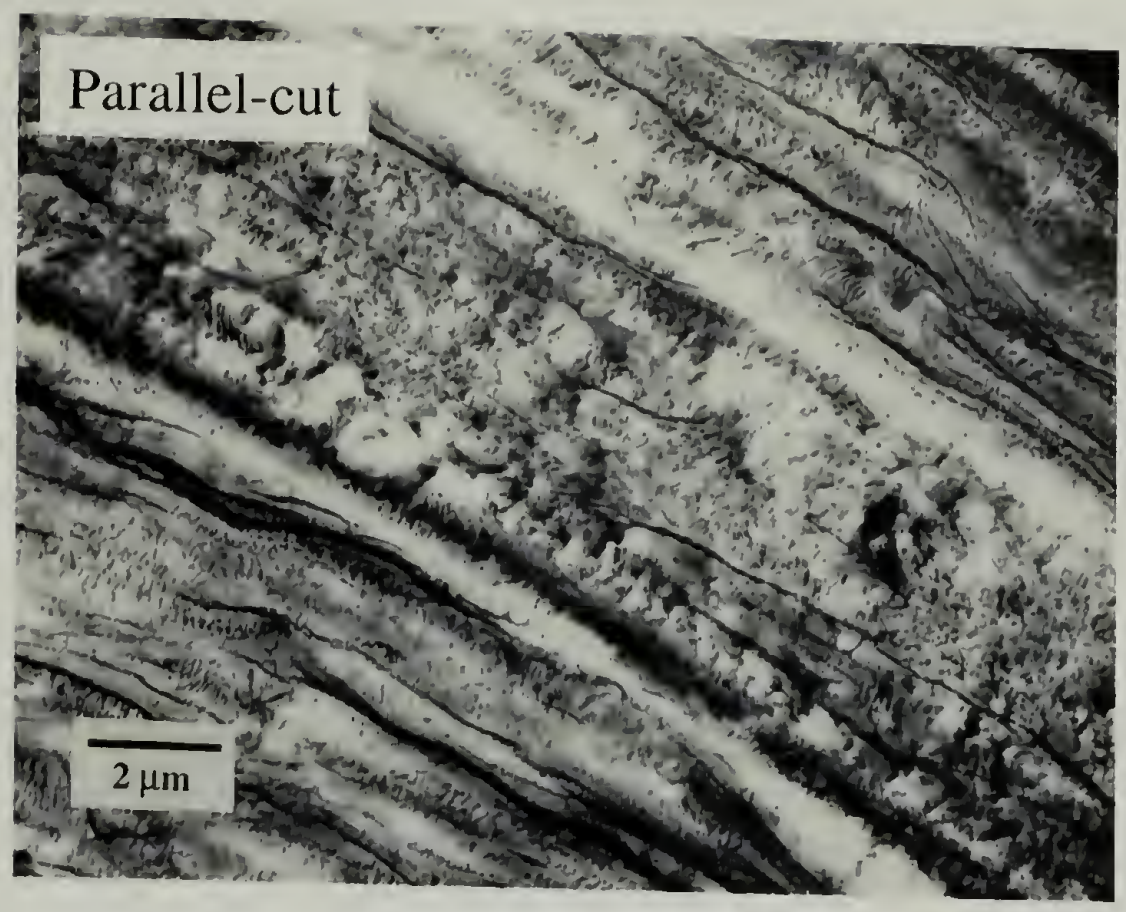

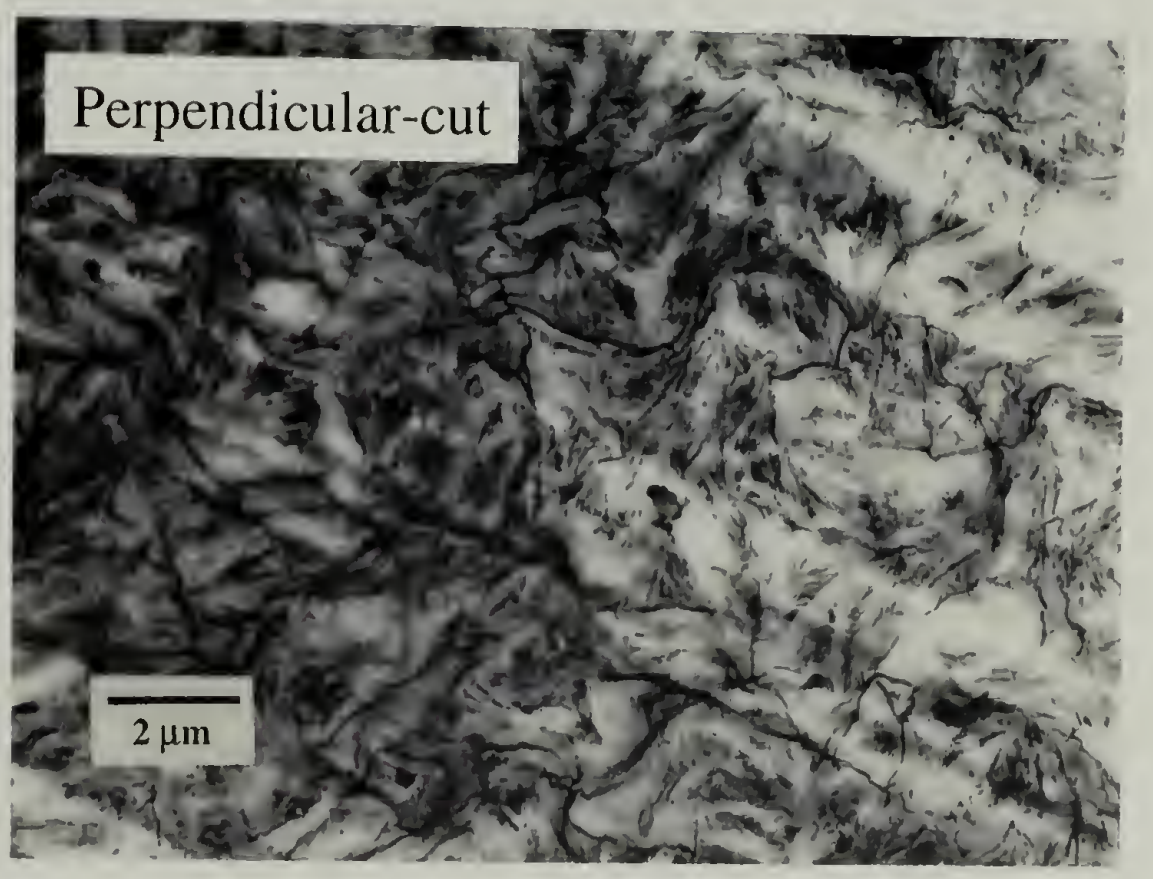

Figure 4.10: TEM micrographs of a PCO/PMP composite containing a14.4 wt% PCO after it was stretched to break at about 560% strain. (Microtoming was performed both parallel and perpendicular to the tensile direction.)

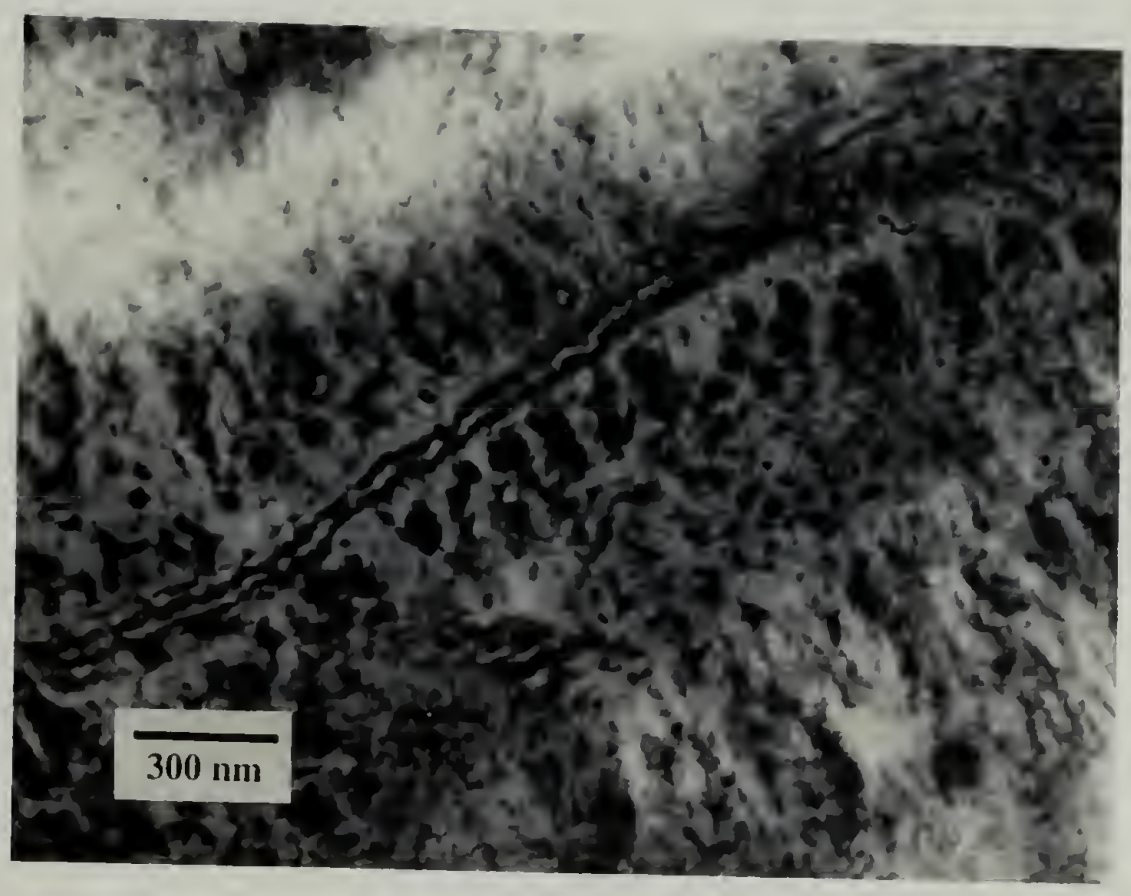

Figure 4.11: A high magnification TEM micrograph of a PCO/PMP composite containing 14.4 wt% PCO after it was stretched to break at about 560% strain. (Microtoming was performed parallel to the tensile direction.)

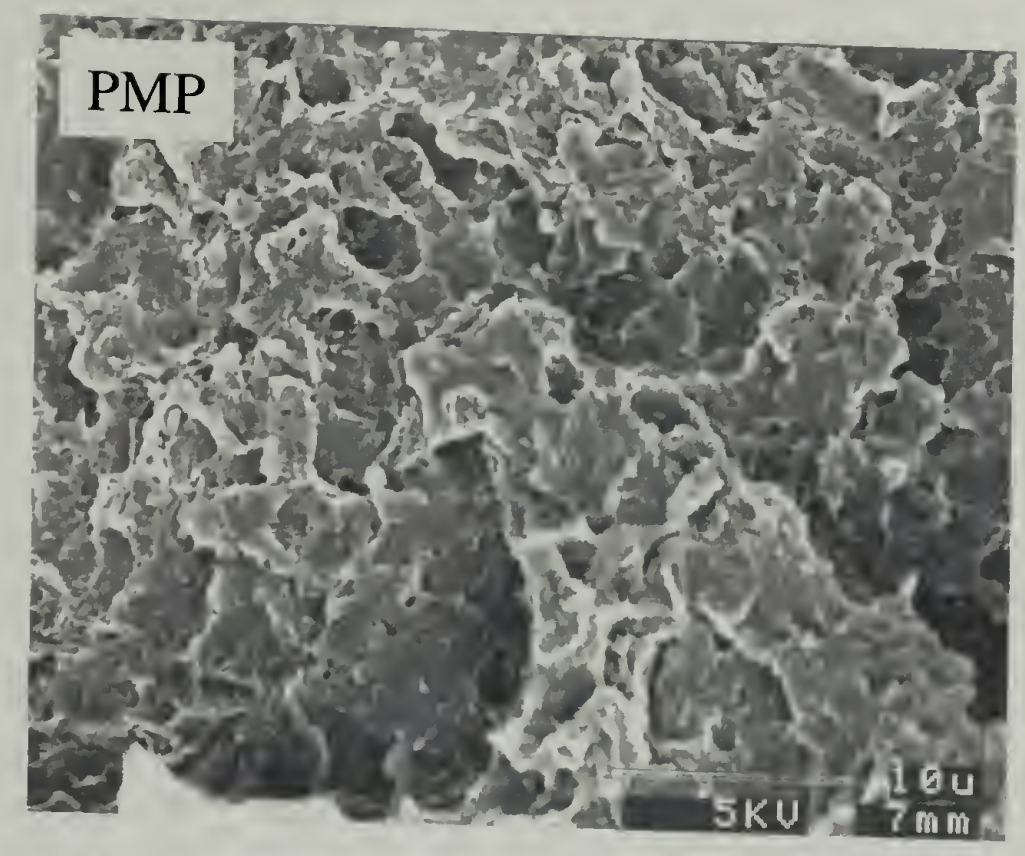

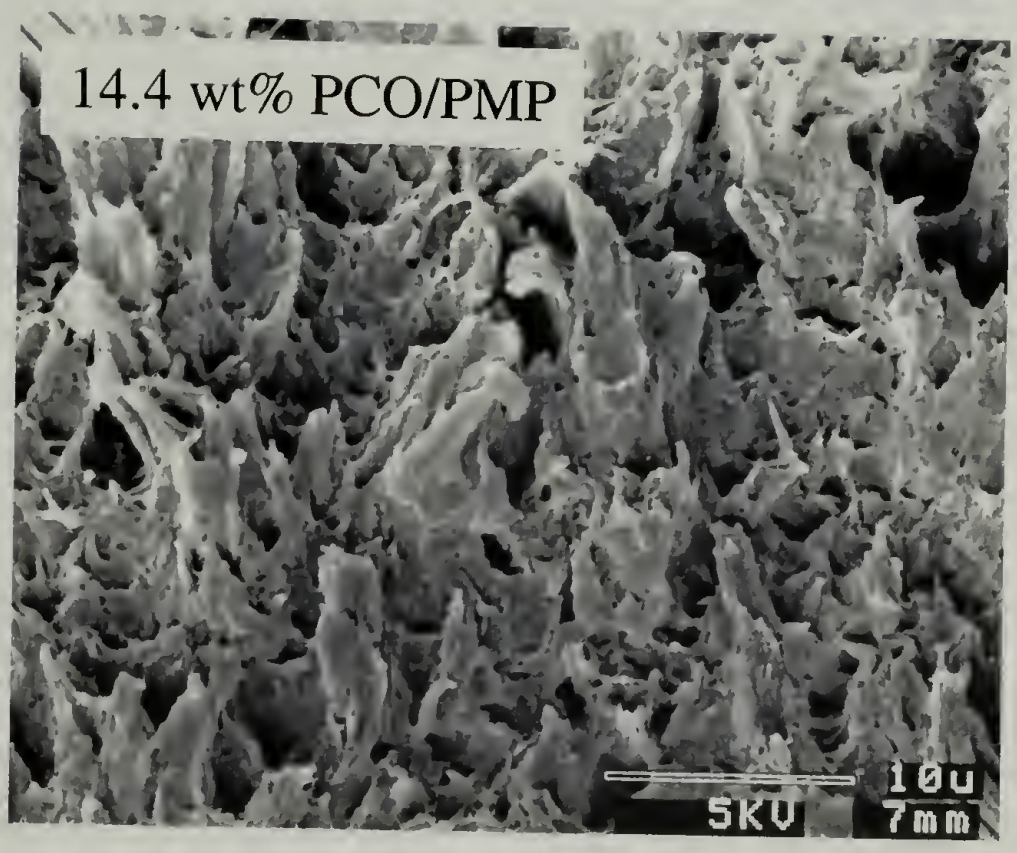

Figure 4.12: SEM images of the fractured surface of both pure PMP and a PCO/PMP composite with 14.4 wt% PCO after tensile testing.

Monitoring the morphology changes in situ during the tensile testing gives detailed information about structure deformation. Normally, a large number of samples with the same composition are made, then tensile testing is performed at each desired strain. The tested samples are taken for morphology analysis, and the results are related to the strain-stress curve. In our case, it is difficult to synthesize composites with repeatable compositions. Dr. Lesser recommended a modified dog-bone method. It is shown in Figure 4.13. Normal dog-bone specimen has a test area with a uniform width. It is assumed that the load is added to this part evenly, and other parts do not contribute to the measured strain. If we have a circular-cut specimen, it will not have a test part with the uniform width. Instead, the middle line of the specimen has the smallest width, and the width gradually increases to both directions. When a load is applied, the middle line has the largest stress, and stress gradually decrease to both "up" and "down" directions. In this way, different areas on the same sample have different strain, and different damaging morphologies. Figure 4.14 is a series of TEM micrographs taken from four different sections of a damaged circular-cut dog-bone sample. Microtoming was performed parallel to the tensile direction. Area 1 is taken from the middle line, and area 2, 3, 4 are sections taken away gradually from the middle line. It is ease to observe, there are much more damage and more ordered orientation of the PCO rubbery phase in area 1 where it has the largest strain. In area 2, the PCO orientation along the tensile direction becomes less. Area 4 is almost like an undamaged PCO/PMP sample except a few crazes.

To have more precise assessment of strain-morphology relationship, we managed to produce several samples with the same PCO composition of about 24 wt%.

Figure 4.15 shows a series of TEM studies on this PCO/PMP composite at different strain conditions. Microtoming was performed parallel to the tensile direction. At 100% stain, small crazes begin to appear in the PMP domains while PCO domains are largely unchanged. When the strain goes to 200%, much more crazes appear. However, they do not grow longer. It looks like they are stopped at the interface of PCO and PMP. At the same time, the PCO domains begin to orient towards the tensile direction. At the maximum strain, most PCO domains are highly orientated along the tensile direction. Some lamellae are broken. There are a lot of damaged zones at the interface between PCO and PMP.

4.3.6 Miscellaneous

In this chapter, the mechanical behavior of new nanocomposites is the main focus. Beyond that, we also conducted several structure manipulations to explore other new structures. There are no systematic studies. Some of them are just tests. A short review will be presented in the following paragraphs.

We performed some foaming studies on PCO/PMP nanocomposites, following the work of Arora, former joined student between McCarthy and Lesser.[41] The finding there is that it is easy to foam PCO/PMP nanocomposites with CO_2 under the conditions used for PMP. However, the cell size does not have a significant dependence on composition up to 40 wt% of PCO.

We also looked at annealing of PCO/PMP samples above the PMP melting temperature. The results are similar to PN/PMP cases in Chapter 3. The materials still kept their original geometry, indicating that PCO has very high molecular weight and is

continuous even when it is only a minor component. Another interesting observation is that no large-scale phase separation appeared. The PCO phase is still continuous. The only change is that the crystalline lamellae inside of PCO domains disappear upon annealing. This indicates that the materials may be used at higher temperature.

Synthesis of macroporous poly(dicyclopentadiene) was reported in literature[155] for a variety of applications, like ion-exchange resins, solid support materials, ect. Chemically induced phase separation was used to generate pores. As the PDCPD/PMP nanocomposites contain crosslinked PDCPD phase with tens-of-nanometer thick PMP crystalline lamellae inside, we think that a novel nanoporous thermoset will be produced if the PMP is removed. Hot carbon tetrachloride extraction was carried out on PDCPD/PMP nanocomposites. Unfortunately, there are no good results. We did succeed in removing all PMP, but the capillary force applied by the solvent crushed all of the nanopores. It would be better if there could be some kind of supercritical extraction procedure.

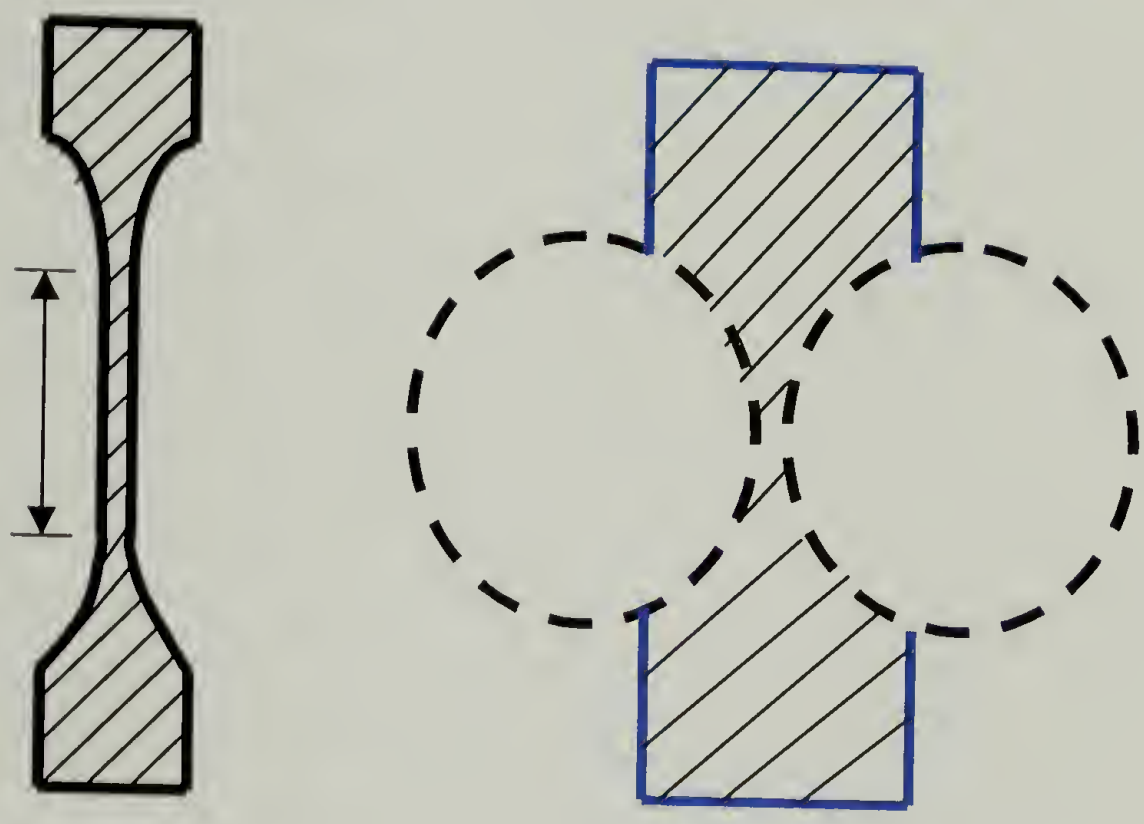

Dog-bone specimen Circular-cut specimen

Figure 4.13: Illustration of the tensile testing specimens with two different geometries.

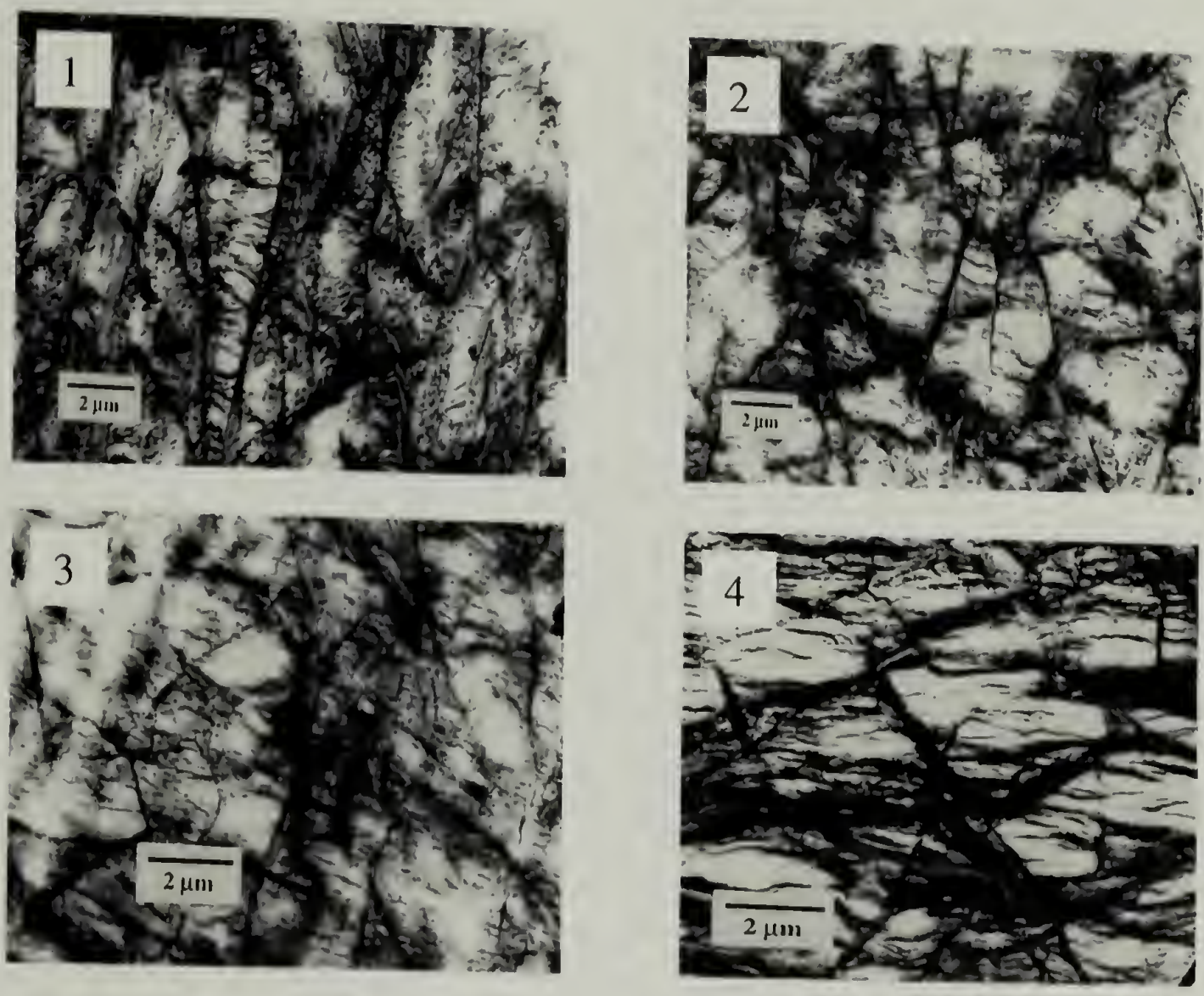

Figure 4.14: TEM micrographs of four different areas on a damaged PCO/PMP with 20 wt% PCO after tensile testing. (From 1 to 4 , local strains gradually decrease.)

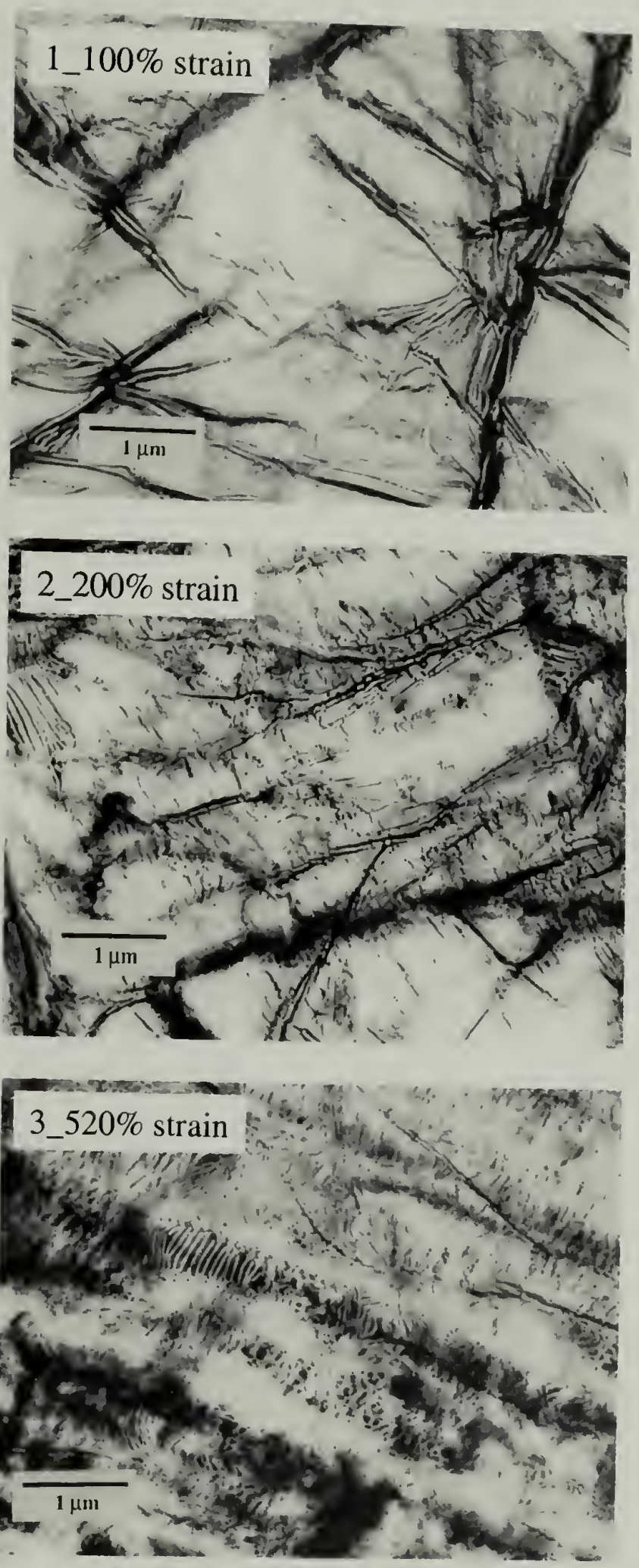

Figure 4.15: TEM micrographs of a PCO/PMP composite with 34 wt% PCO at different strain conditions. (Microtoming was performed parallel towards the tensile direction.)

4.4 Conclusions

Following the templating method developed in Chapter 3, two types of novel nanocomposites were synthesized by performing ring-opening metathesis polymerizations inside of CO_2-swollen semicrystalline polymer substrates. One is a rubber/plastics nanocomposite, polyoctenamer/PMP (PCO/PMP) and the other is a thermoset/thermoplastics nanocomposite, poly(dicyclopentadiene)/PMP (PDCPD/PMP). The distribution of the second polymer is homogeneous in the PCO/PMP case. This phenomenon helped us to explain the gradient structure of PN/PMP composites by monomer diffusion, reaction rate, and the barrier effect of the new-formed polymer. Both PCO/PMP and PDCPD/PMP show co-continuous morphology even when the minor component is present in only about 10 wt% concentration. The tensile test of PCO/PMP composites shows very interesting results. With only a small portion of PCO incorporated, the maximum strain increased five times while the modulus decreased sharply. We effectively transformed a brittle plastic into a rubbery material. Electron microscopy studies on the deformed sample also revealed detailed information on damaging.

The work presented here is merely wondering around the doorstep. A new area is open. With thousands of reactions and tons of substrates to choose from, we can predict that more and more new materials with novel properties will appear using this method.

BIBLIOGRAPHY

(1) Cao, C.; McCarthy, T. J. *Polym. Prepr. (Am. Chem. Soc., Div. Polym. Chem.)* **1999**, *40(2)*, 841.

(2) Cao, C.; Fadeev, A. Y.; McCarthy, T. J. *Langmuir* **2001**, *17*, 757.

(3) Cao, C.; McCarthy, T. J. Polym. Prepr. (Am. Chem. Soc., Div. Polym. Chem.) **2000**, 41(1), 490.

(4) Cao, C.; McCarthy, T. J. *polym. Prepr. (Am. Chem. Soc., Div. Polym. Mater. Sci. Eng.)* **2001**, *84*, 47.

(5) Plueddemann, E. P. *Silane Coupling Agents*; 2nd ed.; Plenum Press: New York, 1991.

(6) Tada, H.; Nagayama, H. *Langmuir* **1994**, *10*, 1472.

(7) Chen, W.; Fadeev, A. Y.; Hsieh, M. C.; Oner, D.; Youngblood, J.; McCarthy, T. J. *Langmuir* **1999**, *15*, 3395.

(8) Fadeev, A. Y.; McCarthy, T. J. *Langmuir* **1999**, *15*, 3759.

(9) Sagiv, J. *J. Am. Chem. Soc.* **1980**, *102*, 92.

(10) Korosi, G.; Kovats, E. s. *Colloids Surf.* **1981**, *2*, 315.

(11) Brzoska, J. B.; Ben Azouz, I.; Rondelez, F. *Langmuir* **1994**, *10*, 4367.

(12) Fadeev, A. Y.; Soboleva, O.; Summ, B. D. *Colloid J.* **1997**, *59*, 273.

(13) Abel, F. W.; Pollard, F. H.; Uden, P. C.; Nickless, G. *J. Chromatogr.* **1966**, *22*, 23.

(14) Sander, L. C.; Wise, S. A. *Crit. Rev. Anal. Chem.* **1987**, *18(4)*, 299.

(15) Regnier, F. E.; Unger, K. K.; Majors, R. E. *J. Chromatogr.* **1991**, *47*, 544.

(16) Biernat, J. F.; Konieczka, P.; Tarbet, B. J.; Bradshaw, J. S.; Izatt, R. M. *Sep. Purif. Methods* **1994**, *23*, 77.

(17) Stenger, D. A.; Hichman, J. J.; Calvert, J. M. *J. Am. Chem. Soc.* **1994**, *114*, 8435.

(18) Takahara, A.; Kojio, K.; Ge, S.-R.; Kajiyama, T. *J. Vac. Sci. Technol. A* **1996**, *14*, 1747.

(19) Sofia, S. J.; Premnath, V.; Merrill, E. W. *Macromolecules* **1998**, *31*, 5059.

(20) Zhang, M. Q.; Desai, T.; Ferrari, M. *Biomaterials* **1998**, *19*, 953.

(21) Dulcey, C. S.; Georger, J. H.; Krauthamer, V.; Fare, T. L.; Stenger, D. A.; Calvert, J. M. *Science* **1991**, *252*, 551.

(22) Ross, C. B.; Sun, L.; Crooks, R. M. *Langmuir* **1993**, *9*, 632.

(23) Xia, Y.; Zhao, X.; Whitesides, G. M. *Microelectron. Eng.* **1996**, *32*, 255.

(24) Jeon, N. L.; Finnie, K.; Bradshaw, K.; Nuzzo, R. G. *Langmuir* **1997**, *13*, 3382.

(25) Allara, D. L. *Biosens. Bioelectron.* **1995**, *10*, 771.

(26) Yang, J. Y. M.; Frank, C. W. In *Organic thin films (ACS synposium series 695)*; Frank, C. W., Ed.; American Chemical Society: Washington, DC, 1998; pp 67.

(27) Xia, Y.; Mrksich, M.; Kim, E.; Whitesides, G. M. *J. Am. Chem. Soc.* **1995**, *117*, 9576.

(28) Riedo, F.; Czencz, M.; Liardon, O.; Kovats, E. s. *Helv. Chim. Acta.* **1978**, *61*, 1912.

(29) Balachander, N.; Sukenik, C. *Langmuir* **1990**, *6*, 1621.

(30) Ulman, A. *Thin Solid Films* **1996**, *273*, 48.

(31) Webzler, L. A.; Moyes, G. L.; Raikar, G. N.; Hansen, R. L.; Harris, J. M.; Beebe, T. P., Jr.; Wood, L. L.; Saavedra, S. S. *Langmuir* **1997**, *13*, 3761.

(32) Ulman, A. *Chem. Rev.* **1996**, *96*, 1533.

(33) Fadeev, A. Y.; McCarthy, T. J. *Langmuir* **2000**, *16*, 7268.

(34) Tripp, C. P.; Hair, M. L. *Langmuir* **1991**, *7*, 923.

(35) Tripp, C. P.; Hair, M. L. *Langmuir* **1992**, *8*, 1961.

(36) McHugh, M. A.; Krukonis, V. *Supercritical Fluid Extraction*; 2nd ed.; Butterworth-Heinemann: Boston, 1994.

(37) Noyori, R.; // Kajimoto, O.; // Tucker, S. C.; // Peters, C. J.; Gauter, K.; // Brennecke, J. F.; Chateauneuf, J. E.; // Baiker, A.; // Jessop, P. G.; Ikariya, T.; Noyori, R.; // Darr, J. A.; Poliakoff, M.; // Kendall, J. L.; Canelas, D. A.; Young, J. L.; DeSimone, J. M.; // Kirby, C. F.; McHugh, M.; // Savage, P. E.; // Mesiano, A. J.; Bechman, E. J.; Russell, A. J. *Chem. Rev.* **1999**, *99*, 353.

(38) Jessop, P. G.; Leitner, W., Eds. *Chemical Synthesis Using Supercritical Fluids*; WILEY-VCH: Weinheim, 1999.

(39) Hayes, H. J. In *Polymer Science and Engineering*; University of Massachusetts: Amherst, 1999; p 8.

(40) Newitt, D. M., et. al. In *Thermodynamic Functions of Gases*; Din, F., Ed.; Butterworths Scientific Publications: Londen, 1956; Vol. 1.

(41) Arora, K. A. In *Polymer Science and Engineering*; University of Massachusetts: Amherst, 1999; p 18.

(42) Swaddle, T. W. *Inorganic Chemistry: An Industrial and Enviromental Perspective*; Academic Press: San Diego, 1997.

(43) Fricke, J. *Springer Proc. Phys.* **1986**, *6*, 2.

(44) Hrubesh, L. W. *Chem. Ind. (London)* **1990**, 824.

(45) Loy, D. A.; Russick, E. M.; Yamanaka, S. A.; Baugher, B. M. *Chem. Mater.* **1997**, *9*, 2264.

(46) Combers, J. R.; Mahabadi, H. K.; Tripp, C. P. In *United States Patent*; US patent 5,725,987, 1998.

(47) Tripp, C. P.; Combers, J. R. *Langmuir* **1998**, *14*, 7348.

(48) Combers, J. R.; White, L. D.; Tripp, C. P. *Langmuir* **1999**, *15*, 7870.

(49) Zhuravlev, L. T. *Langmuir* **1987**, *3*, 316.

(50) Israelachvili, J. N.; Gee, M. L. *Langmuir* **1989**, *5*, 288.

(51) Tompkins, H. G. *A User's Guide to Ellipsometry*; Academic Press: Boston, 1993.

(52) McCrackin, F. L.; Passaglia, E.; Stromberg, R. R.; Steinberg, H. J. *J. Res. Natl. Bur. Stand., Sec. A* **1963**, *67*, 363.

(53) Wasserman, S. R.; Tao, Y.; Whitesides, G. M. *Langmuir* **1989**, *5*, 1074.

(54) Stenger, D. A.; Georger, J. H.; Dulcey, C. S.; Hichman, J. J.; Rudolph, A. S.; Nielsen, T. B.; McCort, S. M.; Calvert, J. M. *J. Am. Chem. Soc.* **1992**, *114*, 8435.

(55) Chan, C. M. *Polymer Surface Modification and Characterization*; Hanser:: Munich, New York, 1994.

(56) Fadeev, A. Y.; McCarthy, T. J. *Langmuir* **1999**, *15*, 7238.

(57) Szabo, K.; Ha, N. L.; Schneider, P.; Zeltner, P.; Kovats, E. s. *Helv. Chim. Acta.* **1984**, *67*, 2128.

(58) Bohsanyi, L.; Liardon, O.; Kovats, E. s. *Adv. Colloid Interface Sci.* **1976**, *6*, 95.

(59) Morel, D.; Tabar, K.; Serpinet, J.; Claudy, P.; Letoffe, J. M. *J. Chromatogr.* **1987**, *395*, 73.

(60) Staroverov, S.; Fadeev, A. Y. *J. Chromatogr.* **1991**, *544*, 77.

(61) Kessel, C. R.; Granick, S. *Langmuir* **1991**, *7*, 532.

(62) Allara, D. L.; Parikh, A. N.; Rondelez, F. *Langmuir* **1995**, *11*, 2357.

(63) Parikh, A. N.; Liedberg, B.; Atre, S. V.; Ho, M.; Allara, D. L. *J. Phys. chem.* **1995**, *99*, 9996.

(64) Edelstein, A. S.; Cammarata, R. C., Eds. *Nanomaterials: Synthesis, Properties and Applications*; Institute of Physics Publishing: Bristol and Philadelphia, 1996.

(65) Feynman, R. P. *Eng. Sci.* **1960**, *23*, 22.

(66) Ito, Y.; Bleloch, A. L.; Brown, L. M. *Nature* **1998**, *394*, 49.

(67) Peckerar, M. C.; Maldonado, J. *Proc. IEEE* **1993**, *81*, 1249.

(68) Hawker, C. J.; Frechet, J. M. J. *J. Am. Chem. Soc.* **1990**, *112*, 7638.

(69) Ebbesen, T. W.; Ajayan, P. M. *Nature* **1992**, *358*, 220.

(70) Kong, J.; Soh, H. T.; Cassell, A. M.; Quate, C. F.; Dai, H. J. *Nature* **1998**, *395*, 878.

(71) Whitesides, G. M.; Mathias, J. P.; Seto, C. T. *Science* **1991**, *254*, 1312.

(72) Stroscio, J. A.; Eigler, D. M. *Science* **1991**, *254*, 1319.

(73) Snow, E. S.; Campbell, P. M. *Science* **1995**, *270*, 1639.

(74) Piner, R. D.; Zhu, J.; Xu, F.; Hong, S. H.; Mirkin, C. A. *Science* **1999**, *283*, 661.

(75) Henselwood, F.; Liu, G. *Macromolecules* **1998**, *31*, 4213.

(76) Huang, E.; Rockford, L.; Russell, T. P.; Hawker, C. J. *Nature* **1998**, *395*, 757.

(77) Balogh, L.; Tomalia, D. A. *J. Am. Chem. Soc.* **1998**, *120*, 7355.

(78) Ajayan, P. M.; Iljima, S. *Nature* **1993**, *361*, 333.

(79) Usuki, A.; Kojima, Y.; Kawasumi, M.; Okada, A.; Fukushima, Y.; Kurauchi, T.; Kamigaito, O. *J. Mater. Res.* **1993**, *8*, 1179.

(80) Johnson, S. A.; Ollivier, P. J.; Mallouk, T. E. *Science* **1999**, *283*, 963.

(81) Werne, T. v.; Patten, T. E. *J. Am. Chem. Soc.* **1999**, *121*, 7409.

(82) Alivisatos, A. P.; Johnsson, K. P.; Peng, X. G.; Wilson, T. E.; Loweth, C. J.; Bruchez, M. P.; Schultz, P. G. *Nature* **1996**, *382*, 609.

(83) Liu, G.; Ding, J.; Hashimoto, T.; Kimishima, K.; Winnik, F. M.; Nigam, S. *Chem. Mater.* **1999**, *11*, 2233.

(84) Strobl, G. *The Physics of Polymers*; Springer-Verlag: Berlin, 1996.

(85) Haward, R. N. *Br. Polym. J.* **1970**, *2*, 209.

(86) DeSimone, J. M.; Guan, Z.; Elsbernd, C. S. *Science* **1992**, *257*, 945.

(87) Goel, S. K.; Beckman, E. J. *Polym. Eng. Sci.* **1994**, *34*, 1137.

(88) Arora, K. A.; Lesser, A. J.; McCarthy, T. J. *Macromolecules* **1998**, *31*, 4614.

(89) Reverchon, E. *J. Supercrit. Fluids.* **1999**, *15*, 1.

(90) Wood, C. D.; Cooper, A. I. *Macromolecules* **2001**, *34*, 5.

(91) Sundararajan, N.; Yang, S.; Ogino, K.; Valiyaveettil, S.; Wang, J.; Zhou, X.; Ober, C. K.; Obendorf, S. K.; Allen, R. D. *Chem. Mater.* **2000**, *12*, 41.

(92) Hoggan, E.; DeSimone, J. M.; Carbonell, R. G. *Polym. Prepr. (Am. Chem. Soc., Div. Polym. Mater. Sci. Eng.)* **1999**, *81*, 218.

(93) Howdle, S. M.; Watson, M. S.; Whitaker, M. J.; Popov, V. K.; Davies, M. C.; Mandel, F. S.; Wang, J. D.; Shakesheff, K. M. *Chem. Commun.* **2001**, 109.

(94) Watkins, J. J.; McCarthy, T. J. *Chem. Mater.* **1995**, *7*, 1991.

(95) Kendall, J. L.; Canelas, D. A.; Young, J. L.; DeSimone, J. M. *Chem. Rev.* **1999**, *99*, 543.

(96) Kirby, C. F.; McHugh, M. A. *Chem. Rev.* **1999**, *99*, 565.

(97) Cooper, A. I. *J. Mater. Chem.* **2000**, *10*, 207.

(98) Wells, S. L.; DeSimone, J. M. *Angew. Chem. Int. Ed.* **2001**, *40*, 518.

(99) Watkins, J. J.; McCarthy, T. J. *Macromolecules* **1994**, *27*, 4845.

(100) Hyatt, J. A. *J. Org. Chem.* **1984**, *49*, 5097.

(101) Shieh, Y.; Su, J.; Manivannan, G.; Lee, P. H. C.; Sawan, S. P.; Spall, W. D. *J. Appl. Polym. Sci.* **1996**, *59*, 695.

(102) Manson, J. A.; Sperling, L. H. *Polymer blends and composites*; Plenum Press: New York, 1976.

(103) Sun, Y.; Willemse, R. J. G.; Liu, T. M.; Baker, W. E. *Polymer* **1998**, *39*, 2202.

(104) Majundar, B.; Paul, D. R.; Oshinski, A. J. *Polymer* **1997**, *38*, 1787.

(105) Brown, H. R.; Char, K.; Deline, V. R.; Green, P. F. *Macromolecules* **1993**, *26*, 4155.

(106) Kung, E.; Lesser, A. J.; McCarthy, T. J. *Macromolecules* **1998**, *31*, 4160.

(107) Rajagopalan, P.; McCarthy, T. J. *Macromolecules* **1998**, *31*, 4791.

(108) Watkins, J. J.; McCarthy, T. J. *Macromolecules* **1995**, *28*, 4067.

(109) Arora, K. A.; Lesser, A. J.; McCarthy, T. J. *Macromolecules* **1999**, *32*, 2562.

(110) Sperling, L. H.; Mishra, V. In *IPNs Around the World: Science and Engineering*; Kim, S. C., Sperling, L. H., Eds.; John Wiley & Sons: Chichester, 1997; pp 1.

(111) Sperling, L. H. In *Interpenetrating Polymer Networks*; Klempner, D., Sperling, L. H., Utracki, L. A., Eds.; American Chemical Society: Washington, DC, 1994; pp 3.

(112) Liu, J.-H.; Chen, J.-L.; Wang, H.-Y.; Tsai, F.-R. *Macromol. Chem. Phys.* **2000**, *201*, 126.

(113) Akovali, G.; Biliyar, K.; Shen, M. *J. Appl. Polym. Sci.* **1976**, *20*, 2419.

(114) Milczarek, P.; Kryszewski, M. *Colloid j& Polymer Sci.* **1987**, *265*, 481.

(115) Kryszewski, M. *Polym. Adv. Tech.* **1998**, *9*, 244.

(116) Jasso, C. F.; Martinez, J. M.; Mendizabal, E.; Laguna, O. *J. Appl. Polym. Sci.* **1995**, *58*, 2207.

(117) Duijnhoven, F. v.; Bastiaansen, C. *Adv. Mater.* **1999**, *11*, 567.

(118) Calderon, N. *J. Macromol. Sci. Revs.* **1972**, *C7(1)*, 105.

(119) Ivin, K. J. *Olefin Metathesis*; Academic Press: London, 1983.

(120) Tebbe, F. N.; Parshall, G. W.; Orenall, D. W. *J. Am. Chem. Soc.* **1979**, *101*, 5074.

(121) Gilliom, L. R.; Grubbs, R. H. *J. Am. Chem. Soc.* **1986**, *108*, 733.

(122) Schrock, R. R.; DePue, R. T.; Feldman, J.; Schaverien, C. J.; Dewan, J. C.; Liu, A. H. *J. Am. Chem. Soc.* **1988**, *110*, 1423.

(123) Schrock, R. R.; Murdzek, J. S.; Bazan, G. C.; Robbins, J.; DiMare, M.; O'Regan, M. *J. Am. Chem. Soc.* **1990**, *112*, 3875.

(124) Nguyen, S.-B. T.; Johnson, L. K.; Grubbs, R. H. *J. Am. Chem. Soc.* **1992**, *114*, 3974.

(125) Wu, Z.; Benedicto, A. D.; Grubbs, R. H. *Macromolecules* **1993**, *26*, 4975.

(126) Ivin, K. J.; Mol, J. C. *Olefin Metathesis And Metathesis Polymerization*; Academic Press: San Diego, 1997.

(127) Mistele, C. D.; Thorp, H. H.; DeSimone, J. M. *J.M.S.-Pure Appl. Chem.* **1996**, *A33(7)*, 953.

(128) Furstner, A.; Koch, D.; Langemann, K.; Leitner, W.; Six, C. *Angew. Chem. Int. Ed. Engl.* **1997**, *36*, 2466.

(129) Hayes, H. J.; McCarthy, T. J. *Macromolecules* **1998**, *31*, 4813.

(130) Lopez, L. C.; Wilkes, G. L. *J.M.S.-Rev. Macromol. Chem. Phys.* **1992**, *C32(3,4)*, 301.

(131) Zoller, P.; Starkweather, H. M.; Jones, G. A. *J. Polym. Sci., Polym. Phys.* **1986**, *24*, 1451.

(132) Rybnikar, F.; Geil, P. H. *J. Macromol. Sci.-Phys.* **1973**, *B7(1)*, 1.

(133) Armarego, W. L. F.; Perrin, D. D. *Purification of Laboratory Chemicals*; 4th ed.; Butterworth-Heinemann: Oxford, 1996.

(134) Berens, A. R.; Huvard, G. S.; Korsmeyer, R. W.; Kunig, F. W. *J. Appl. Polym. Sci.* **1992**, *46*, 231.

(135) Crank, J. *The Mathematics of Diffusion*; 2nd ed.; Clarendon Press: Oxford, 1975.

(136) Schwab, P.; Grubbs, R. H.; Ziller, J. W. *J. Am. Chem. Soc.* **1996**, *118*.

(137) Doroudiani, S.; Park, C. B.; Kortschot, M. T. *Polym. Eng. Sci.* **1996**, *36*, 2645.

(138) Baldwin, D. F.; Suh, N. P. *Proc. SPE-ANTEC* **1992**, 1503.

(139) Khandpur, A. K.; Macosko, C. W.; Bates, F. S. *J. Polym. Sci., Polym. Phys.* **1995**, *33*, 247.

(140) Hase, Y.; Geil, P. H. *Poly. J.* **1971**, *2*, 560.

(141) Wang, Z.; J., P. T. *Chem. Mater.* **1998**, *10*, 1820.

(142) Sarbu, T.; Styranec, T.; Beckman, E. J. *Nature* **2000**, *405*, 165.

(143) Reginato, L. *Makromol. Chem.* **1970**, *132*, 113.

(144) Gilman, J. W.; Jackson, C. L.; Morgan, A. B.; Harris, R. J.; Manias, E.; Giannelis, E. P.; Wuthenow, M.; Hilton, D.; Phillips, S. H. *Chem. Mater.* **2000**, *12*, 1866.

(145) Yu, J. M.; Dubois, P.; Jerome, R. *Macromolecules* **1996**, *29*, 8362.

(146) Dair, B. J.; Honeker, C. C.; Alward, D. B.; Avgeropoulos, A.; Hadjichristidis, N.; Fetters, L. J.; Capel, M.; Thomas, E. L. *Macromolecules* **1999**, *32*, 8145.

(147) Weidisch, R.; Michler, G. H.; Arnold, M.; Hofmann, S.; Stamm, M.; Jerome, R. *Macromolecules* **1997**, *30*, 8078.

(148) Martuscelli, E.; Palumbo, R.; Kryszewski, M. In *Polymer Blends: Processing, Morphology, and Properties*; Palumbo, R., Martuscelli, E., Kryszewski, M., Eds.; Plenum Press: New York and London, 1980.

(149) Utracki, L. A.; Walsh, D. J.; Weiss, R. A. In *Multiphase Polymers: Blends and Ionomers*; Utracki, L. A., Weiss, R. A., Eds.; American Chemical Society: Washington, DC, 1989.

(150) Riew, C. K.; Kinloch, A. J. In *Toughened Plastics I: Science and Engineering*; Riew, C. K., Kinloch, A. J., Eds.; American Chemical Society: Washington, DC, 1993.

(151) Riew, C. K.; Kinloch, A. J. In *Toughened Plastics II: Novel Approaches in Science and Engineering*; Riew, C. K., Kinloch, A. J., Eds.; American Chemical Society: Washington, DC, 1996.

(152) Young, R. J.; Lovell, P. A. *Introduction to Polymers*; 2nd ed.; Chapman & Hall: London, 1991.

(153) Weidisch, R.; Stamm, M.; Michler, G. H.; Fischer, H.; Jerome, R. *Macromolecules* **1999**, *32*, 742.

(154) Sjoerdsma, S. D.; Bleijenbeg, A. C. A. M.; Heikens, D. In *Polymer Blends: Processing, Morphology, and Properties*; Martuscelli, E., Palumbo, R., Kryszewski, M., Eds.; Plenum Press: New York and London, 1980.

(155) Martina, A. D.; Hilborn, J., G.; Muhlebach, A. *Macromolecules* **2000**, *33*, 2916.